AD-A167 004 A VISUALISATION STUDY OF THE VORTEX FLOW AROUND DOUBLE-DELTA WINGS(U) AERONAUTICAL RESEARCH LABS MELBOURNE (AUSTRALIA) D H THOMPSON AUG 85 1/1

UNCLASSIFIED ARL/AERO-R-165 F/G 20/4 NL

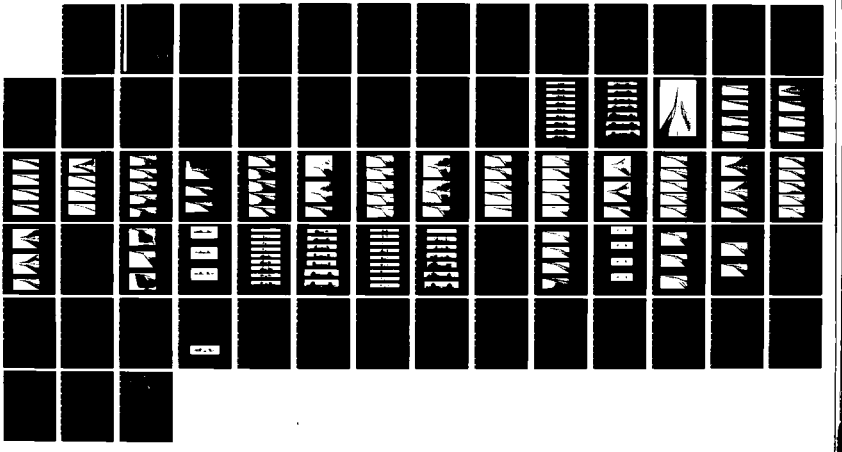

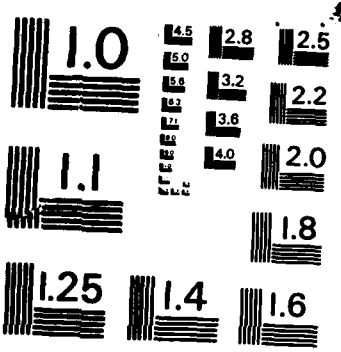

ARL-AERO-R-165

AR-004-047

(12)

DEPARTMENT OF DEFENCE

DEFENCE SCIENCE AND TECHNOLOGY ORGANISATION

AERONAUTICAL RESEARCH LABORATORIES

MELBOURNE, VICTORIA

AERODYNAMICS REPORT 165

A VISUALISATION STUDY OF THE VORTEX FLOW AROUND DOUBLE-DELTA WINGS

by

D. H. THOMPSON

Approved for Public Release

COPY No

AUGUST 1985

AR-004-047

DEPARTMENT OF DEFENCE
DEFENCE SCIENCE AND TECHNOLOGY ORGANISATION
AERONAUTICAL RESEARCH LABORATORIES

AERODYNAMICS REPORT 165

A VISUALISATION STUDY OF THE VORTEX FLOW AROUND DOUBLE-DELTA WINGS

by

D. H. THOMPSON

SUMMARY

A family of double-delta wings with leading-edge sweep combinations of 80/80, 80/70, 80/60, 80/50, and 80/40 deg. was tested in a small towing tank. The hydrogen bubble technique was used to visualise the vortex patterns above the wings over a range of Reynolds numbers (based on centreline chord) from 7,000 to 100,000. The effects of variations in incidence and leading-edge kink angle were examined. Reynolds number and leading-edge cross-section shape were found to have significant effects on the vortex structure. Attempts to visualise details of the upper surface secondary vortex flows met with only partial success.

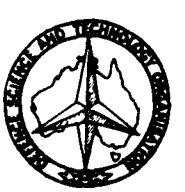

POSTAL ADDRESS: Director, Aeronautical Research Laboratories,
Box 4331, P.O., Melbourne, Victoria 3001, Australia

CONTENTS

1. INTRODUCTION

The controlled generation of seperated vortex flows is an important feature of the aerodynamic design of many current and proposed combat aircraft, particularly those requiring a manoeuvring capability at high angles of attack. Such designs often incorporate delta or double-delta wings, or a highly swept strake combined with a moderately swept wing. Some canard configurations also make use of controlled vortex flows.

Significant features of those flows are the interactions which may occur between multiple vortices, or between vortices and parts of the aircraft. Although techniques are available for modelling the flow around delta wings and modified delta wings (1–6), models which incorporate interacting vortices (1, 2, 7, 8) are less well developed, and an understanding of the fluid mechanics of such interactions is important.

The work described in the report forms part of a general study of vortex flow aerodynamics. In particular, the flow patterns over a family of double-delta wings were studied using water flow visualisation techniques in a small towing tank, with the aim of determining the conditions under which multiple vortex systems formed and interacted above such wings. The effects of changes in wing geometry were investigated, as were the conditions under which vortex breakdown occurred.

Justification for the study at low Reynolds number in water of vortex flows originating from sharp leading-edges is based on the assumption that such flows are relatively insensitive to Reynolds number, provided that certain conditions are met (9, 10). However, this assumption has been queried (11), and doubts expressed as to the relevance of results obtained using water flow visualisation techniques. Thus in the tests described here, particular attention was given to assessing the effects on the flow of changes in Reynolds number.

The flows around double-delta wings have been studied in wind tunnels using smoke (12, 16), surface flow visulisation techniques (13–16), flow field surveys (13–18), and force and moment measurements (12–18). The studies by Brennenstuhl and Hummel (13–15) are particually detailed, and the smoke flow photographs by Verhaagen (12) illustrate well the vortex patterns above such wings. Strake/wing combinations, which exhibit many flow features similar to those for double-delta wings, have also been studied extensivily in wind tunnels (19–22) and water tunnels (23).

2. EXPERIMENTAL APPARATUS AND TECHNIQUES

2.1. Test facility

A small towing tank, 5 m long and with a 0.3 m square cross-section, was used for the experiments described in this report. The tank is shown schematically in Fig. 1. It is constructed of Perspex and is in four sections, joined by bolted flanges. The towing carriage is mounted on cylinderical linear bearings running on steel rails. A variable speed-DC motor drives a pulley and cable system through a reduction gearbox. Coarse speed control is provided by changing the diameter of the drive pulley around which the towing cable passes. The maximum velocity of the carriage, currently limited by available acceleration and deceleration distances, is approximately 0.85 m/s.

2.2 Models

The planforms of the models used in the tests are shown in Fig. 2. The leading-edge sweep of the front half (or strake) of each model is 80 deg. The leading-edge sweep of the rear half (or wing) of each model varies from 80 deg. to 40 deg., giving values of the leading-edge kink angle ranging from 0 deg. to 40 deg.

All the models have a centreline chord of 150 mm, and are made of Perspex sheet 2 mm thick, giving a thickness/chord ratio of 0.0133. There are two sets of models. In one set, each model has symmetrically bevelled edges, with an included edge angle of 30 deg. In the second set, each model has one flat surface and one bevelled surface, again with an included edge angle of 30 deg., and can be mounted with either surface uppermost. A sting mounting beneath the towing carriage allowed the incidence of each model to be varied over the range 0–30 deg.

2.3. Flow visualisation techniques

The hydrogen bubble technique (24) was used to visualise the vortex flows around the double delta models. A strip of aluminum foil, 2 mm wide, was cemented along the underside of each leading-edge of each model. The strips acted as the cathodes of an electrolytic circuit. The anode was a brass plate mounted on the towing carriage, in contact with the water in the tank. A voltage applied between the foil cathodes and the anode produced fine bubbles of hydrogen gas on the surface of the aluminum. The bubbles were swept off the strips into the separating flow at the leading edge-and into the vortex system above the model. The formation of the bubbles was promoted by the addition of the sodium sulphate to the tank water at a concentration of 0.1 g/l.

Two lighting arrangements were used to illuminate the bubble pattern. To obtain plan views of the model and flow pattern, a small 100 watt slide projector was mounted on a frame attached to the towing carriage in such a way that the light from the projector passed through one side of the tank. A camera positioned directly above the model and pointing down into the tank was used to photograph the flow patterns. A Perspex sled, fixed to the towing carriage and moving on the surface of the water, prevented any optical distortion due to the surface waves.

To obtain cross-sectional views of the bubble patterns, the lighting arrangement shown schematically in Fig. 3 was used. An air-cooled argon ion laser (typical output 38mW at a wavelength of 514 nm) was positioned at one end of the tank. The output beam from the laser passed through the pair of cylindrical lenses to form a horizontal sheet of light. The sheet of light passed along the tank to the towing carriage, where a second pair of lenses expanded the beam in a horizontal plane and converged it in a vertical plane. The beam was deflected down into the water by a front surfaced plane mirror, providing a vertical sheet of light orientated normal to the direction of the travel of the model and focussed to a line on the upper surface of the model. The lens system and mirror on the towing carriage could be adjusted to position the light plane at any desired chordwise station on the model. The accuracy of the linear motion of the carriage provided by the linear bearing system ensured that once the laser had been aligned, the position of the light sheet on the model did not change as the carriage traversed the length of the tank.

The bubble pattern cross-sections were viewed via a mirror mounted behind the model, reflecting upward into a camera mounted on the rear of the towing carriage.

Flow patterns were recorded using a video system comprising a Philips LDH 26 monochrome camera and a National NV-100 video cassette recorder, and by still photography using an Olympus OM2N 35 mm single lens reflex camera. Ilford HP5 film rated at 1600 ASA and developed in Microphen was used.

Sodium fluorescein dye was used also to a limited extent for flow visualisation, in conjunction with the crossflow illumination technique outlined above. The model mounting system allowed the model to be swung easily out of the water without affecting the incidence setting. The model undersurface was painted with a concentrated solution of the dye. The model was replaced in the water and the test run started immediately. The dye from the lower surface passed into the vortex system and fluoresced brightly when stimulated by the 488 nm line of the argon ion laser. This technique was effective only at low speeds, as the dye washed off the model too quickly at higher speeds. In addition, the dye rapidly contaminated the tank water, reducing the optical contrast between the pattern of interest and the background. Nevertheless, the technique did provide a useful check on some of the results obtained using hydrogen bubbles.

2.4. Test range and results format

Tests were carried out over a velocity range of 0.05–0.85 m/s, corresponding to a Reynolds number range (dependent on water temperature) of approximately 7,000 to 130,000, based on model centreline chord. Most of the models were tested at angles of incidence or 6, 8, 10, 12, 15, 20, 25, and 30 degrees, although other angles were used as neccessary to provide additional information.

Results are presented for the most part in the form of photographs, although in a number of cases vortex trajectories have been plotted graphically from measurements made from still photographs or video recordings.

3. RESULTS AND DISCUSSION

3.1 General flow features

The flow over the 80/60 deg. wing model with symmetrically bevelled edges provides good examples of the features observed in typical double-delta vortex flows, and will be described in this section. This description will provide a basis for the subsequent discussions of the effects of model geometry and Reynolds number.

Fig. 4 shows cross-sections of the vortex system at various chordwise stations along the 80/60 deg. wing at a Reynolds number of 103,000 and an incidence of 15 deg. At $X/C = 0.5$, the position of the leading-edge kink, the flow is typical of that over a single-delta wing. Separation occurs along each leading-edge of the strake, and the separated fluid rolls up to form a spiral vortex system above each side of the strake. The core of each vortex stretches downstream from the strake apex, and lies above and inboard of the leading-edge.

Downstream of the leading-edge kink, at $X/C = 0.525$, a second small vortex has appeared outboard of the strake vortex. This second vortex has its origin at the leading-edge kink. With increasing downstream distance, the outboard (or wing) vortex moves inboard and upwards over the strake vortex, which in turn moves outboard and downwards to the wing surface. The strake vortex cross-section becomes increasingly distorted as the two vortices intertwine and merge, and separate wing and strake cores can no longer be discerned beyond $X/C = 0.8$.

Fig. 5 shows a plan view of the flow pattern in which the cores of the strake and wing vortices are clearly visible, and can be separately distinguished almost back to the trailing-edge. The strake vortex core is straight from the strake apex back to about $X/C = 0.7$, when it starts to curve outboard under the influence of the wing vortex. The wing vortex core also is almost straight back to the same chordwise station, when it starts to curve inboard under the influence of the strake vortex. The two cores first cross over in plan view at about $X/C = 0.77$, subsequently intertwining and merging into one core before the trailing-edge- is reached.

Downstream of the wing leading-edge kink, the strake vortex is no longer fed by vorticity shed from the leading-edge, and so remains constant in strength, or may weaken due to viscous effects. The wing vortex, onthe other hand, is fed by vorticity from the leading-edge, and so will gain strength with increasing downstream distance. The degree to which one or other of the two vortices will dominate the interaction will depend on the relative strengths of the two vortices and the distance between them at any particular chordwise station. Any change in flow conditions or model geometry which influences either of these two factors will affect the interaction process.

3.2 Effect of incidence

Figs. 6–10 show in plan view how the vortex system is affected by changes in incidence for the 80 deg., 80/60 deg., 80/50 deg. and 80/40 deg. wings. All the photographs were taken at a Reynolds number of approximately 100,000. The flow patterns for each wing will be discussed in turn.

(*a*) 80 deg. wing. (Fig. 6)

For this wing, with a straight leading-edge, a single vortex core forms above each wing half at all the incidence angles tested. A single sheet of bubbles rolls up unbroken from each leading-edge. In plan view, each core is straight from the apex to the trailing edge, and each core moves inboard slightly as incidence increases.

At an incidence of 30 degrees, vortex bursting occurs in the starboard vortex at $X/C = 0.85$; the other vortex remains unburst. The asymmetry may be due to asymmetry in the model itself, or in the model mount.

(*b*) 80/70 deg. wing. (Fig. 7)

For this wing, at an incidence of 6 deg., the strake vortex core is reasonably well defined. Downstream of the leading edge kink, the wing vortex core is just discernible as it passes over the strake vortex at about $X/C = 0.75$, causing the latter to move slightly outboard. At an incidence of 8 deg., the flow pattern is generally similar, although the wing vortex core is more sharply defined. At an incidence of 10 deg., the intertwining of the two vortices is discernible. At an incidence of 12 deg., the wing vortex core is well defined, and becomes more so as the incidence increases further. The flow pattern appears to take the form of an unbroken sheet of bubbles separating from the leading-edge and rolling up to form a single vortex. Nevertheless, there are slight kinks in the strake vortex core, indicating that some form of interaction is occurring, perhaps with a very weak wing vortex. The resolution of the visualisation technique was not good enough to allow this point to be clarified.

At an incidence of 30 deg., the starboard vortex bursts at about $X/C = 0.65$, and the port vortex remains unaffected back to and beyond the trailing-edge.

(*c*) 80/60 deg. wing. (Fig. 8)

At an incidence of 6 deg., the core of the strake vortex is well defined and lies in an approximately straight line from the strake apex back to about $X/C = 0.9$, and then curves slightly inboard to align with the freestream direction. Over the wing and outboard of the strake vortex, there is a region of separated flow within which a vortex core can just be discerned.

At an incidence of 8 deg., both the strake and wing vortices are visible. They do not cross over above the wing itself, although the strake vortex core now curves outboard slightly near the trailing-edge. At an incidence of 10 deg., the strake and wing vortices interact over the wing, with the crossover point occurring at about $X/C = 0.85$. The wing vortex appears to dominate the interaction, as its core remains almost upright while the strake vortex core is sharply deflected outboard beneath it.

At an incidence of 12 deg., the vortex crossover has moved slightly upstream, and the wing vortex appears to be less dominant. It moves inboard during the interaction and the outboard deflection of the strake vortex is more gradual than was the case at an an incidence of 10 deg.

As the incidence further increased beyond 12 deg., the same general flow structure is maintained, except that the vortex crossover point moves gradually upstream, reaching $X/C = 0.75$ at an incidence of 25 deg. Also, the dominance of the wing vortex appears to continue to decrease, as it is its core which undergoes increasingly greater deflections as it intertwines with the strake vortex.

There is again asymmetry in the flow patterns at angles of incidence greater than 25 deg. At an incidence of 30 deg., the starboard strake vortex bursts at about X/C 0.65, while the port strake vortex bursts at about X/C 0.85.

(*d*) 80/50 deg. wing. (Fig. 9)

The development of the flow over this wing is generally similar to that over the 80/60 deg. wing. At low angles of incidence, the strake vortex core is well defined and straight (in plan view), and the wing vortex core becomes increasingly well defined as incidence is increased. However, at an incidence of 10 deg., the vortices do not cross over above the wing. The interaction is beginning just upstream of the trailing-edge at an incidence of 12 deg. At an in-

cidence of 15 deg., the vortex crossover is at $X/C = 0.82$, and moves further upstream as incidence increases.

For angles of incidence of 15 and 20 deg., both the strake and wing vortices burst after interacting. At an incidence of 25 deg., a similar situation exists above the port side of the wing, but on the starboard side, the strake vortex has burst further upstream and there is little evidence of a wing vortex having formed at all. At an incidence of 30 deg., the port strake vortex bursts before interaction occurs, and the wing vortex is entrained in the turbulent flow downstream of the burst. On the starboard side, the strake vortex has burst close to the leading-edge kink, and there is again little evidence of a fully formed wing vortex.

(*e*) 80/40 deg. wing. (Fig. 10)

For this wing, at an incidence of 6 deg., the strake vortex core is well defined. The flow over the outboard part of the wing does not appear to have a well ordered structure. As the incidence increases to 8 deg., a wing vortex core becomes visible. However, the core appears to expand after a short distance (at about $X/C = 0.6$ for an incidence of 10 deg.). This expansion may be a form of burst, although it appears to be more gradual than the normal burst. With further increase in incidence, the wing vortex core expansion moves further downstream, reaching $X/C = 0.75$ at an incidence of 15 deg. This effect has been noted by Brennenstuhl and Hummel (15) in some of their wind tunnel tests. They attribute it to an interference effect between the unburst strake vortex and the wing vortex, with the former exerting a stabilising influence on the core of the latter as incidence is increased.

At an incidence of 15 deg., the strake vortex is influenced by the expanding wing vortex and moves outboard beneath the latter. At an incidence of 20 deg., the position of the wing vortex burst has moved upstream again and the strake vortex is entrained in the turbulent flow downstream of the burst. The strake vortex itself bursts at about $X/C = 0.8$. At an incidence of 25 deg., the flow pattern becomes asymmetrical. The port wing vortex bursts at $X/C = 0.7$ and the port strake vortex bursts at $X/C = 0.75$. On the starboard side, the strake vortex bursts at $X/C = 0.65$. The wing vortex appears to have burst almost as soon as it is formed. At an incidence of 30 deg., the flow pattern is also asymmetrical, with the starboard strake vortex bursting at $X/C = 0.5$, and no starboard wing vortex being visible. The port strake vortex bursts at $X/C = 0.7$.

3.3. Effect of leading-edge kink angle

The flow patterns for the five different wings at the same incidence of 15 deg., and a Reynolds number of 100,000 are compared in Fig. 11 to show directly the effects of changes in the leading-edge kink angle.

For this incidence and Reynolds number, the effect of increasing the leading-edge kink angle from zero is to cause the formation of a separate wing vortex. The initial spanwise distance between the wing and the strake vortices increases as the kink angle increases. The wing vortex and the strake vortex interact over the wing at low values of kink angle, but the position of the interaction moves downstream past the trailing-edge as the kink angles increase.

For a kink angle of 30 deg., both wing and strake vortices burst in the vicinity of the trailing-edge, after the vortex cores have interacted. For a kink angle of 40 deg., only the wing vortex has burst at about $X/C = 0.8$, before the vortex cores have interacted.

3.4. Effect of leading-edge cross-section shape

The results described so far were obtained using models with symmetrically bevelled edges. To investigate the effects of edge cross-section shape on the vortex patterns, wing models with asymmetrically bevelled edges were tested. Each of these models had edges bevelled on one surface only and could be mounted with the bevelled surface uppermost (positive camber) or the flat surface uppermost (negative camber). An additional 80 deg. 60 deg. model with rounded leading-edges was also tested.

The development with incidence of the flow over the 80 deg./60 deg. wing models with asymmetrically bevelled edges and with rounded edges is shown in Figs. 12–14.

For the model with a flat upper surface, Fig. 12 shows that the vortex patterns are quite similar to those for the model with symmetrically bevelled edges (see Fig. 8). However, the wing vortex core is more sharply defined at the lower angles of incidence, and the interaction between the strake and wing vortices occurs further upstream for a particular incidence. Thus, for example, at an incidence of 12 deg., vortex crossover occurs at $X/C = 0.7$ for the flat-topped wing.

Fig. 13 shows that for a model with a flat lower surface, the differences in flow pattern relative to the symmetrically bevelled wing are more marked. At all angles of incidence tested, the strake vortex lies further outboard over the strake. For angles of incidence of 8 deg. or more, the wing vortex appears to originate from a point on the leading-edge outboard and aft of the kink. The wing vortex lies further outboard, and the interaction between the strake and wing vortices occurs further aft than is the case for the symmetrically bevelled wing. For example, at an incidence of 15 deg., the vortex crossover occurs at $X/C = 0.9$, 0.77, and 0.70 for the flat-bottomed, symmetrical, and flat-topped wings respectively.

For the model with rounded leading-edges, Fig. 14 shows that the ortex positions liep between those for the symmetrically bevelled model and those for the mvodel with a flat to surface. An interesting feature of the flow patterns around this model at the higher angles of incidence is that they are much less asymmetrical than is the case for the sharp-edged wings. Also, the wing vortex cores are discernible almost back to the trailing-edge at incidence angles of 25 and 30 deg.

The vortex paths for the three edge bevel shapes are compared graphically in Fig. 15, for an incidence of 12 deg.

Similar effects of leading-edge shape were observed for other models in the series. For example, Fig. 16 shows how the three different types of edge bevel affect the vortex pattern above the 80/40 deg. wings, and Fig 17 shows the effect of edge shape on vortex cross-sections above the same models at $X/C = 0.65$ and an incidence of 15 deg. For the flat bottomed wing, the wing vortex lies closer to the wing upper surface, and further outboard, than is the case for the symmetrically bevelled wing. The proximity of the wing vortex to the wing surface means that its motion under the influence of its image in the wing tend to keep it further outboard and further away from the strake vortex, thus delaying any interaction between the two. Elle (25) has reported similar effects of edge shape on vortex position for single-delta wings.

The effects of edge cross-section shape on the initial stages of wing vortex formation are not unexpected. The changes to the edge bevel, although small in relation to the overall dimensions of the models, constitute significant changes to local surface geometry. For example, in the case of the 80/40 deg. wings, at $X/C = 0.5$ the spanwise extent of the actual bevelled part of the leading-edge comprises some 36 per cent of the local semispan for the asymmetrical bevelled wing, and half that amount for the symmetrically bevelled wing.

3.5. Effect of Reynolds number

It is assumed generally that separated vortex flows where primary separation occurs at a sharp leading-edge are relatively insensitive to Reynolds number. This assumption provides the justification for flow visualisation tests in water at Reynolds numbers typically in the range 1,000–10,000, some two or three orders of magnitude less than usual wind tunnel and flight values. Erickson (10) has examined results from water flow tests in a wide range of facilities and has provided guidelines for testing at low Reynolds number, based on Maskell's description (9) of the influence of Reynolds number on vortex structure. Wortman (11) has queried the assumption of Reynolds number independence, and has expressed doubts as to the results obtained using water flow visualisation techniques. He concludes that:

> "the relation between the currently popular low speed water tunnel studies and realistic aircraft flows is tenuous in a qualitative sense and either misleadimg or nonexistent in quantitative terms. Inferences regarding actual flows which are based on low speed flow observations should be viewed as wishful thinking denying realities or pleasant distractions with strong publicity potential."

Thus it is of considerable importance to evaluate the effect of Reynolds number on vortex

flows, and this was one objective of the present tests. The towing tank is particually useful in this respect, as the free stream turbulence is effectively zero, irrespective of the test Reynolds number. This removes one variable which might otherwise contribute to an apparent Reynolds number effect.

The effect of Reynolds number on the flow over the 80/60 deg. wing with symmetrically bevelled edges is discussed below.

Figs. 18 and 19 show the downstream development of the vortex system for Reynolds numbers of 32,000 and 17,000 respectively, at an incidence of 15 degrees. In each case, the general features of the flow are similar to those for a Reynolds number of 103,000. However, at a given chordwise station just downstream of the leading-edge kink, as the Reynolds number is reduced, both wing and strake vortices move inboard, the wing vortex to a greater extent than the strake vortex. The wing vortex also moves upward away from the wing surface and the strake vortex moves down towards the wing surface. Again, the vertical movement of the wing vortex is greater than that of the strake vortex. These relative movements are plotted in Fig. 20(*a*), which shows the vortex positions at $X/C = 0.675$. One effect of the changes in positions of the vortices is that the point at which the strake and wing vortex cores cross over (in plan view) moves upstream as Reynolds number decreases.

The position of the merged vortex near the trailing-edge is also affected by changes in Reynolds number, as shown in Fig. 20(*b*), where the vortex position at $X/C = 0.95$ is plotted. In this case, the vertical position of the vortex is constant, but the spanwise outboard movement amounts to about 12 per cent of the local semispan as the Reynolds number increases from 17,000 to 103,000.

Further illustrations of the effect of Reynolds number are provided in Fig. 21, which shows plan views of the flow over the 80/60 deg. wing at an incidence of 12 deg. and Reynolds numbers of 8,400, 29,000, 57,000 and 100,000. The aft movement of the crossover of the strake and wing vortices with increasing Reynolds number is apparent for the three highest Reynolds numbers. At a Reynolds number of 8,400, there appears to be no separate wing vortex, and the flow separating from the leading-edge rolls up in a continuous sheet into a single vortex above each wing half. This effect is also demonstrated in Fig. 22, which shows vortex cross-sections over the same wing at $X/C = 0.6$ for Reynolds numbers of 7,100, 15,000, 30,000, and 52,000, at an incidence of 12 deg. At the lowest Reynolds number, the sheet of bubbles is continuous from the leading edge into the strake vortex core, with no indication of a wing vortex outboard of the strake vortex. At a Reynolds number of 15,000, the wing vortex is present, and becomes larger as the Reynolds number increases further.

Similar effects were observed for other wings in the series. For example, Fig. 23 shows the flow patterns above the 80/50 deg. wing at an incidence of 12 deg. and Reynolds numbers of 7,400, 20,000, 34,000, 63,000, and 100,000. The formation of a single vortex at the lowest Reynolds number and the outboard and aft movement of the crossover point at the higher Reynolds numbers are again features of the flow. In addition, the bubble sheet shed from the wing leading-edge at a Reynolds number of 20,000 has a distinct banded appearance. The reason for this banding is not known, but one possible explanation is that small scale vortices, with their axes parallel to the leading-edge, are forming in the sheet of fluid separating from the leading-edge. Bubbles concentrating in the cores of these vortices are appearing as bands in the photographs. Similar patterns have been observed by Gad-el-Hak and Blackwelder (26) in the flow over single delta wings.

The vortex positions above the 80/60 deg. wing are compared graphically in Fig. 24. Results of towing tank tests at three Reynolds numbers are an incidence of 12 deg. are shown, and also included are results obtained by Brennenstuhl and Hummel (15) at a Reynolds number of 1.5 million in a windtunnel. Their model differed slightly from the towing tank model in that it was thinner ($t/c = 0.006$) and had rounded leading edges. Nevertheless, the trend of the towing tank results appears to be continued to the higher Reynolds numbers of the wind tunnel results in that the point at which the strake and wing vortices cross over moves outboard and aft with increasing Reynolds number, and the position of the merged vortex at the trailing edge also moves outboard.

Similar Reynolds number effects were observed at higher angles of incidence in the towing tank tests. For example, at an incidence of 20 deg. and a Reynolds number of 13,000, vortex crossover occurs at $X/C = 0.68$, and at a Reynolds number of 100,000, crossover occurs at

X/C = 0.75. (See Fig. 8, for example). However, at this angle of incidence. Brennenstuhl and Hummel (15) found that the merging of the two vortices was complete at the leading-edge kink. In other words, only one vortex forms above each side of the wing, in contrast to the two vortices clearly visible in the towing tank tests at the same incidence. A possible explanation for this difference is that the wind tunnel results were based on the interpretation of surface flow patterns. The lack of surface traces of the wing vortex has been interpreted as indicating that vortex merging has occurred. This may not be the case, as the wing vortex may have moved upwards and inboard over the strake vortex before it can affect the surface flow pattern. Alternatively, the wing vortex may have been too weak to produce discerible surface flow traces.

A further indication of the effect of Reynolds number is provided in Fig. 25(*a*), in which the position of the merged vortex at the trailing edge of the 80/60deg. wing is plotted against Reynolds number for an incidence of 12 deg. The results are taken from both still photographs and videotape recordings. Wind tunnel results from Ref.(15) are included. The overall movement of the merged vortex is about 35 per cent of the local semispan for a range of Reynolds number from 5,000 to 1.5 million. Fig. 25(*b*) shows further towing tank results for incidence angles of 10, 15, and 20 degrees. In each case the trend is similar, with the merged vortex moving outboard by some 15–20 per cent of the local semispan, as Reynolds number increases from 10,000 to 100,000.

Downstream of the leading edge kink, the initial spanwise separation of the wing and strake vortices increases with Reynolds number, allowing the wing vortex to gain strength before interacting with the strake vortex. The wing vortex thus becomes increasingly dominant in the interaction process. The result is that the merged vortex moves outboard, closer to the extended line of the wing vortex, as the Reynolds number increases.

To check that the effects of Reynolds number on vortex position were not due only to the interaction mechanism between the wing and the strake vortices over the double-delta wing, measurements were made of the vortex positions above a single-delta wing. An existing model with a leading-edge sweep of 70 deg. was used. The thickness/chord ratio and edge bevel matched those of the symmetrically bevelled double-delta models. The vortex positions at X/C 0.9 were measured from videotape recordings and are plotted in Fig. 26. Some measurements were made using dye for flow visualisation. The results obtained did not differ significantly from those obtained using hydrogen bubbles. The outboard movement of the vortex with increasing Reynolds number is apparent, amounting to some 10–15 percent of the local semispan over the range of Reynolds number in the towing tank. The trends are similar for all three test angles of incidence. For comparison, some results from Ref. (25), obtained in a water tunnel at Reynolds number of 1.2 million, are included. The trend of the towing tank results is continued to the higher Reynolds numbers of the water tunnel results.

Reynolds number effects observed in wind tunnel tests of delta wings (27, 28) have been attributed to the transition behaviour of the boundary layer on the wing upper surface. Beneath the primary vortex, the upper surface boundary layer is moving outboard and aft. Outboard of the primary vortex, the boundary layer encounters an unfavourable pressure gradient, and separates to roll up into a secondary vortex of opposite sense to the primary vortex. If the upper surface boundary layer undergoes transition before separation, the separation will be delayed and the secondary vortex will be smaller than is the case following laminar separation. The displacement effect of the secondary vortex on the primary vortex will be reduced, allowing the latter to move outboard and downwards towards the wing surface.

The observed Reynolds number effects on the flow over double-delta wings could be explained in the same way. However, in the case of the towing tank tests described here, the maximum Reynolds number is approximately 100,000, and all the upper surface boundary layers would have been laminar. Thus if the observed effects are due to movements of the secondary vortex, these movements must be caused by changes in the position of laminar separation only, and not by changes due to transition.

In view of the definite Reynolds number effect observed in the tests on both the double-delta and single-delta models, and particularly, in the case of the former, of the change from a single to a double vortex system above each wing half at a Reynolds number of approximately 9,000, the majority of the tests described in this report were carried out at a Reynolds number of at least 50,000, and most at a Reynolds number of approximately 100,000.

Maskell (9) and Erickson (10) suggest that for a separated vortex flow to be insensitive to Reynolds number, the relationship:

$$L/X >> 1/\sqrt{R(x)}$$

should be valid, where L is a typical lateral dimension of the large scale vortex structure at a distance X from the origin of the vortex (the wing apex) and $R(x)$ is the Reynolds number based on the distance X and the freestream velocity. This relationship basically gives the condition under which the structure of the vortex is determined mainly by vorticity convection rather than by vorticity diffusion. Alternatively, the relationship can be interpreted as stating that typical lateral dimension of the vortex should be much greater than the local wing boundary layer thickness (as the latter is inversely proportional to the square root of the Reynolds number).

In the case of the towing tank tests described here, typical values of the parameters in the relationship are:

L	10 mm	
X	150 mm (the trailing-edge)	
thus L/X	0·069	
For $R(x)$	100,000, $\sqrt{R(x)}$ 0·003, and $\{L/X\}/\{1/\sqrt{R(x)}\}$	23
For $R(x)$	10,000, $\sqrt{R(x)}$ 0·01, and $\{L/X\}/\{1/\sqrt{R(x)}\}$	7·7

(the value of L does not change much with $R(x)$).

If we arbitrarily assume that ">>" means "at least 10 times as large as", then the relationship is satisfied for Reynolds numbers greater than about 20,000, the region within which most of the results shown in this report lie.

Wortman's (11) examination of available experimental measurements of such parameters as axial velocity in the vortex core, vortex trajectories, and vortex breakdown position, together with his analysis of the size and position of the vortex, led him to conclude that the vortex flow pattern is strongly influenced by Reynolds number, particually in the 10,000 to 1 million range.

The results described in this report tend to confirm Wortman's observations. However, his conclusions that little can be learnt about high Reynolds number flows by visualisation at low Reynolds numbers appears to be rather harsh. Some of the basic mechanisms of vortex interaction will be qualitatively similar, irrespective of Reynolds number, and trends established at low Reynolds numbers appear to be continued to higher values. It appears that, provided that the obvious restrictions are borne in mind, low speed flow visualisation can serve a useful purpose in increasing the understanding of separated vortex flows.

3.6 Vortex system structure

Having investigated the parameters which affect the overall flow pattern over the family of double-delta wings, it is of interest to consider in some detail the structure of the vortex system in the vicinity of the leading-edge kink. The influence of the strake flow in this region has been investigated by Fiddes and Smith (29). They have shown that the strake vortex induces upwash and sidewash near the kink, thus increasing the effective incidence and sweepback of the wing leading edge, and causing earlier and more pronounced separation than would occur on the wing alone.

Flow in the kink region, and in particular, the initial stages of wing vortex formation, will be influenced by local wing surface geometry. This has been shown by the effects of changes in leading-edge bevel, for example.

Possible flow structures downstream of the leading-edge kink have been discussed by Smith (2) and Verhaagen (12), and are considered here in relation to the towing tank tests.

At small values of leading-edge kink angle and at moderate incidence, Smith suggests that

downstream of the kink, the wing vortex is double-branched, linked by a stream surface to the strake vortex (Fig. 27). A similar structure is suggested by Verhaagen, on the basis of smoke and surface flow visualisation tests on two wind tunnel models with 76/60 deg. and 76/40 deg. sweep combinations. The majority of the flow patterns observed in the towing tank tests appear to show a double-branched structure. At the higher test Reynolds numbers, the details of the flow in the region between the strake and wing vortices are not clearly visible, but at lower Reynolds numbers the bubble sheet linking the two vortices can be discerned (Figs. 19 and 22). Fig. 28 shows a further example of such a flow, in this case, over the 80 deg. wing with symmetrically bevelled edges at $X/C = 0.6$, an incidence of 15 deg., and a Reynolds number of 34,000.

With a double-branched system, vorticity shed from the leading-edge is convected into the outboard core and does not reach the inboard vortex. The latter remains constant in strength, or may weaken if the outboard vortex becomes strong enough to convect votricity back towards itself. The stream surface linking the two vortex cores may not be a true vortex sheet, as vorticity is being convected away from the central line of inflection in the sheet. The jump in tangential velocity across the sheet in this area may thus decay to zero.

At larger kink angles, or smaller incidence angles, Smith suggests that part of the stream surface connecting the two vortices may collapse on to the wing surface, leading to the possible flow pattern shown in Fig. 29. The structure of the flow between the wing surface and the inboard vortex is not clear, and will depend on whether or not vorticity is being shed from the surface up into the vortex. None of Verhaagen's flow pattern photographs appear to show this type of structure, and neither do the majority of photographs taken in the present towing tank tests. However, some of the photographs of the flow over the 80 deg./40 deg. model with a bevelled upper surface could represent such a pattern as, for example, in Fig. 17(*c*).

Verhaagen has used the crossflow topology theories of Peake and Tobak (30) and Hunt *et al.* (31) to interpret the smoke and surface flow patterns which he observed in his wind tunnel tests. As an example, Fig. 30(*a*), taken from ref. (12), shows the crossflow topology for a 76/40 deg. wing at an incidence of 10 deg. The vortices are represented by the nodes N, and S is a saddle point on the stream surface joining the vortices. $S'(a)$ and $S'(s)$ are half-saddle points of attachment and separation respectively. $N'(a)$ and $N'(s)$ are half-nodes of attachment and separation, but none of these are present in this particular flow pattern. The topological rules give the relationship:

$$\left(\sum N + 1/2 \sum N'\right) - \left(\sum S + 1/2 \sum S'\right) = -1$$

where

$$\sum N' = \sum N'(s) + \sum N'(a)$$

and

$$\sum S' = \sum S'(s) + \sum S'(a)$$

This relationship is satisfied for the flow pattern in Fig. 30(*a*). (Note that the effects of secondary separation from the wing upper surface and the formation of secondary vortices have been included).

The topological approach may be extended to consider what might happern as the outboard wing vortex moves closer to the wing surface, as occurs in Fig. 17(*c*). The saddle point S also moves closer to the surface. The final situation is conjectured in Fig. 30(*b*). The saddle point in the external flow has been replaced by a half-saddle point of attachment and a half-saddle point of separation. The topological equation given above is still satisfied, and the resulting flow pattern resembles that suggested by Smith (2), with a stream surface extending from the wing upper surface to the inboard strake vortex.

3.7. Visualisation of upper surface secondary flows

To clarify the structure of the secondary separations and vortices on the wing upper surface, attempts were made to visualise more details of the flow by placing a foil electrode on the surface, with the aim of injecting bubbles into the secondary vortices. These attempts were only partially successful. Glare from the surface and from the foil made observation of the bubble patterns difficult, and in addition, there was some unsteadiness in the secondary flows under some conditions. No satisfactory photographs were obtained, but examination of videotape records did allow some information to be extracted from the tests in the form of sketches based on the videotapes and direct observation of the flow.

The model chosen for these tests was the 80/40 deg. wing with a flat upper surface and a bevelled lower surface. It was felt that the flat upper surface might facilitate the observation of the secondary flow details. The foil strip was positioned along a chordwise line at approximately 15 per cent of the local semispan of the wing. The bubble patterns were illuminated in the cross-flow plane. Because of unsteadiness of the secondary flows at higher velocities, test Reynolds numbers were restricted to values below 60,000. Some typical flow patterns are shown in Figs. 31–33.

Fig. 31 shows how the secondary flow pattern is affected by Reynolds number at an incidence of 8 deg. The chordwise station is at $X/C = 0.65$. At a Reynolds number of 19,000, there appears to be no secondary separation associated with the inboard strake vortex, but secondary separation does occur outboard of the wing vortex. A secondary vortex forms intermittently. An interesting feature of his flow is the apparent correlation between the formation of the secondary vortex and the development of a slight kink in the primary bubble sheet separating from the leading-edge. The kink is there when the secondary vortex is present, but disappears when there is no secondary vortex.

At a Reynolds number of 34,000, two secondary separations occur, just outboard of the strake and wing vortices respectively, and two secondary vortices form. Fluid passing over the inboard of these two vortices reattaches. In this case, the secondary flow is reasonably steady, without the intermittent vortex formation present at the lower Reynolds number. There appears to be no interaction between the outboard secondary vortex and the primary bubble sheet from the leading-edge.

At a Reynolds number of 61,000, the flow pattern is generally similar to that at a Reynolds number of 34,000.

Fig. 32 shows how the secondary flow at a Reynolds number of 19,000 and $X/C = 0.65$ changes with angle of incidence. At an incidence of 6 deg., the primary vortex system is double branched and a single small secondary vortex forms intermittently outboard of the wing vortex. There is again a correlation between the presence of the secondary vortex and the formation of a kink in the primary bubble sheet. At an incidence of 8 deg., the flow pattern is generally similar, except that the primary wing vortex lies further inboard, and the secondary vortex, when it forms, is larger. The intermittent kink in the primary bubble sheet is also present.

For angles of incidence of 10, 12, and 15 deg., the same general flow pattern is maintained. A single secondary separation occurs outboard of the wing vortex, and a secondary vortex occurs intermittently. At these higher angles of incidence, however, no kink formation in the primary bubble sheet was observed.

Fig. 33 shows how the secondary flow develops with downstream distance at a Reynolds number of 19,000 and an incidence of 20 deg. At X/C 0.5, the vortex system cross-section is typical of that over a single delta wing. The flow separating along the leading-edge rolls up into a primary vortex, the lateral position of which is at about 60 per cent semispan. At about 70 per cent semispan, the upper surface boundary layer, in which fluid is moving outboard and aft, separates and rolls up into a secondary vortex. The secondary vortex is opposite in sense to the primary vortex, and is located at about 90 per cent semispan. Outboard of the secondary vortex, the flow may reattach, but the scale of the model was too small to allow such details to be distinguished.

At X/C 0.503, just downstream of the leading-edge kink, a small double branched wing vortex has appeared in the primary strake vortex sheet. The wing vortex is located about at 94 per cent semispan, outboard of the secondary vortex which now lies at about 85 per cent semispan. The wing vortex and the secondary vortex lie roughly the same distance above the wing upper surface.

At $X/C = 0.513$, the pattern is similar to that at $X/C = 0.506$, (except that the wing vortex has moved inboard slightly to about 90 per cent semispan) and is further from the wing upper surface. The secondary vortex is now at about 80 per cent semispan.

At $X/C = 0.525$, the wing vortex has moved still further inboard and upwards. The structure of the secondary separated flow is now less obvious. Although a secondary vortex does form, it does so only intermittently. The bubble sheet separating from the wing upper surface alternates between rolling up into a secondary vortex and being entrained into the wing vortex.

At $X/C = 0.538$, the secondary separated bubble sheet is carried directly into the wing vortex, which has continued to move inboard and upwards. The behaviour of the flow in the roughly triangular region between the primary bubble sheet, the secondary bubble sheet, and the wing surface could not be distinguished. Bubble movemment in this region appeared to be random.

Similar flow patterns occur at $X/C = 0.55$, 0.575, and 0.6, with the wing vortex moving inboard and upwards as X/C increases.

4. CONCLUSIONS

The formation and interaction of vortices above a family of double-delta wings were studied using flow visualisation techniques in a small towing tank. In general, the flow pattern found consisted of a pair of vortices above each wing half. One vortex originated at the apex of the wings and the other vortex originated at the leading-edge kink. Under certain conditions, the vortices interacted above the wing.

The location of the zone on interaction between the two vortices is a function of angle of incidence and leading-edge kink angle. Generally, the interaction moves downstream with increasing kink angle and decreasing incidence. For small kink angles (less than 10 deg.) and angles of incidence, only a single vortice system appears to form above each wing half.

Over the Reynolds range (7,000-100,000) of the tests, changes in Reynolds number were found to have a significant effect on the vortex system above the double-delta wings. At the lower end of the Reynolds number range, only a single vortex is present above each wing half. At a Reynolds number of approximately 9,000, a double vortex system appears. The effect of increasing Reynolds number generally is to cause the zone of interaction between the vortices to move downstream. Comparison with limited available wind tunnel data indicates that this trend continues to higher Reynolds numbers.

Comparative tests on a single delta model also indicated significant Reynolds number effects, with the vortex system moving outboard with increasing Reynolds number.

Leading-edge cross-section shape was also found to affect the vortex system structure. In particular, on models with an upper surface edge bevel, the vortex interaction zone occurred further downstream than was the case with other edge shapes, and the vortices were closer to the wing upper surfaces.

Attempts to visualise details or the upper surface secondary vortices were only partially successful. However, the patterns observed showed that the secondary vortex structure was dependent on Reynolds number, and was also unsteady under some conditions.

REFERENCES

1. Hoeijmakers, H. W. M. — Numerical computation of vortical flow about wings. NLR MP 83073U (Dec. 1983).

2. Smith, J. H. B. — Theoretical modelling of three-dimensional vortex flows in aerodynamics. Aeronautical J., 88, 874, pp 101–116 (Apr. 1984)

3. Hitzel, F. M., Schmidt, W. — Slender wings with leading-edge vortex separation: a challenge for panel methods and Euler solvers. J. of Aircraft, 21, 10, pp 751–759 (Oct. 1984).

4. Hoeijmakers, H. W. M., Rizzi, A. — Vortex-fitted potential solution compared with vortex-captured Euler solution for delta wing leading-edge vortex separation. AIAA 2nd Applied Aerodynamics Conf., Seattle, wash., 21–23 Aug. 1984. Paper AIAA-84-2144.

5. Chaturvedi, S., Ghaffari, F. — Investigation of aerodynamic characteristics of wings having vortex flow using different numerical codes. NASA CR-173596 (Apr. 1984)

6. Reddy, C. S., Goglia, G. L. — Investigation of aerodynamic characteristics of wings having vortex flow using different numerical codes. NASA CR-165706 (Apr. 1981)

7. Peace, A. J. — A multi-vortex model of leading-edge vortex flows. Intl. J. for Numerical Methods in Fluids, 3, pp. 543–565 (1983)

8. Yın Xieyuan — Roll-up or strake leading/trailing-edge vortex sheets for double-delta wings. J. of Aircraft, 22, 1, pp. 87–89 (Jan. 1985).

9. Maskell, E. C. — Some recent developments in the study of edge vortices. 3rd ICAS Congress, proceedings, pp. 737–749, Paper 33 (1962)

10. Ericksion, G. E. — Vortex flow correlation. AFWAL-TR-80-3143 (Jan. 1981).

11. Wortman, A. — On Reynolds number effects in vortex flow over aircraft wings. AIAA 22nd Aerospace Sci. Mtg., Reno, Nevada, 9–12 Jan. 1984. Paper AIAA-84-0137.

12. Verhaagen, N. G. — An experimental investigation of the vortex flow over delta and double-delta wings at low speed. Delft U. of Tech., Dept. of Aerospace Eng., Report LR-372 (Sep. 1983).

13. Brennenstuhl, U., Hummel, D.
On the vortex formation over wings with kinked leading-edges.
Z. Flugwiss. Weltraumforsch., 5, Heft 6, pp. 375–381 (1981).

14. Brennenstuhl, U., Hummel, D.
Further investigations on the vortex formation over wings with kinked leading-edges.
Z. Flugwiss. Weltraumforsch., 6, Heft 4, pp. 239–247 (1982).

15. Brennenstuhl, U., Hummel, D.
Vortex formation over double-delta wings. 13th ICAS Congress, Seattle, Wash., 22–28.
Aug., 1982. Paper ICAS–82–6.6.3.

16. Nathman, J. K., Norton, D. J., Rao, B. M.
An experimental investigation of incompressible flow over delta and double-delta wings.
ONR–CR–215–213–3 (Dec. 1976).

17. Wentz, W. H., McMahon, M. C.
An experimental investigation of the flow fields about delta wings at low speeds.
NASA CR–521 (Aug. 1966).

18. Wentz, W. H., McMahon, M. C.
Further experimental investigations of delta and double-delta wing flow fields at low speeds.
NASA CR–714 (Feb. 1967).

19. Butterworth, P. J.
Flow measurements in the wake of a wing fitted with a leading-edge root extension (strake).
RAE TR 79120 (Sep. 1979).

20. Liu, M. J., *et al.*
Flow patterns and aerodynamic characteristics of a wing-strake configuration.
J. of Aircraft, 17, 5, pp. 332–338 (May 1980).

21. Luckring, J. M.
Aerodynamics of strake-wing interactions.
J. of Aircraft, 16, 11, pp. 756–762 (Nov. 1979).

22. Lamar, J. E.
Analysis and design of strake-wing configurations.
J. of Aircraft, 17, 1, pp. 20–27 (Jan. 1980).

23. Frink, N. T., Lamar, J. E.
Analyses of strake vortex breakdown characteristics in relation to design features.
J. of Aircraft, 18, 4, pp. 252–258 (Apr. 1981).

24. Thompson. D. H.
Flow visualisation using the hydrogen bubble technique.
ARL Aero. Note 338 (Feb. 1973).

25. Elle, B. J.
An investigation at low speed of the flow near the apex of thin delta wings with sharp leading-edges.
ARC REM 3176 (1961).

26. Gad-el-Hak, M. Blackwelder, R. F.
The discrete vortices from a delta wing.
J. of Aircraft, 23, 6, pp. 961–962 (June 1985).

27. Hummel, D., Redeker, G.
Experimental determination of bound vortex lines and flow in the envioronment of the trailing-edge of a slender delta wing.
Braunschweigische Wissenshaftliche Gesellschaft Abhandlungen, pp. 273–290 (1972).
Available as NASA Tech. Translation TT-F-15012 (Aug. 1973).

28. Smith, J. H. B.
How the state of the boundary layer may affect the flow over slender wings.
RAE TM 1157 (Jul. 1969).

29. Fiddes, F. P., Smith, J. H. B.
Strake-induced separation at moderately swept leading-edges.
RAE TR 77128 (Aug. 1977).

30. Peake, D. J., Tobak. M.
Three dimensional interactions and vortical flows with emphasis on high speeds.
AGARDograph No. 252 (1980).

31. Hunt, J. C. R., Abell, C. J., Peterka, J. A., Woo, H.
Kinematical studies of the flows around free or surface-mounted obstacles: applying topology to flow visualisation.
J. Fluid Mechs., 86, pt. 1, pp. 179–200 (1978).

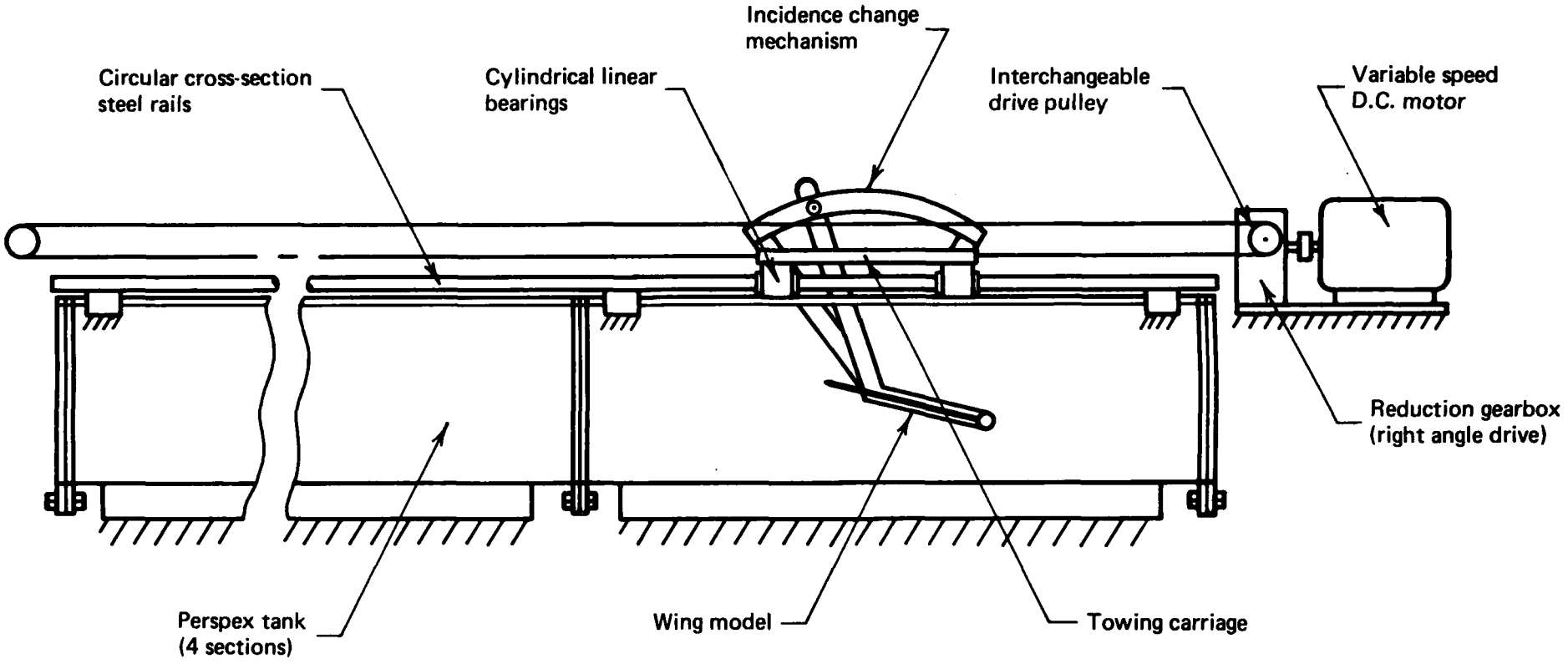

FIG. 1 SCHEMATIC LAYOUT OF TOWING TANK AND CARRIAGE.

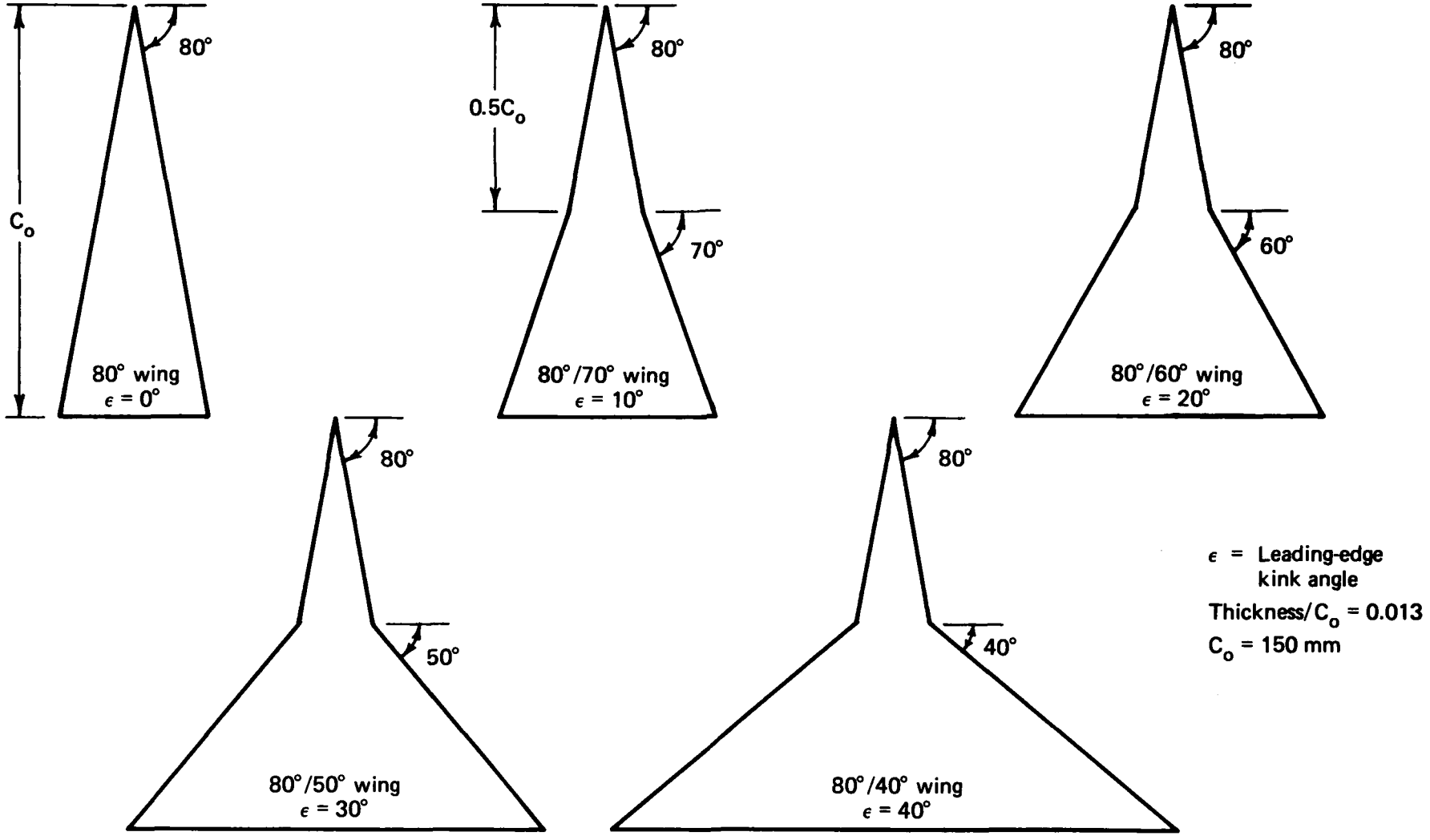

FIG. 2 PLANFORMS OF TEST MODELS.

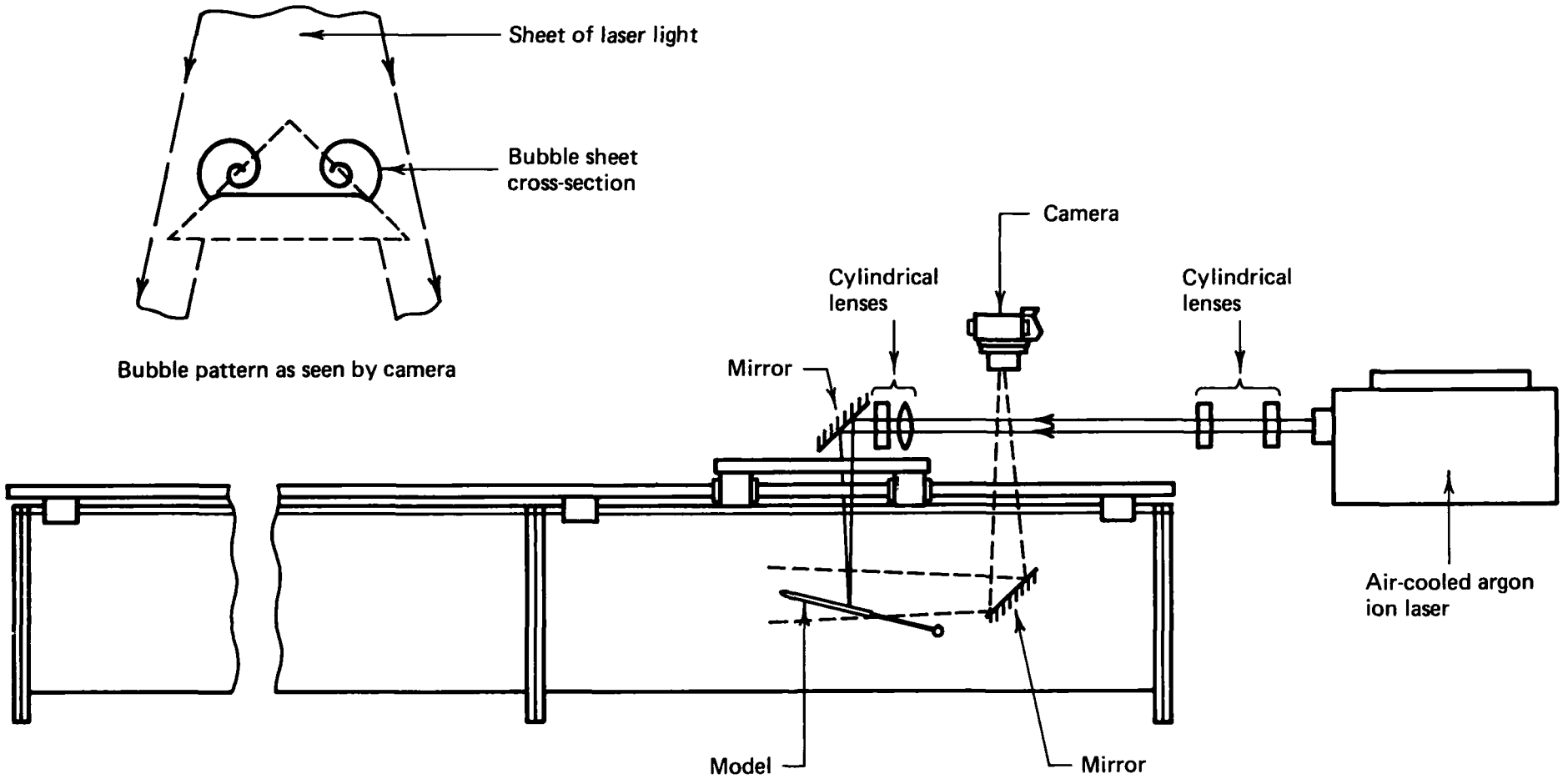

FIG. 3 LIGHTING SET-UP FOR VISUALISATION OF VORTEX CROSS-SECTIONS.

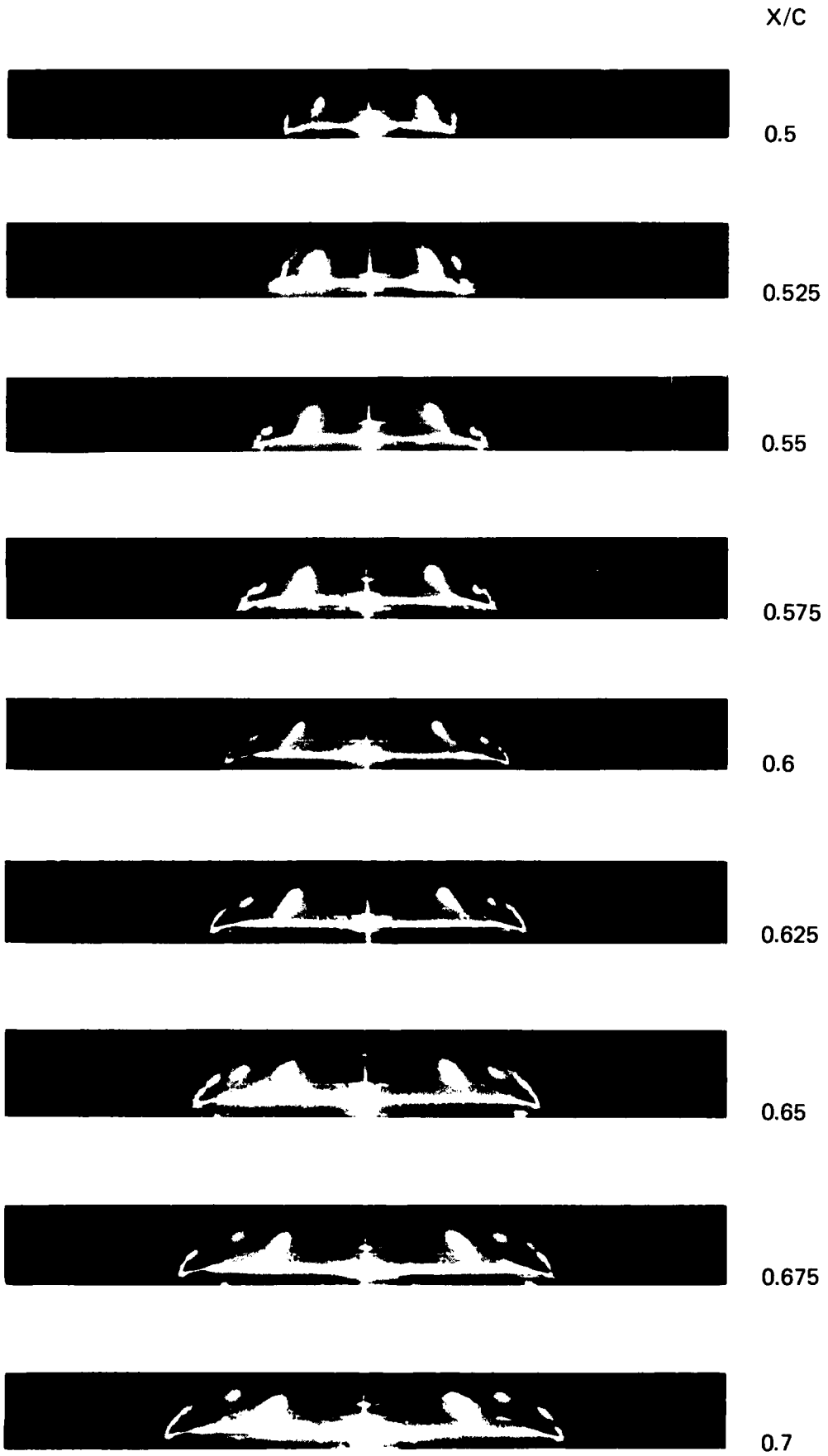

FIG. 4 VORTEX CROSS-SECTIONS OVER 80°/60° WING.
INCIDENCE = 15°. REYNOLDS NO. = 1.03×10^5.

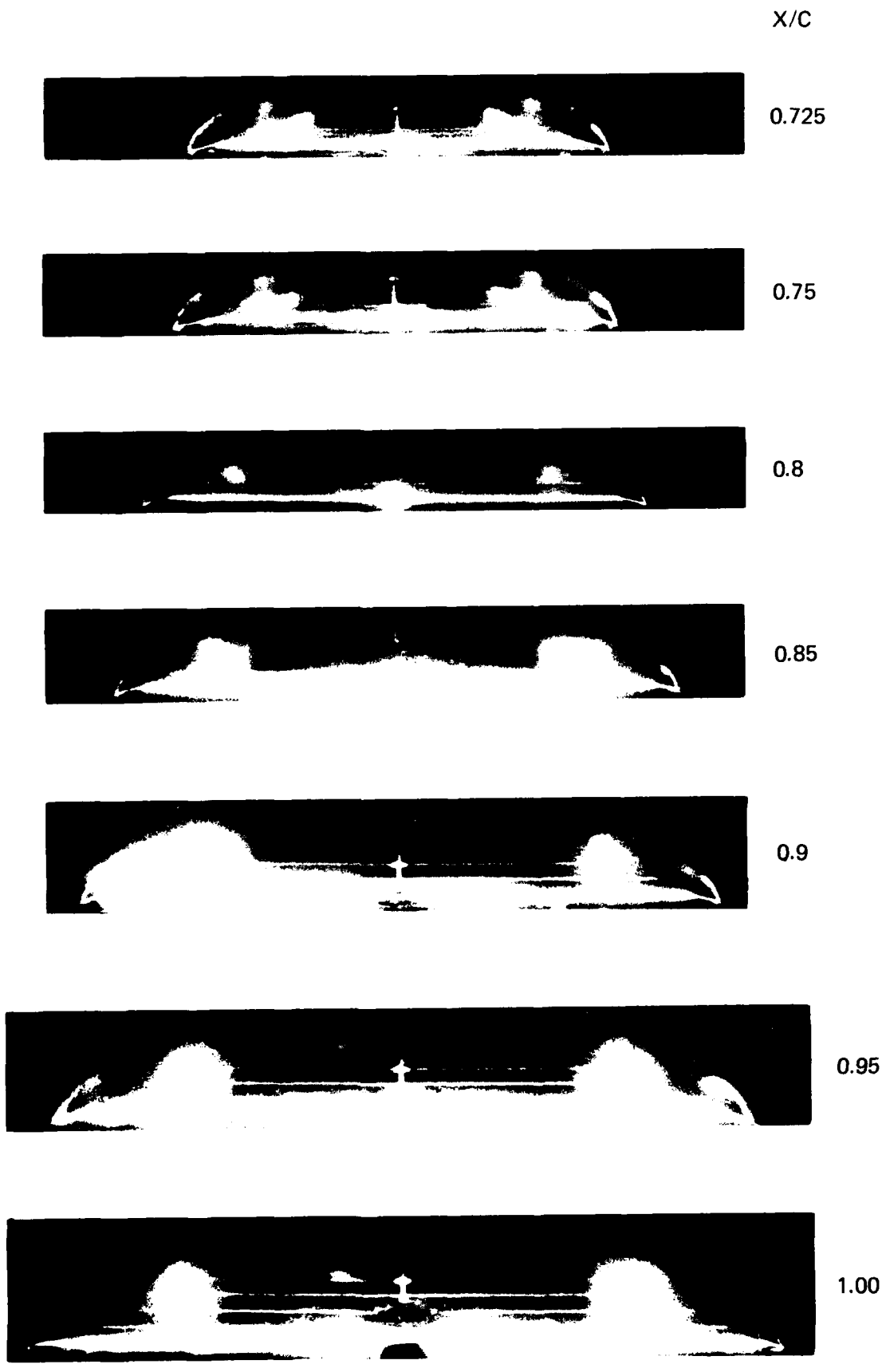

FIG. 4 (contd) VORTEX FLOW OVER 80°/60° WING.
INCIDENCE = 15°. REYNOLDS NO. = 1.03×10^5.

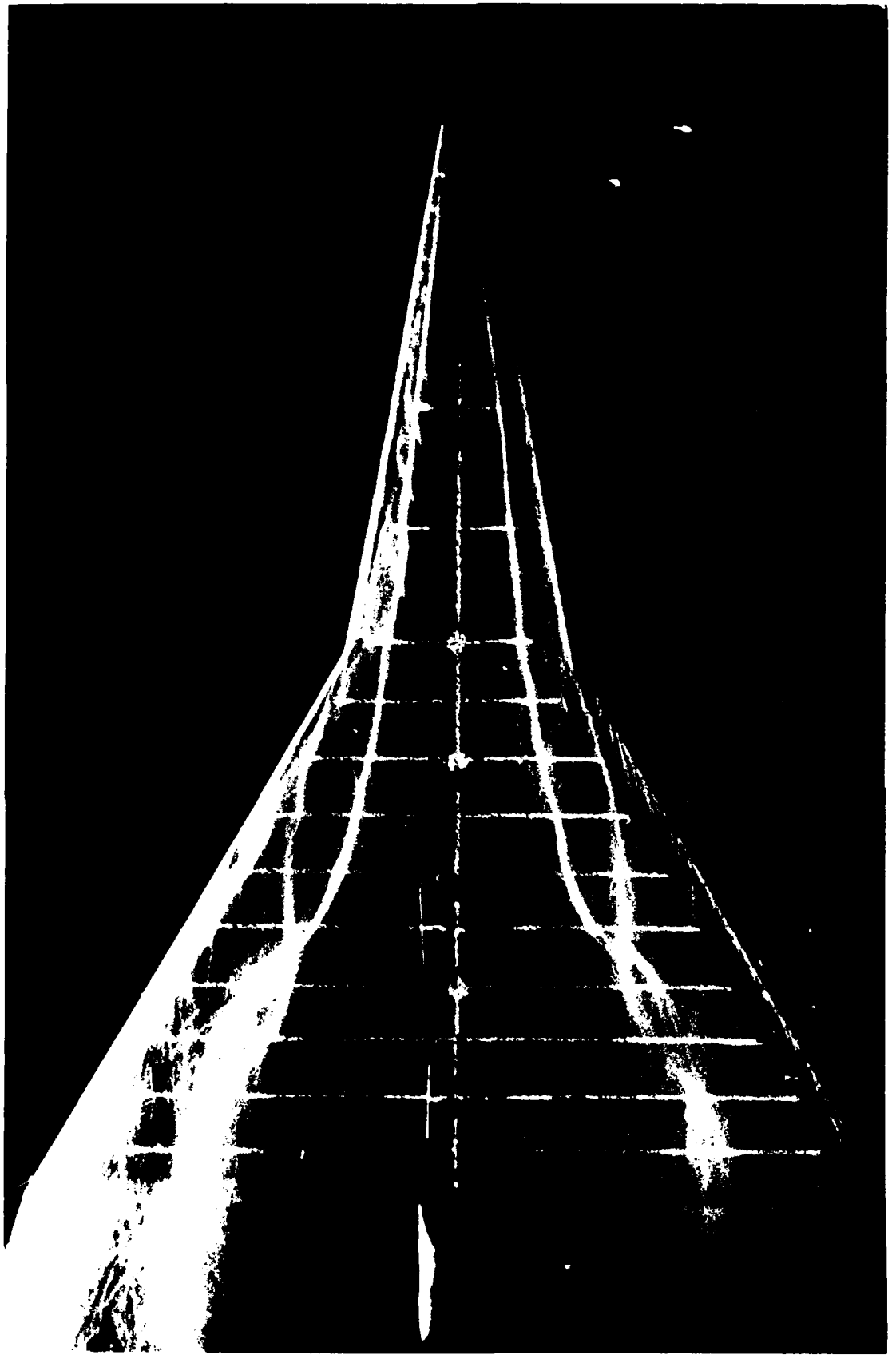

FIG. 5 VORTEX FLOW OVER 80°/60° WING;
$\alpha = 15°$; $R = 1X10^5$.

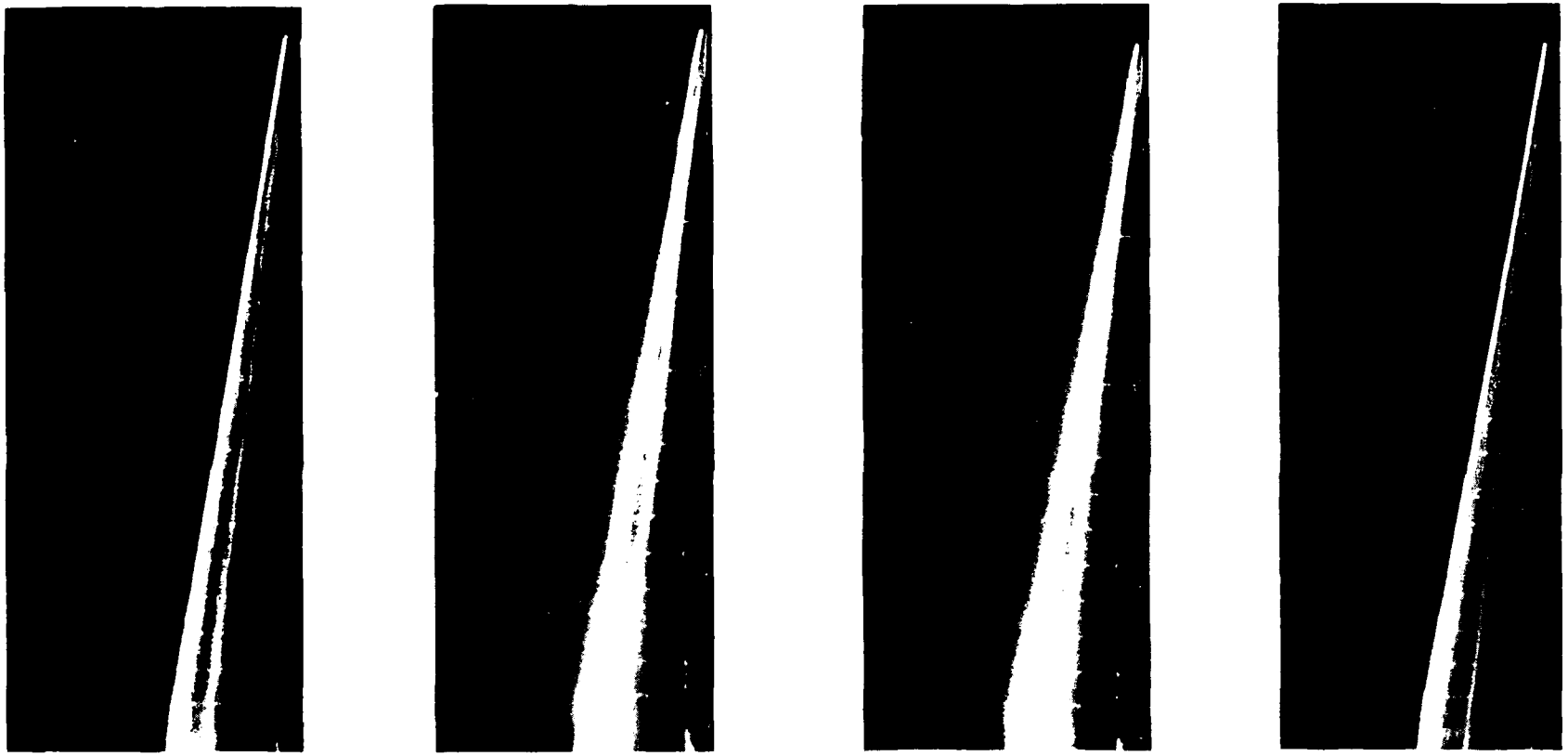

α = 6° α = 8° α = 10° α = 12°

FIG. 6 EFFECT OF INCIDENCE ON VORTEX POSITIONS.
80° WING; REYNOLDS NO. = $1X10^5$.

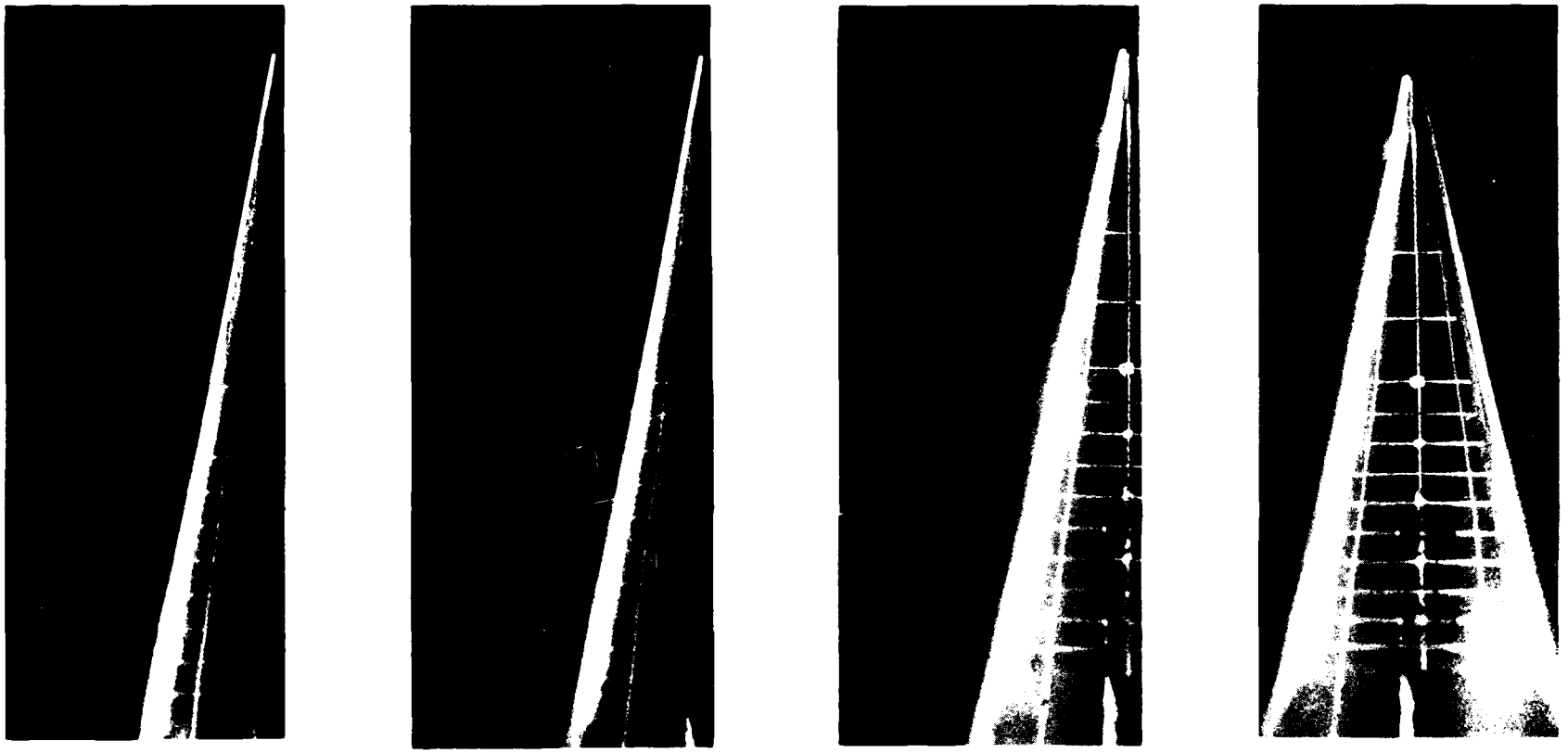

α = 15° α = 20° α = 25° α = 30°

FIG. 6 (contd) EFFECT OF INCIDENCE ON VORTEX POSITIONS.
80° WING; REYNOLDS NO. = $1X10^5$.

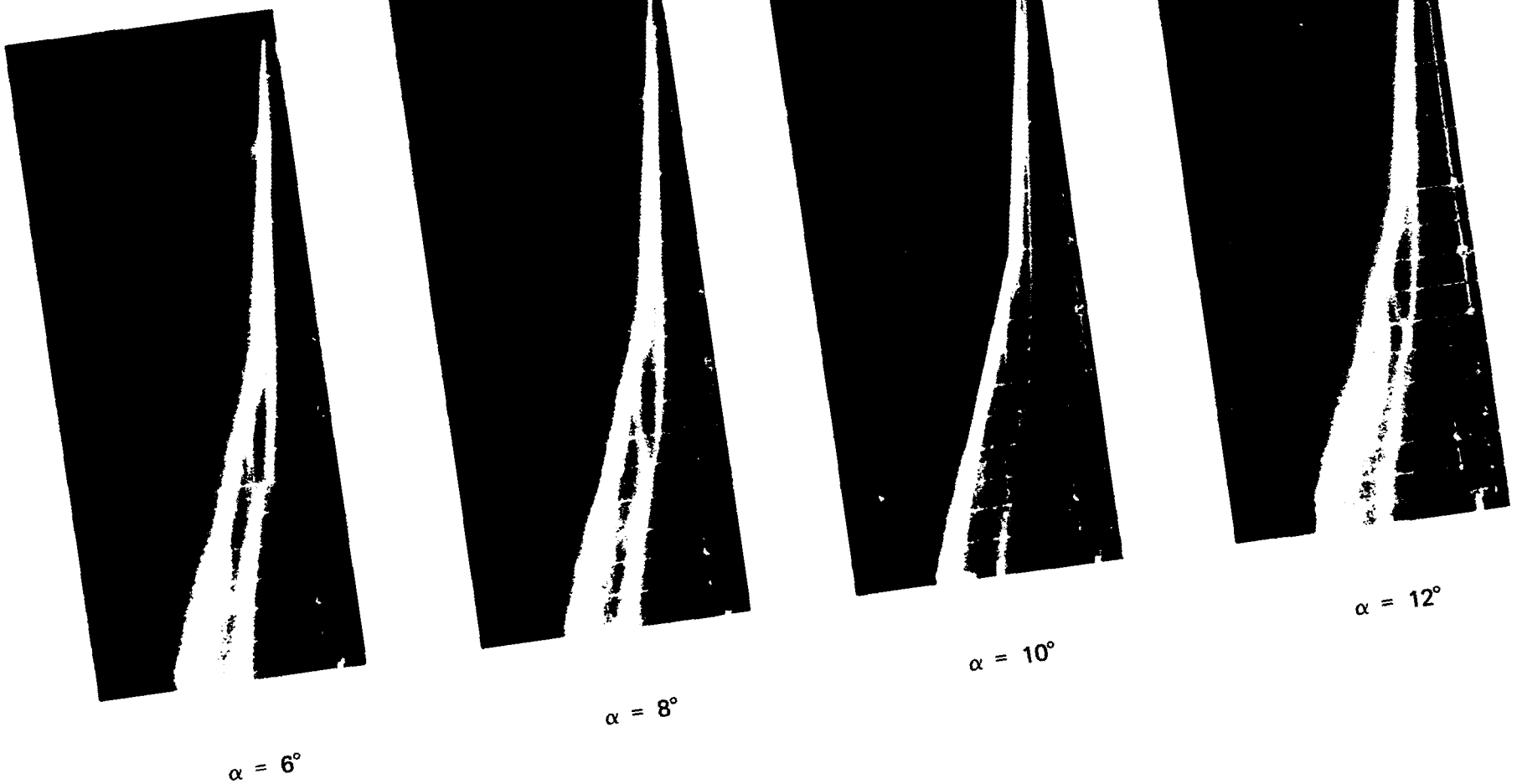

FIG. 7 EFFECT OF INCIDENCE ON VORTEX POSITIONS. 80°/70° WING; REYNOLDS NO. = $1X10^5$.

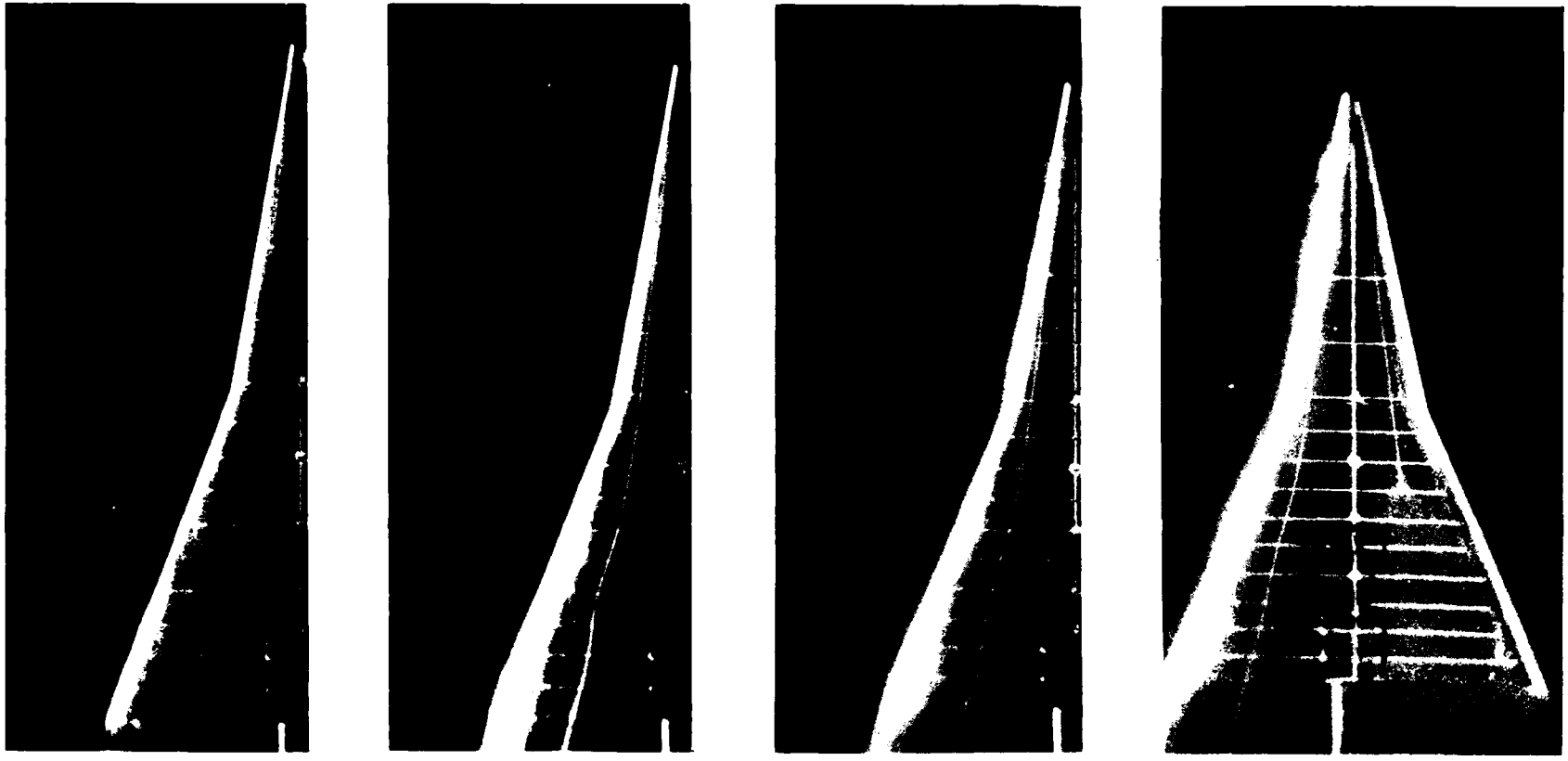

α = 15° α = 20° α = 25° α = 30°

FIG. 7 (contd) EFFECT OF INCIDENCE ON VORTEX POSITIONS.
80°/70° WING; REYNOLDS NO. = $1X10^5$.

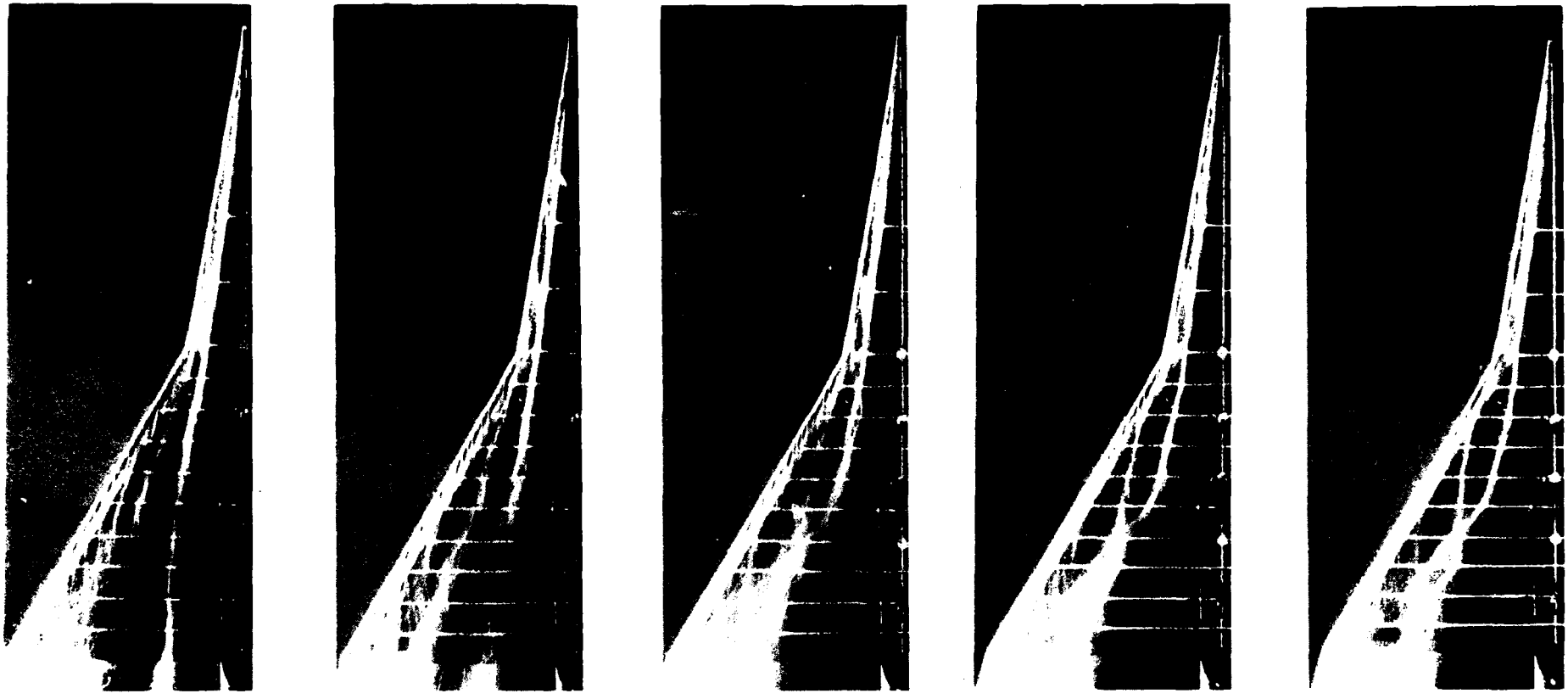

α = 6° α = 8° α = 10° α = 12° α = 15°

FIG. 8 EFFECT OF INCIDENCE ON VORTEX POSITIONS.
80°/60° WING; REYNOLDS NO. = $1X10^5$.

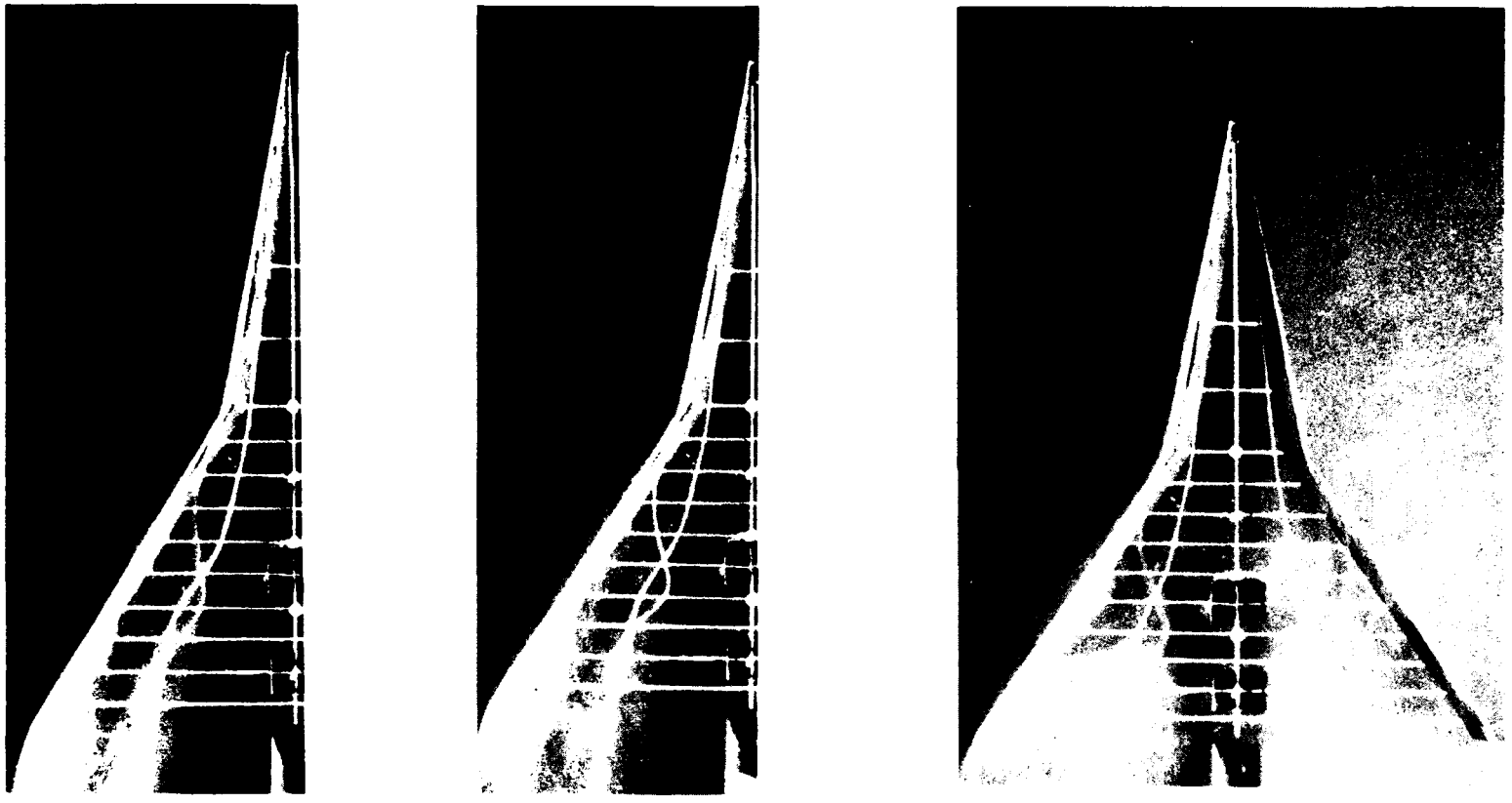

α = 20° α = 25° α = 30°

FIG. 8 (contd) EFFECT OF INCIDENCE ON VORTEX POSITIONS.
80°/60° WING; REYNOLDS NO. = $1X10^5$.

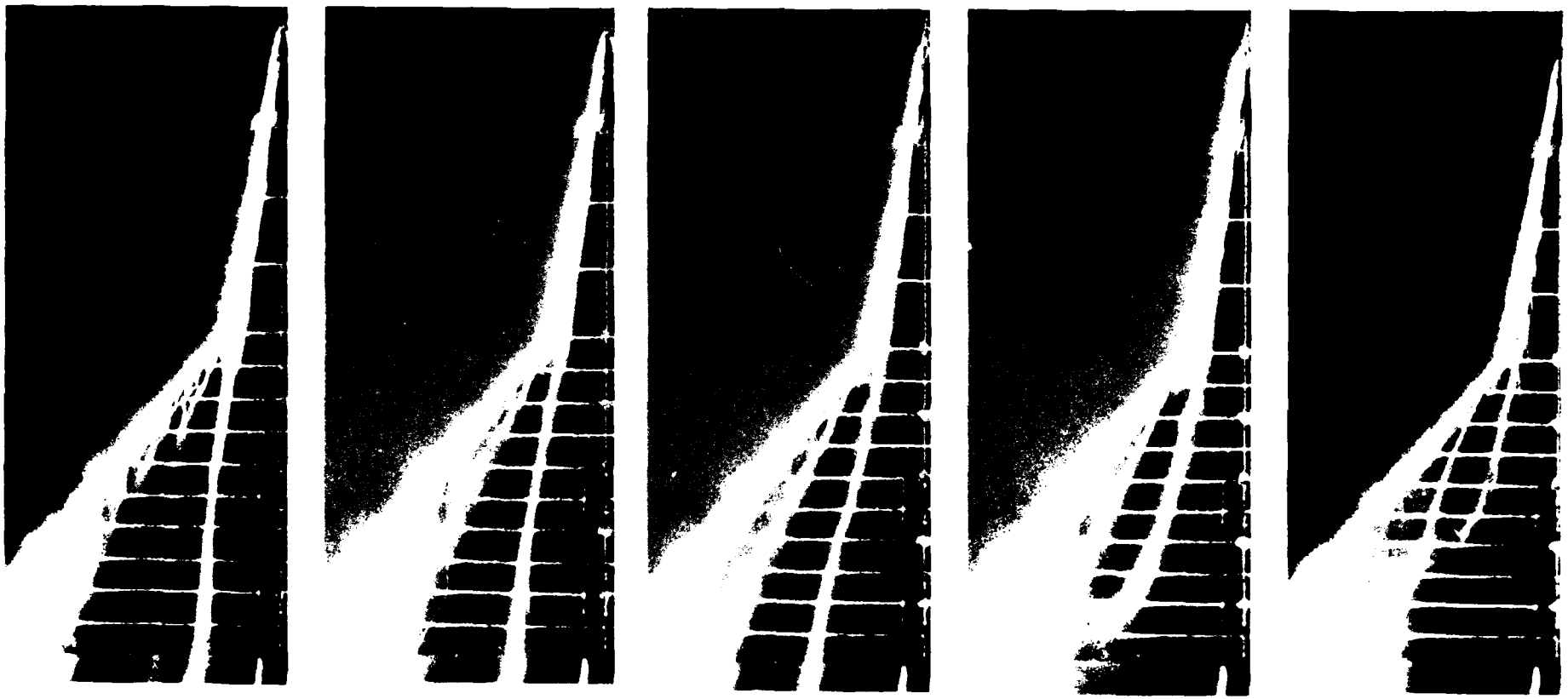

α = 6° α = 8° α = 10° α = 12° α = 15°

FIG. 9 EFFECT OF INCIDENCE ON VORTEX POSITIONS.
80°/50° WING; REYNOLDS NUMBER = $1X10^5$.

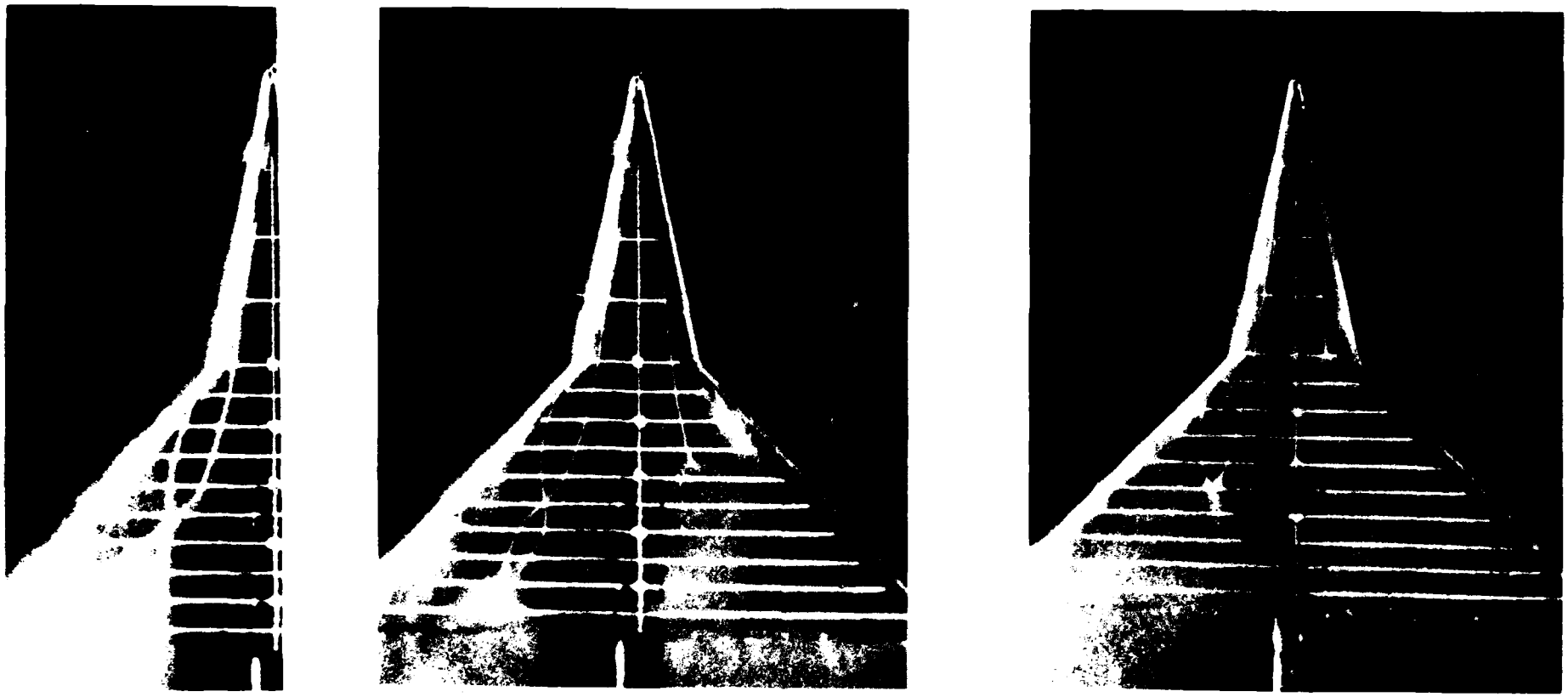

α = 20°

α = 25°

α = 30°

FIG. 9 (contd) EFFECT OF INCIDENCE ON VORTEX POSITIONS.
80°/50° WING; REYNOLDS NO. = $1X10^5$.

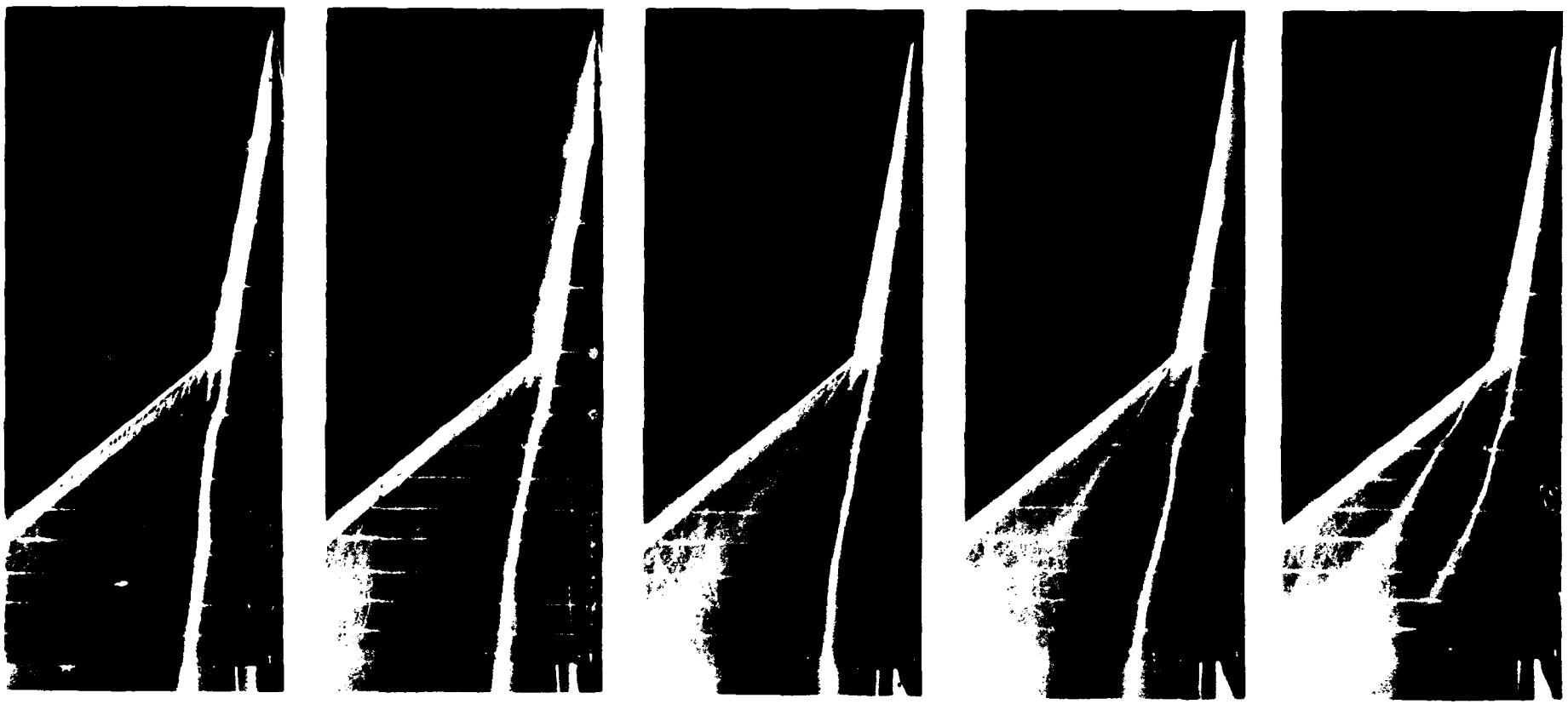

α = 6° α = 8° α = 10° α = 12° α = 15°

FIG. 10 EFFECT OF INCIDENCE ON VORTEX POSITIONS.
80°/40° WING; REYNOLDS NO. = $1X10^5$.

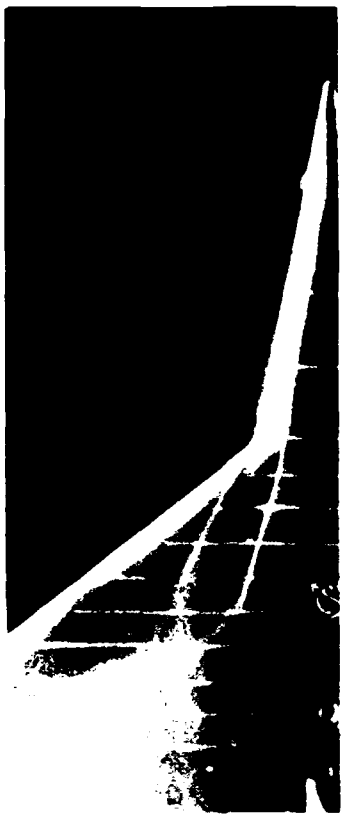

α = 20°

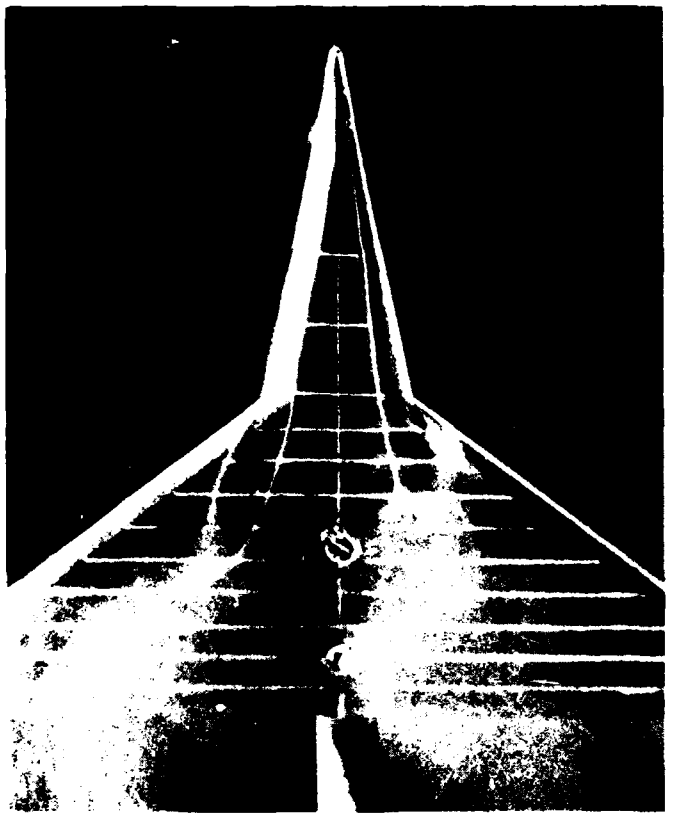

α = 25°

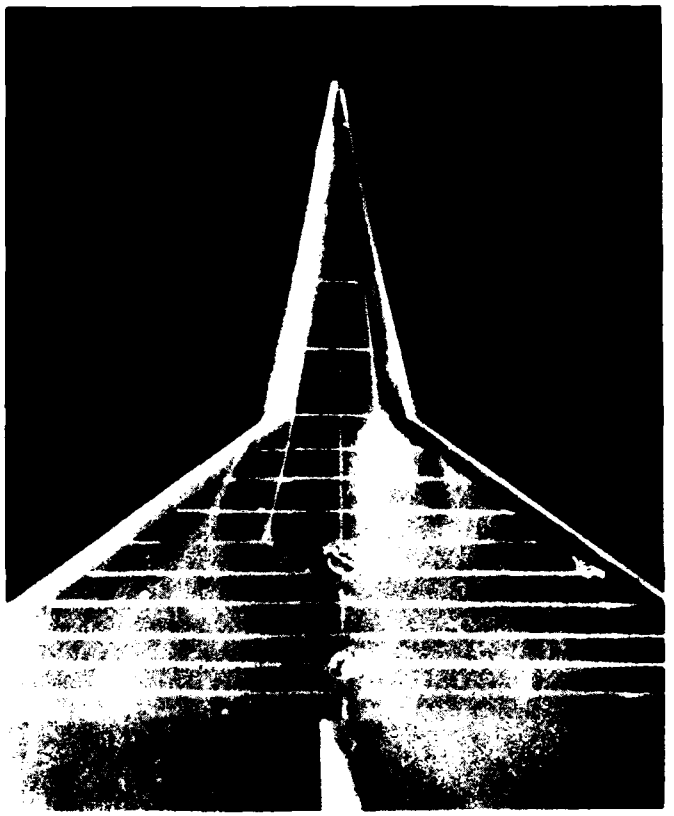

α = 30°

FIG. 10 (contd) EFFECT OF INCIDENCE ON VORTEX POSITIONS.
80°/40° WING; REYNOLDS NO. = $1X10^5$.

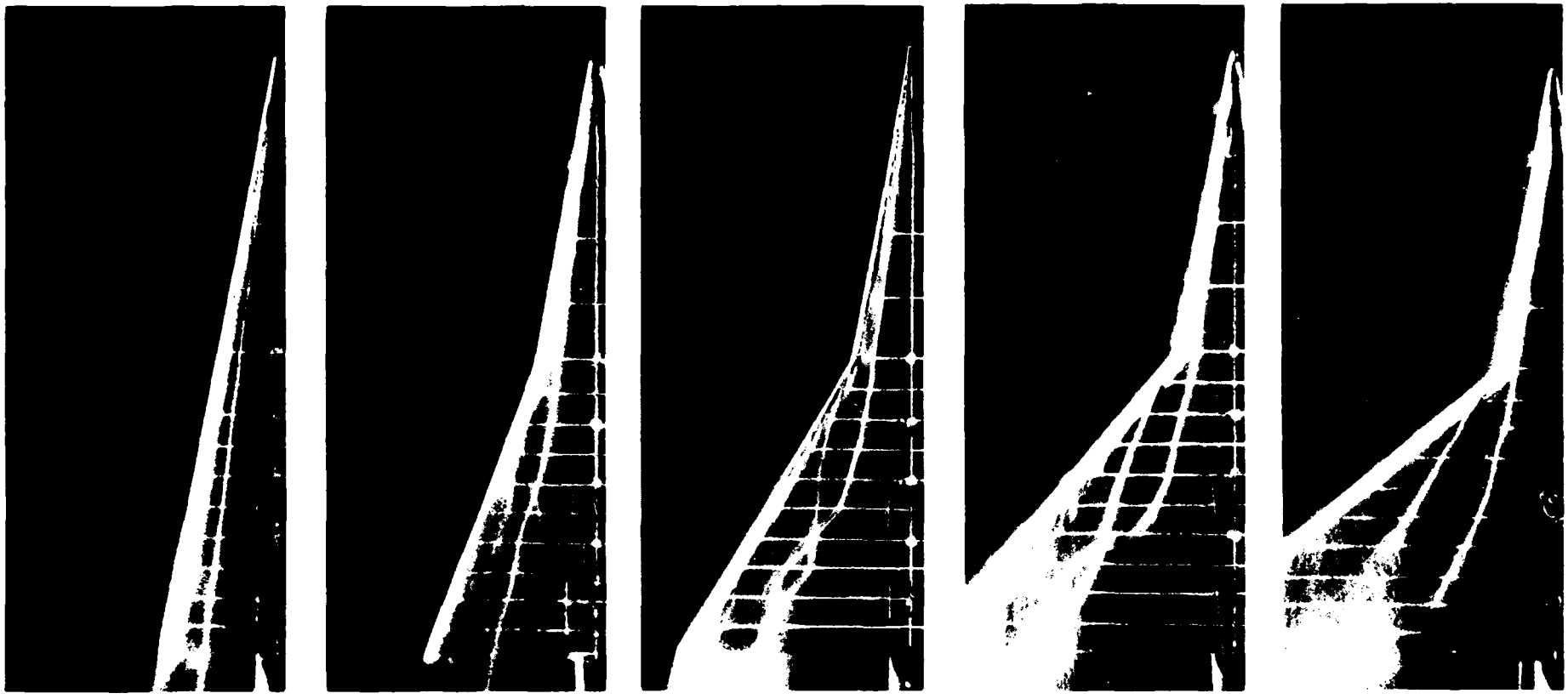

ϵ = 0° ϵ = 10° ϵ = 20° ϵ = 30° ϵ = 40°

FIG. 11 EFFECT OF LEADING EDGE KINK ANGLE, ϵ, ON VORTEX STRUCTURE; $\alpha = 15°$; $R = 1.0X10^5$.

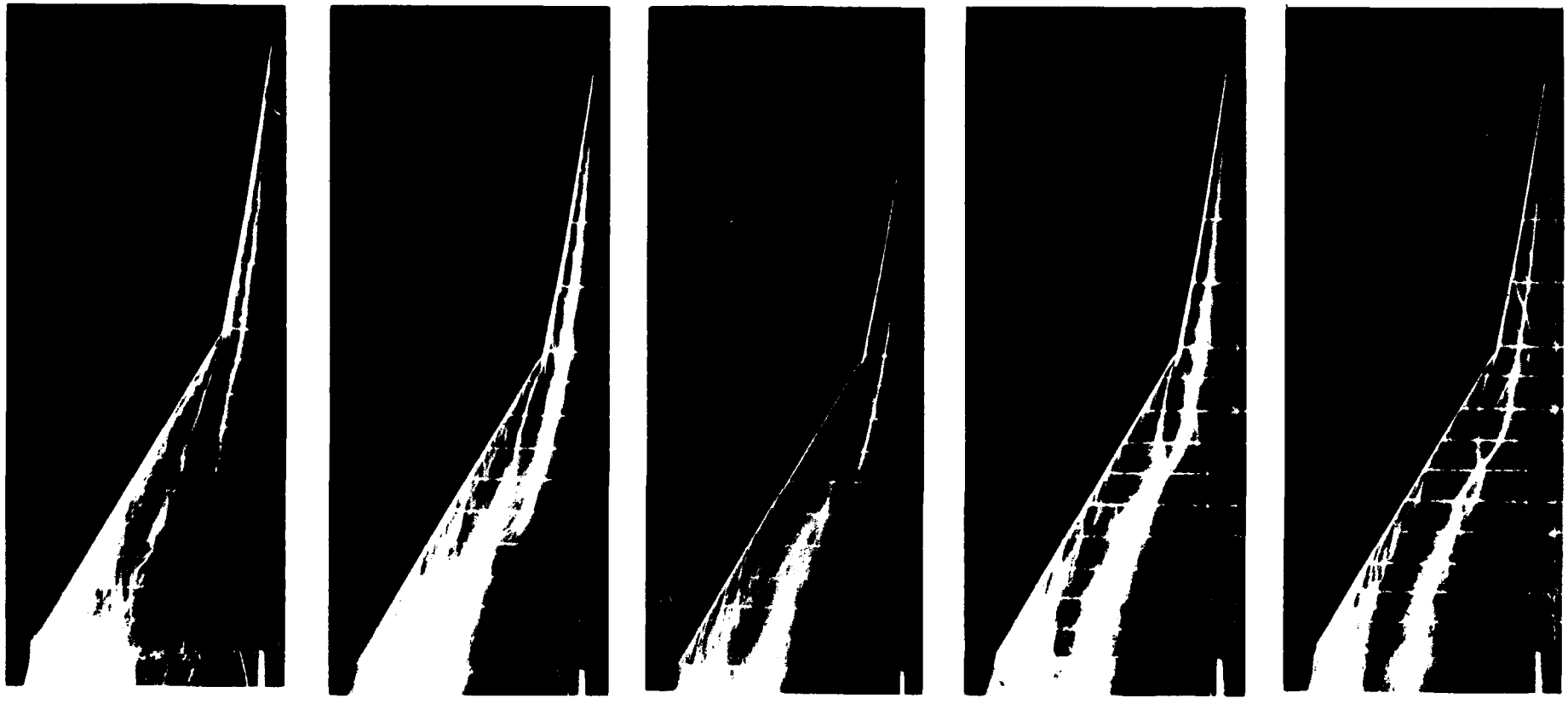

α = 6° α = 8° α = 10° α = 12° α = 15°

FIG. 12 EFFECT OF INCIDENCE ON VORTEX POSITIONS.
80°/60° WING; FLAT UPPER SURFACE; R = $1X10^5$.

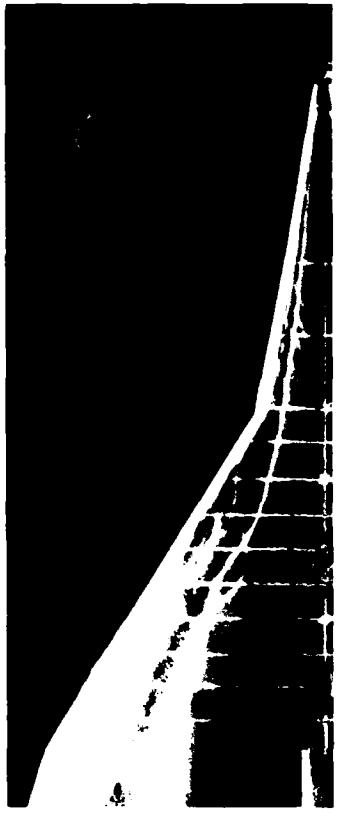

α = 20°

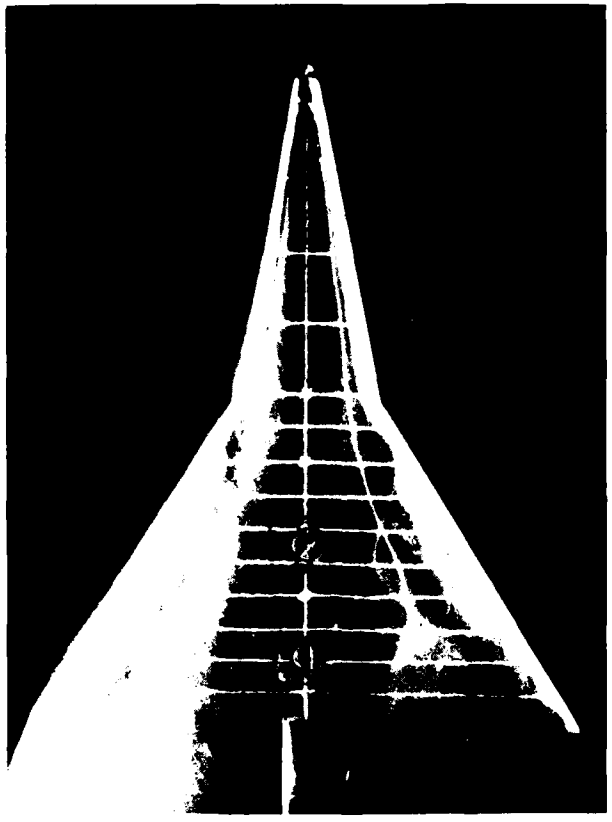

α = 25°

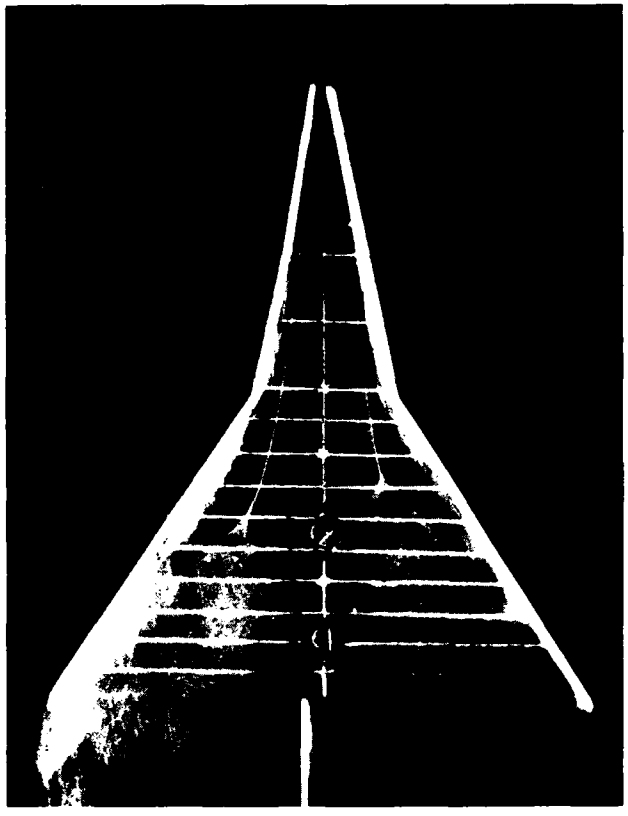

α = 30°

FIG. 12 (contd) EFFECT OF INCIDENCE ON VORTEX POSITIONS.
80°/60° WING; FLAT UPPER SURFACE; R = $1X10^5$.

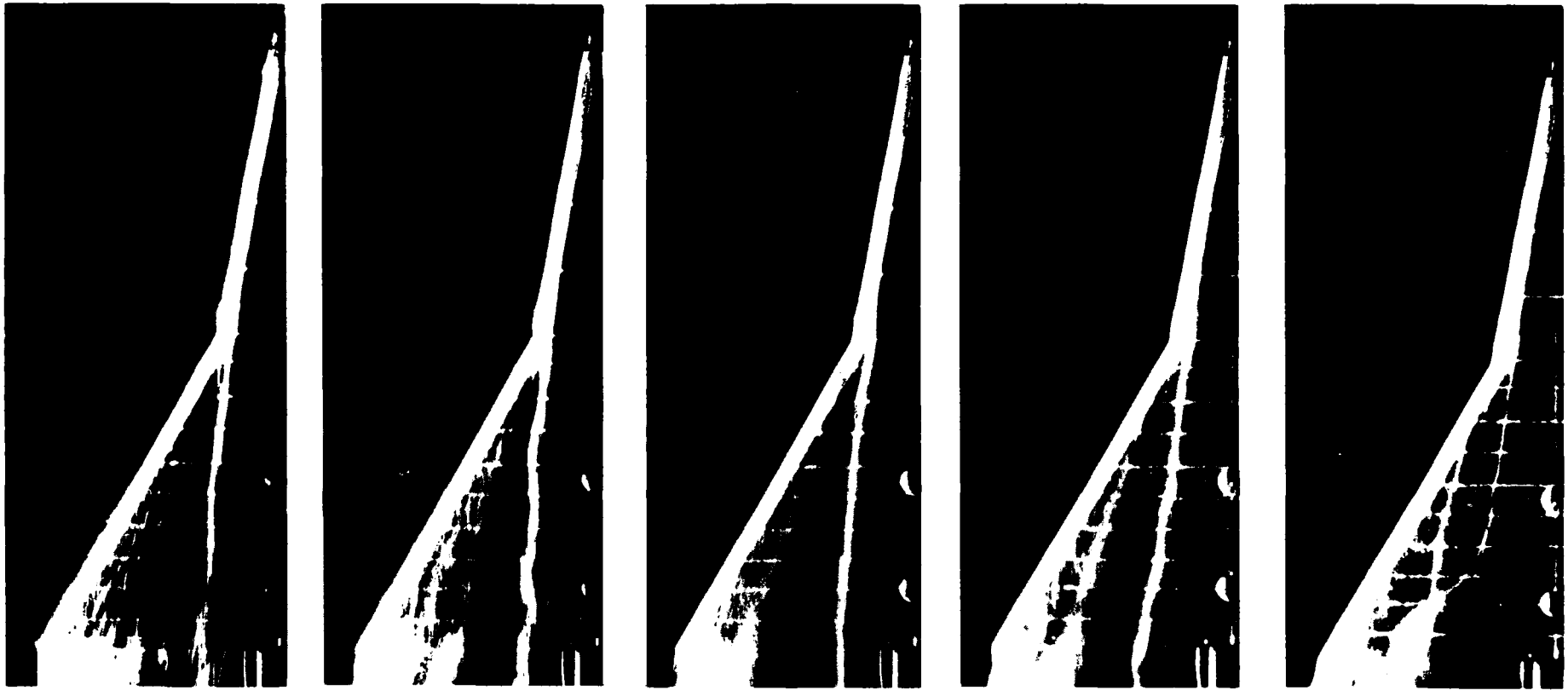

α = 6° α = 8° α = 10° α = 12° α = 15°

FIG. 13 EFFECT OF INCIDENCE ON VORTEX POSITIONS.
80°/60° WING; FLAT LOWER SURFACE; R = $1X10^5$.

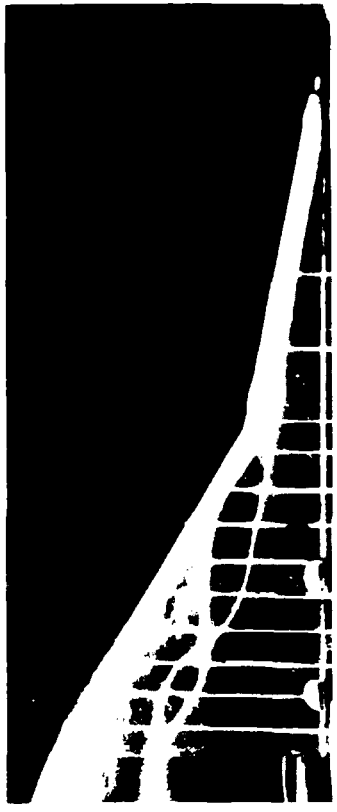

α = 20°

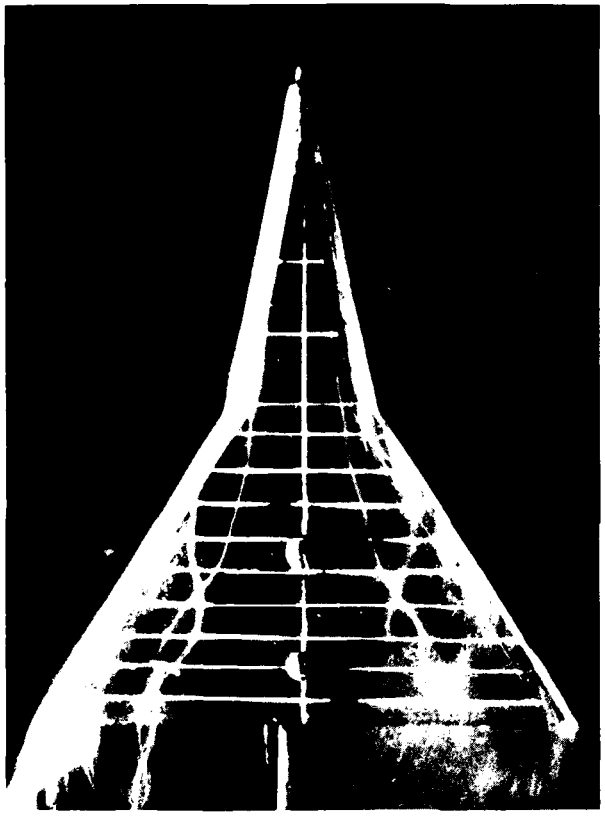

α = 25°

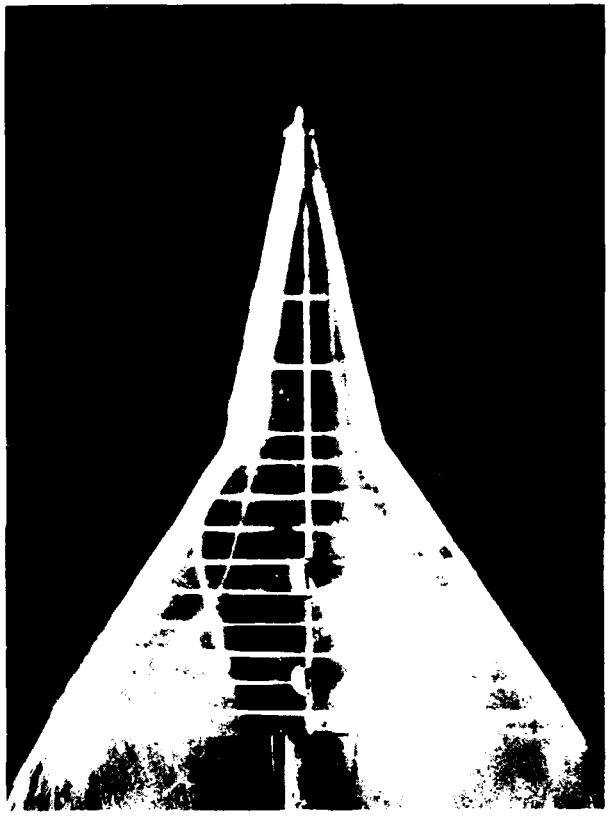

α = 30°

FIG. 13 (contd) EFFECT OF INCIDENCE ON VORTEX POSITIONS.
80°/60° WING; FLAT LOWER SURFACE; R = $1X10^5$.

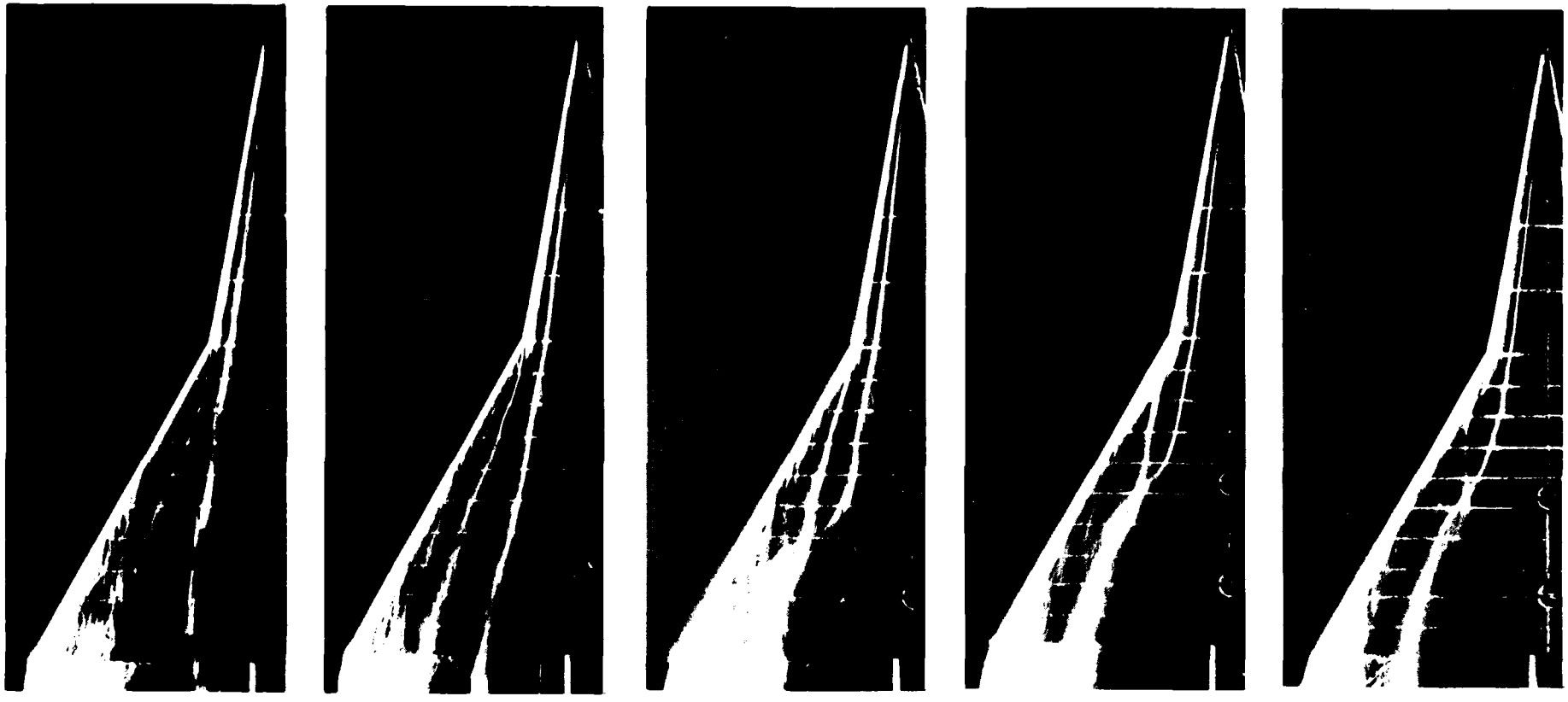

α = 6° α = 8° α = 10° α = 12° α = 15°

FIG. 14 EFFECT OF INCIDENCE ON VORTEX POSITIONS.
80°/60° WING; ROUNDED LEADING EDGE; R = $1X10^5$.

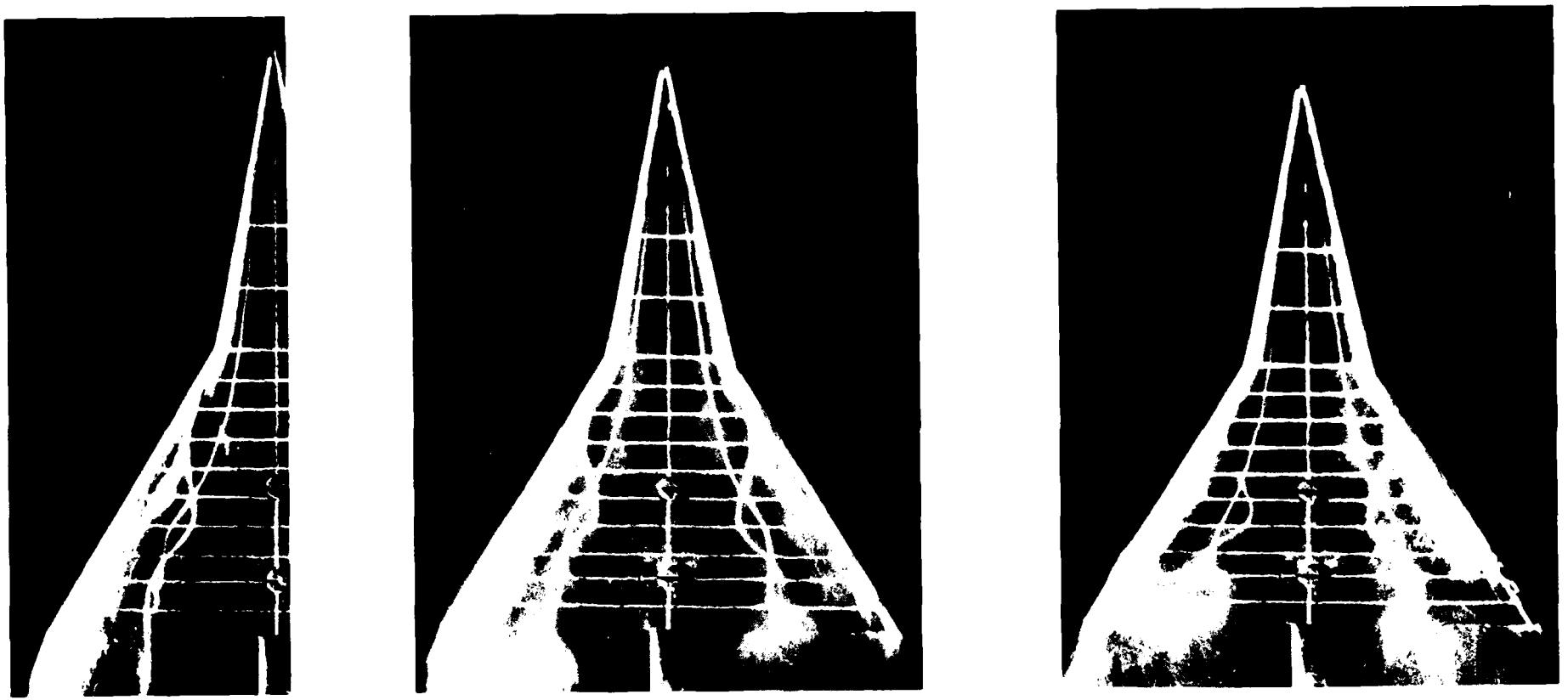

α = 20° α = 25° α = 30°

FIG. 14 (contd) EFFECT OF INCIDENCE ON VORTEX POSITIONS.
80°/60° WING; ROUNDED LEADING EDGE; R = $1X10^5$.

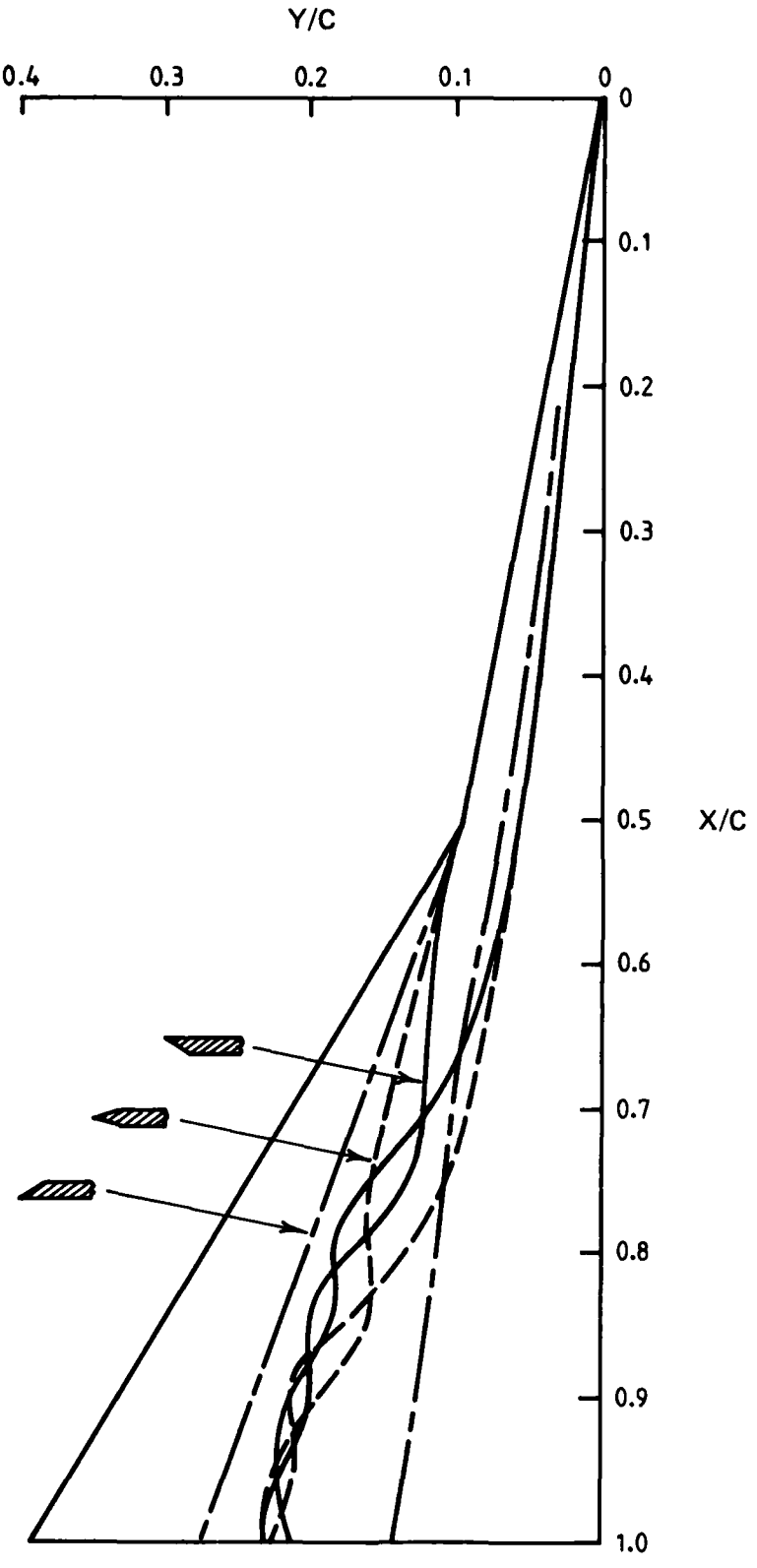

FIG. 15 EFFECT OF WING CROSS-SECTION SHAPE ON VORTEX POSITIONS.
80°/60° WING; $\alpha = 12°$; REYNOLDS NUMBER = $1X10^5$.

(a) Lower surface bevel

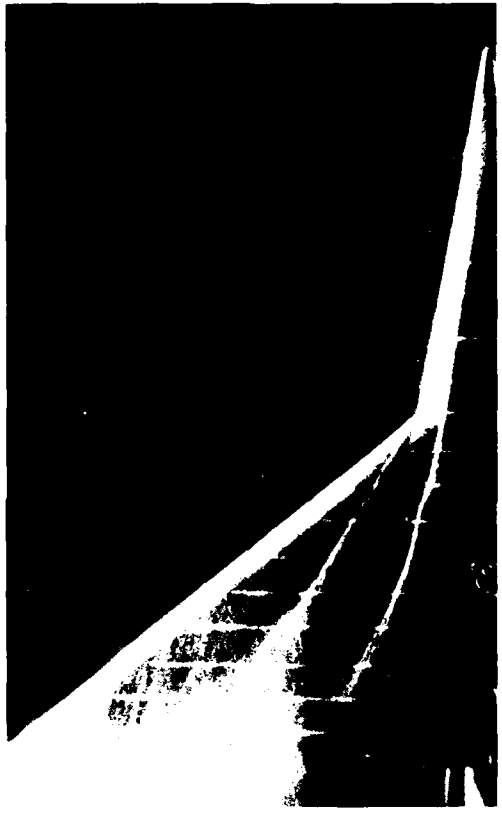

(b) Symmetrical bevel

(c) Upper surface bevel

FIG. 16 EFFECT OF LEADING EDGE SHAPE ON VORTEX STRUCTURE.
80°/40° WING; $\alpha = 15°$; $R = 1X10^5$.

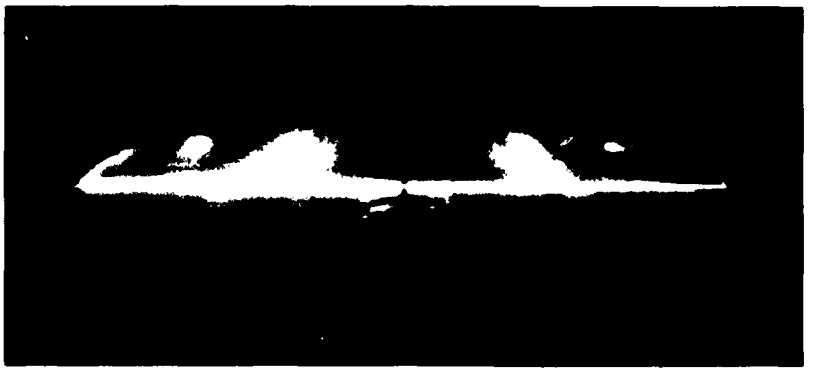

(a) Lower surface bevel

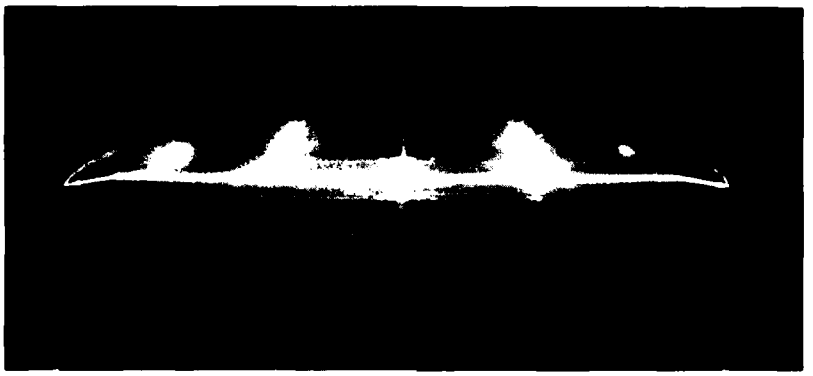

(b) Symmetrical bevel

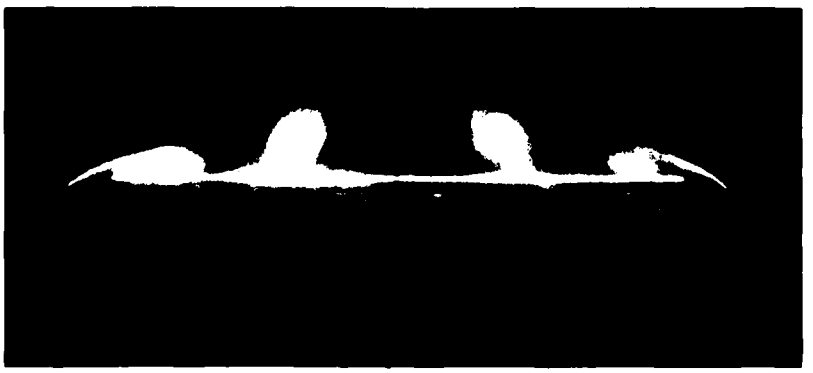

(c) Upper surface bevel

FIG. 17 EFFECT OF LEADING EDGE SHAPE ON VORTEX SYSTEM CROSS-SECTIONS. 80°/40° WING; $\alpha = 15°$; X/C = 0.65; R = $1X10^5$.

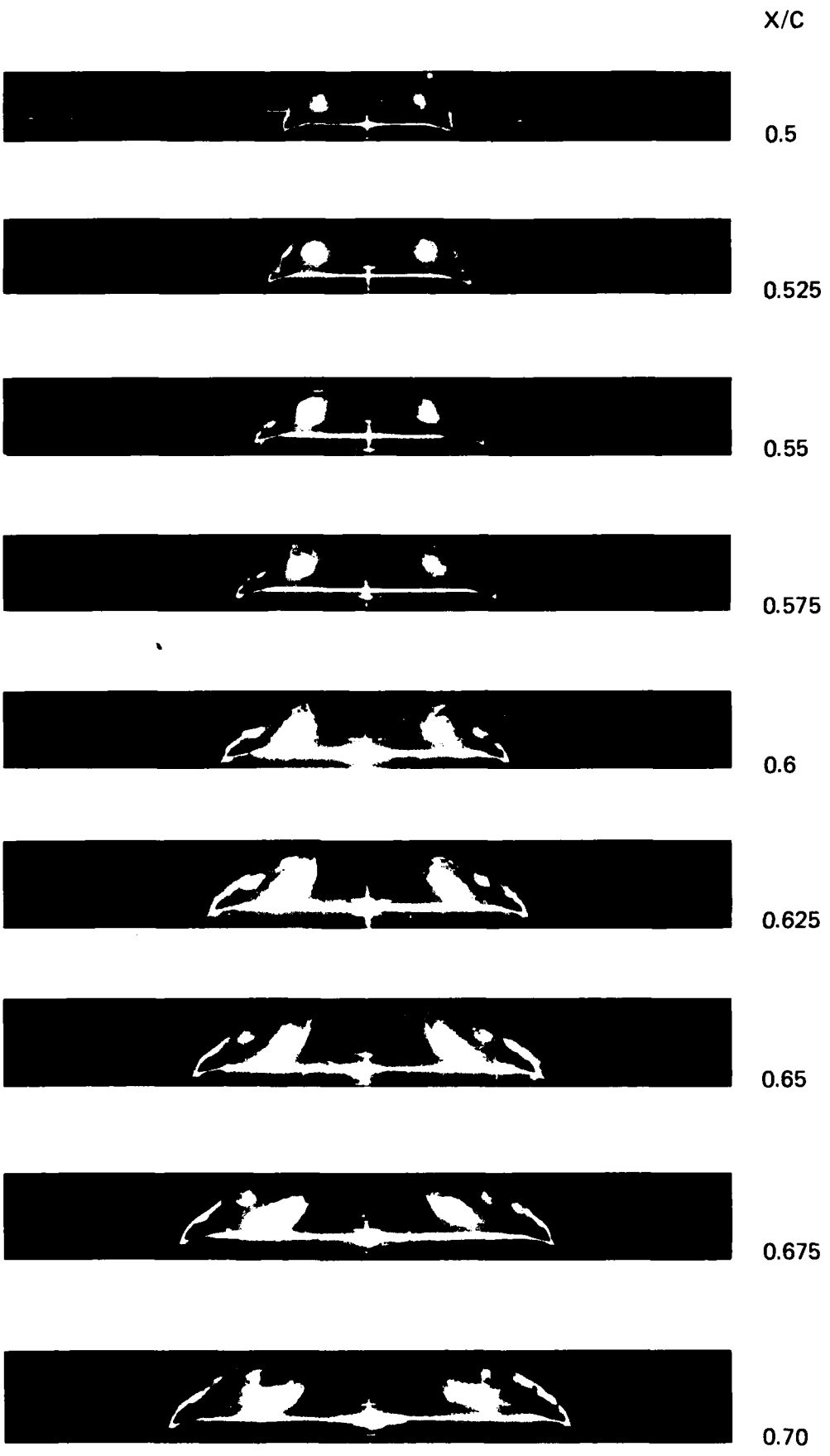

FIG. 18 VORTEX CROSS-SECTIONS OVER 80°/60° WING.
INCIDENCE = 15°. REYNOLDS NO. = 3.2×10^4.

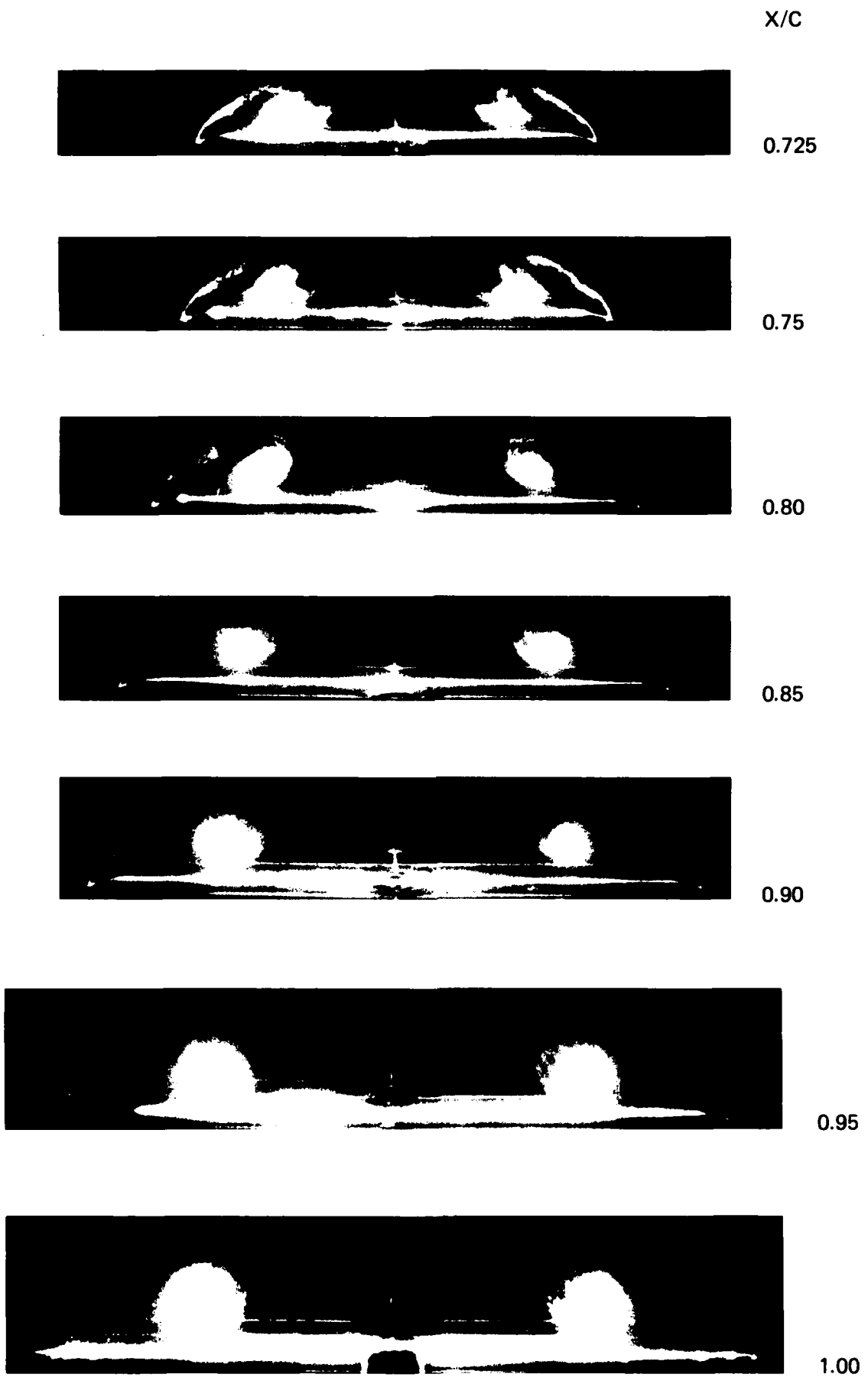

FIG. 18 (contd) VORTEX CROSS-SECTIONS OVER 80°/60° WING. INCIDENCE = 15°. REYNOLDS NO. = 3.2×10^4.

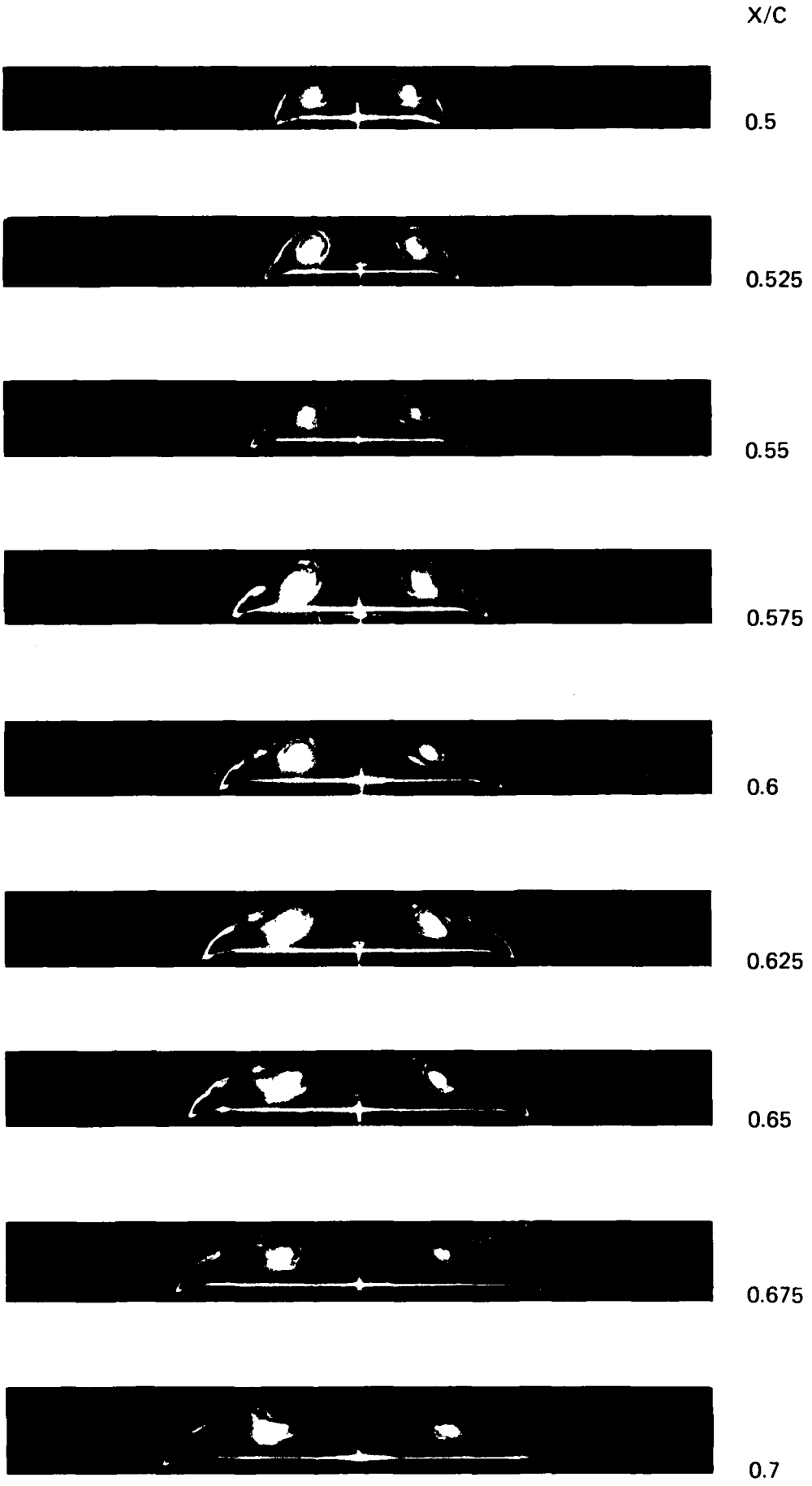

FIG. 19 VORTEX CROSS-SECTIONS OVER 80°/60° WING.
INCIDENCE = 15°. REYNOLDS NO. = 1.74×10^4.

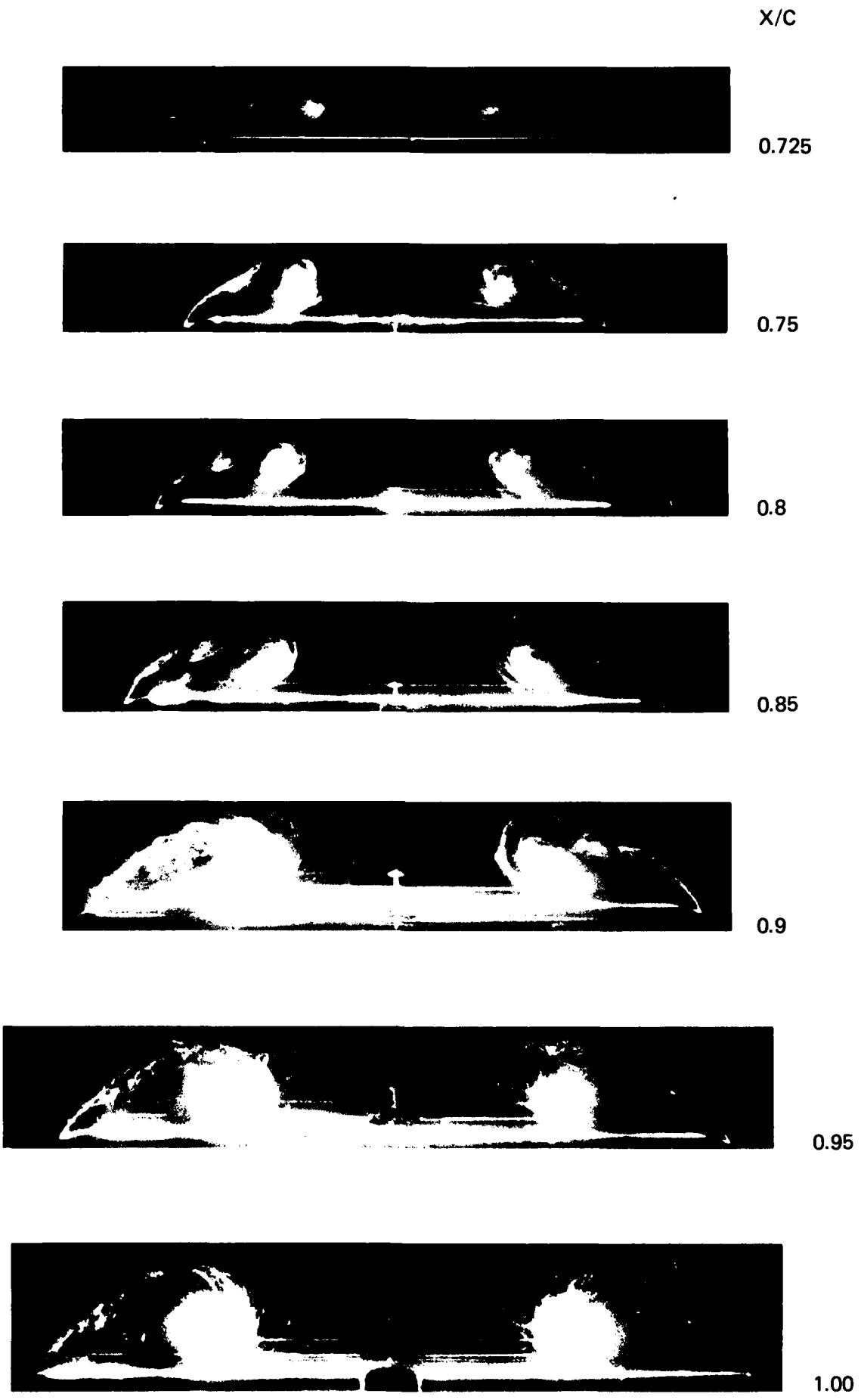

FIG. 19 (contd) VORTEX CROSS-SECTIONS OVER 80°/60° WING.
INCIDENCE = 15°. REYNOLDS NO. = 1.74×10^4.

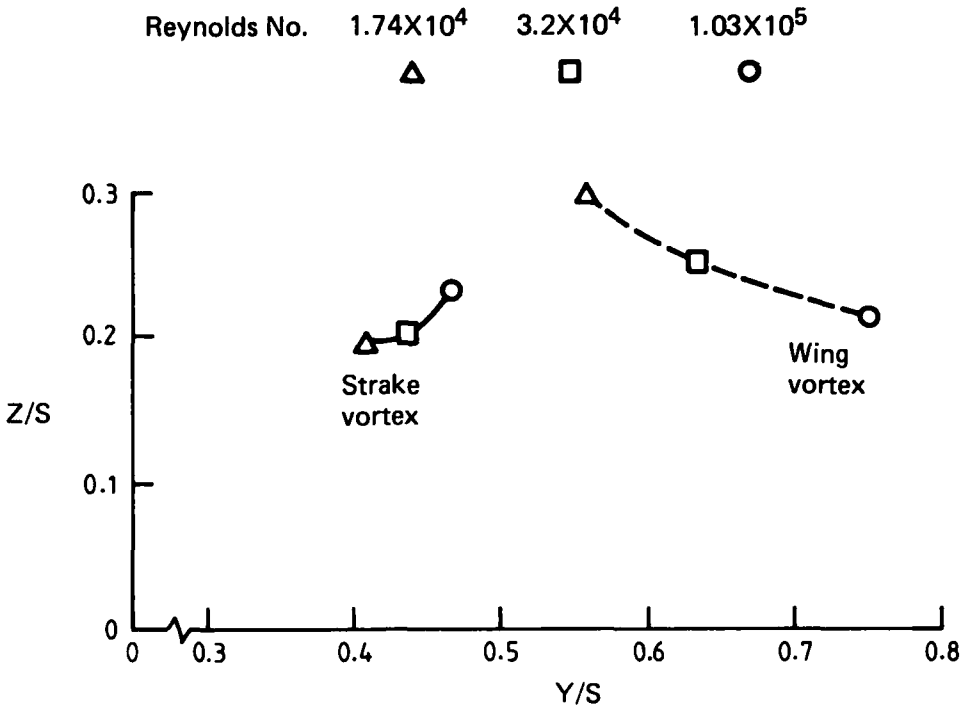

(a) Vortex positions at X/C = 0.675

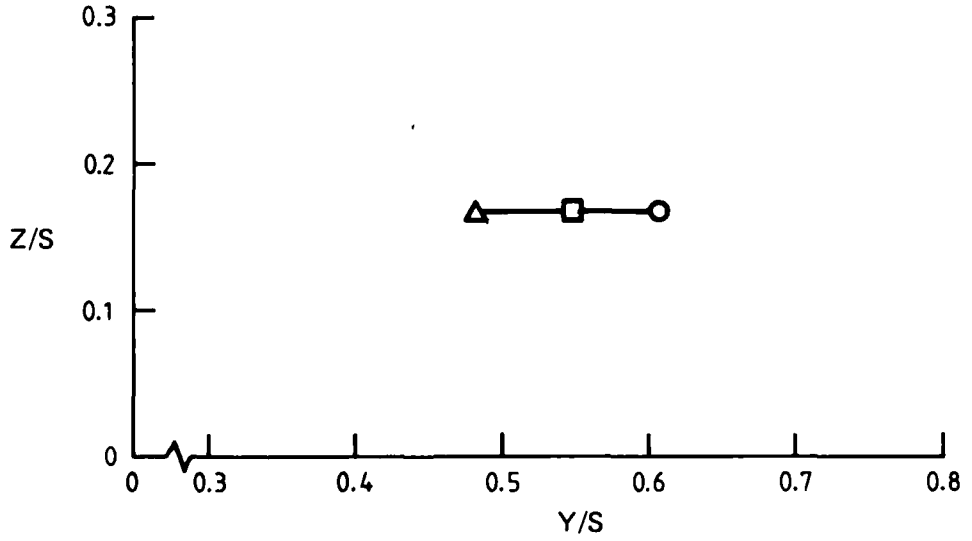

(b) Merged vortex position at X/C = 0.95

FIG. 20 EFFECT OF REYNOLDS NUMBER ON VORTEX POSITIONS. 80°/60° WING; α = 15°.

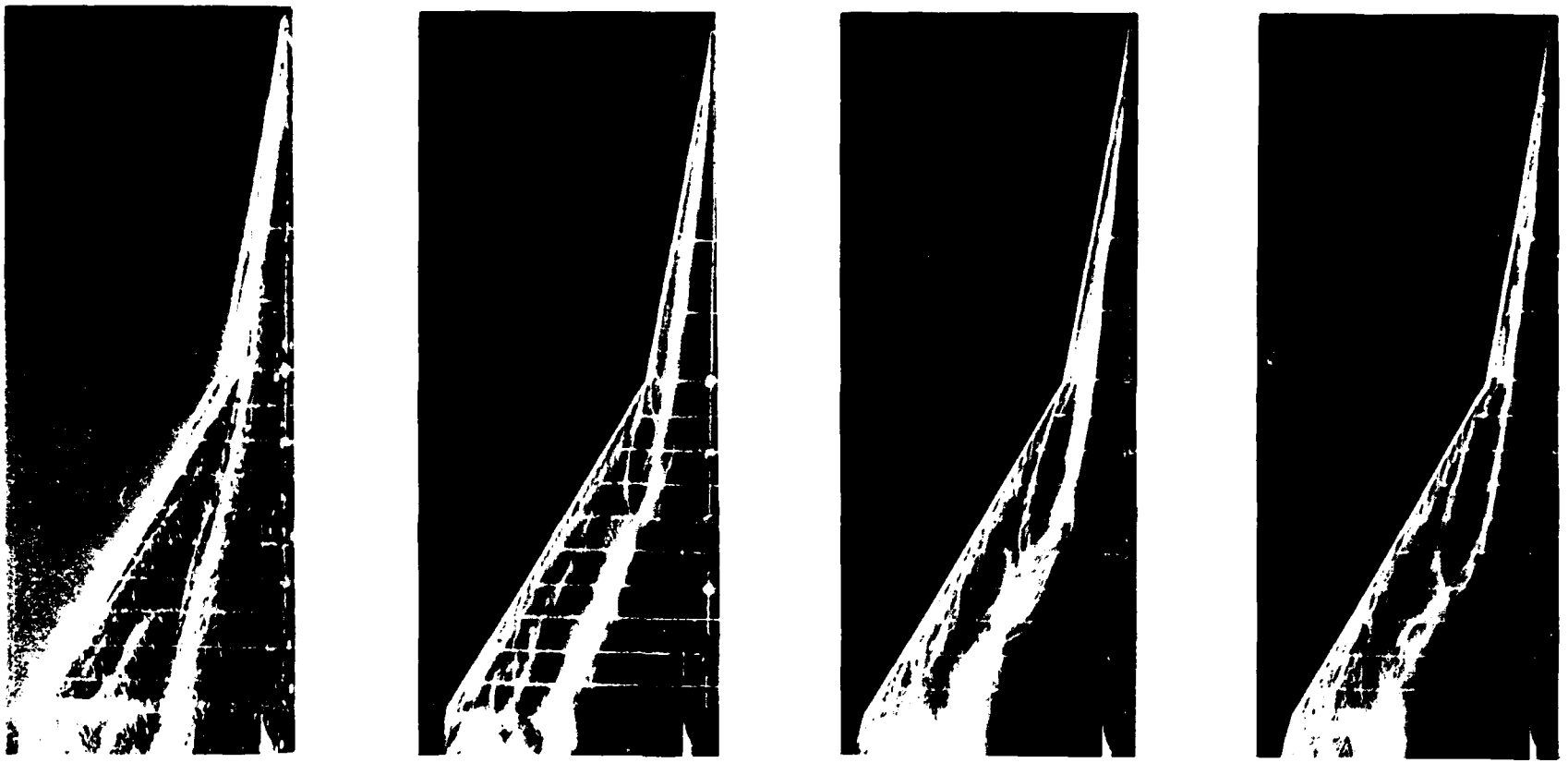

$R = 8.4X10^3$ $R = 2.9X10^4$ $R = 5.7X10^4$ $R = 1.0X10^5$

FIG. 21 EFFECT OF REYNOLDS NO. ON VORTEX FLOW OVER 80°/60° WING. $\alpha = 12°$.

$R = 7.1X10^3$

$R = 2.0X10^4$

$R = 3.0X10^4$

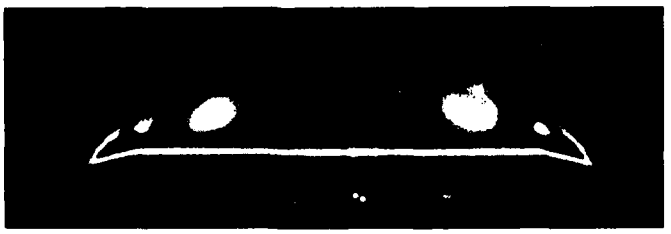

$R = 5.2X10^4$

FIG. 22 EFFECT OF REYNOLDS NO. ON VORTEX CROSS-SECTIONS. 80°/60° WING; $\alpha = 12°$; X/C = 0.6.

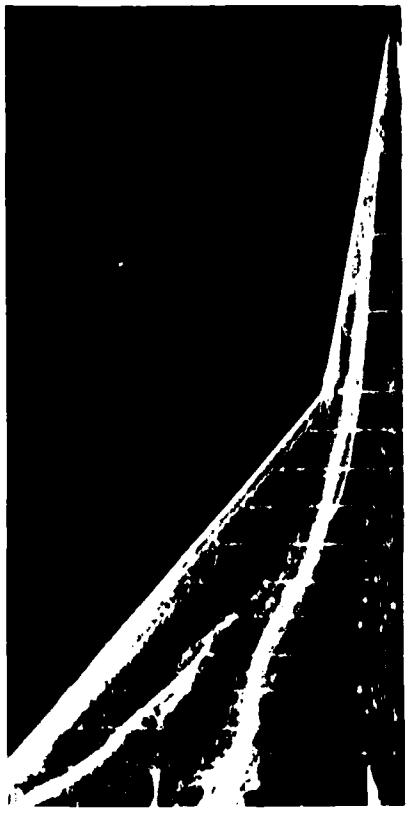

$R = 7.4X10^3$

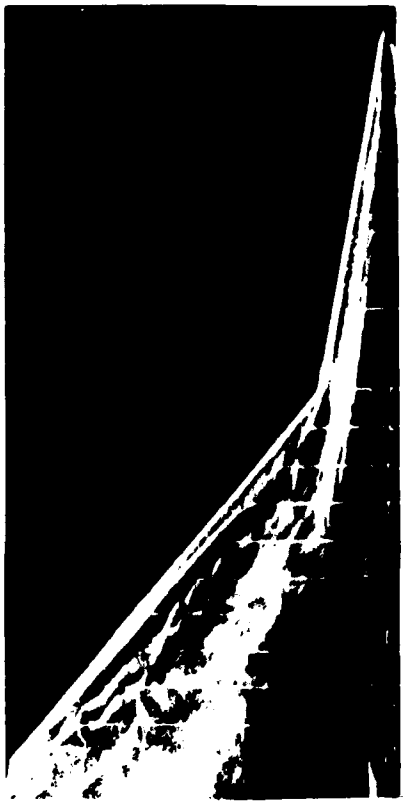

$R = 2.0X10^5$

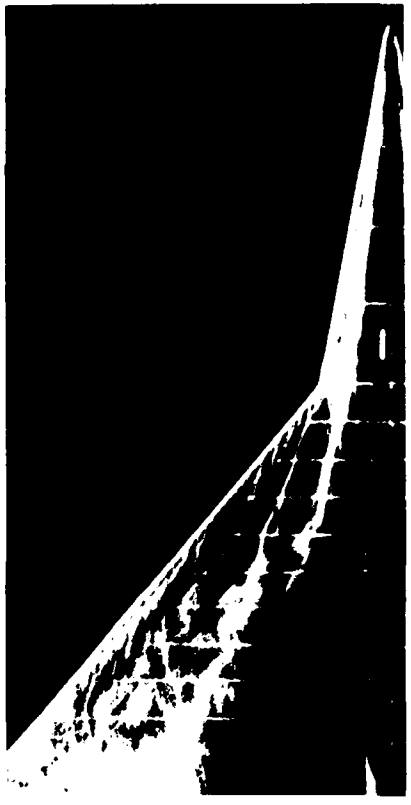

$R = 3.4X10^5$

FIG. 23 EFFECT OF REYNOLDS NO. ON VORTEX FLOW OVER 80°/50° WING. $\alpha = 12°$.

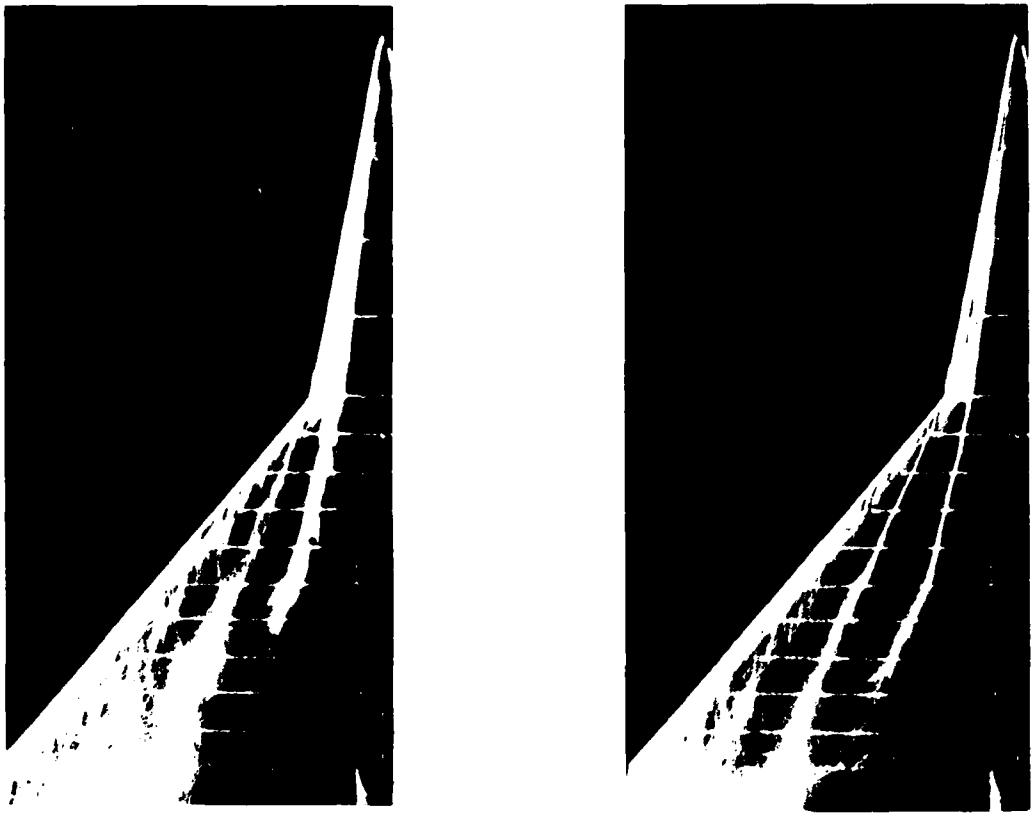

$R = 6.3X10^4$ $R = 1.0X10^5$

FIG. 23 (contd) EFFECT OF REYNOLDS NO. ON VORTEX FLOW OVER 80°/50° WING. $\alpha = 12°$.

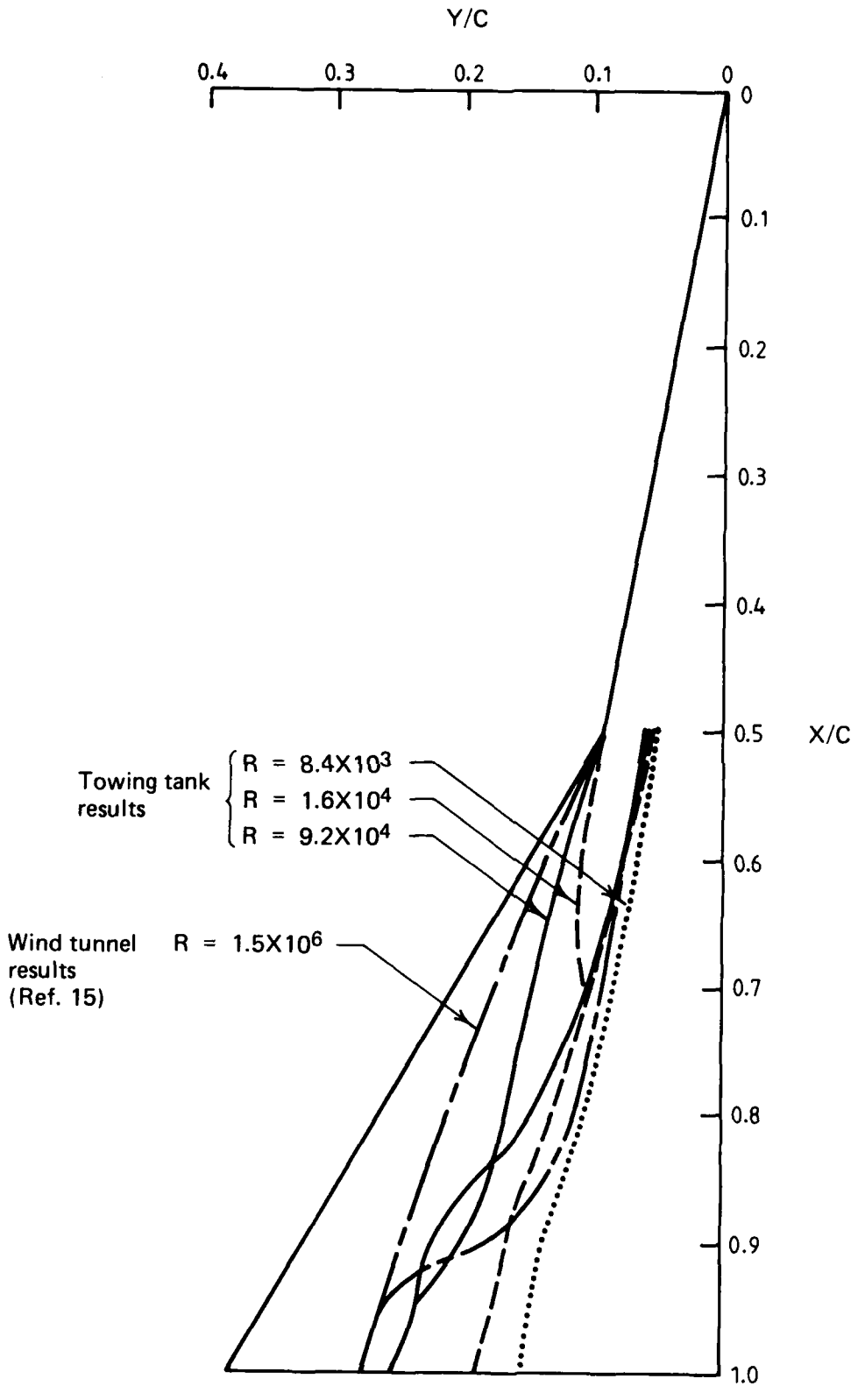

FIG. 24 EFFECT OF REYNOLDS NUMBER ON VORTEX POSITIONS. 80°/60° WING; $\alpha = 12°$.

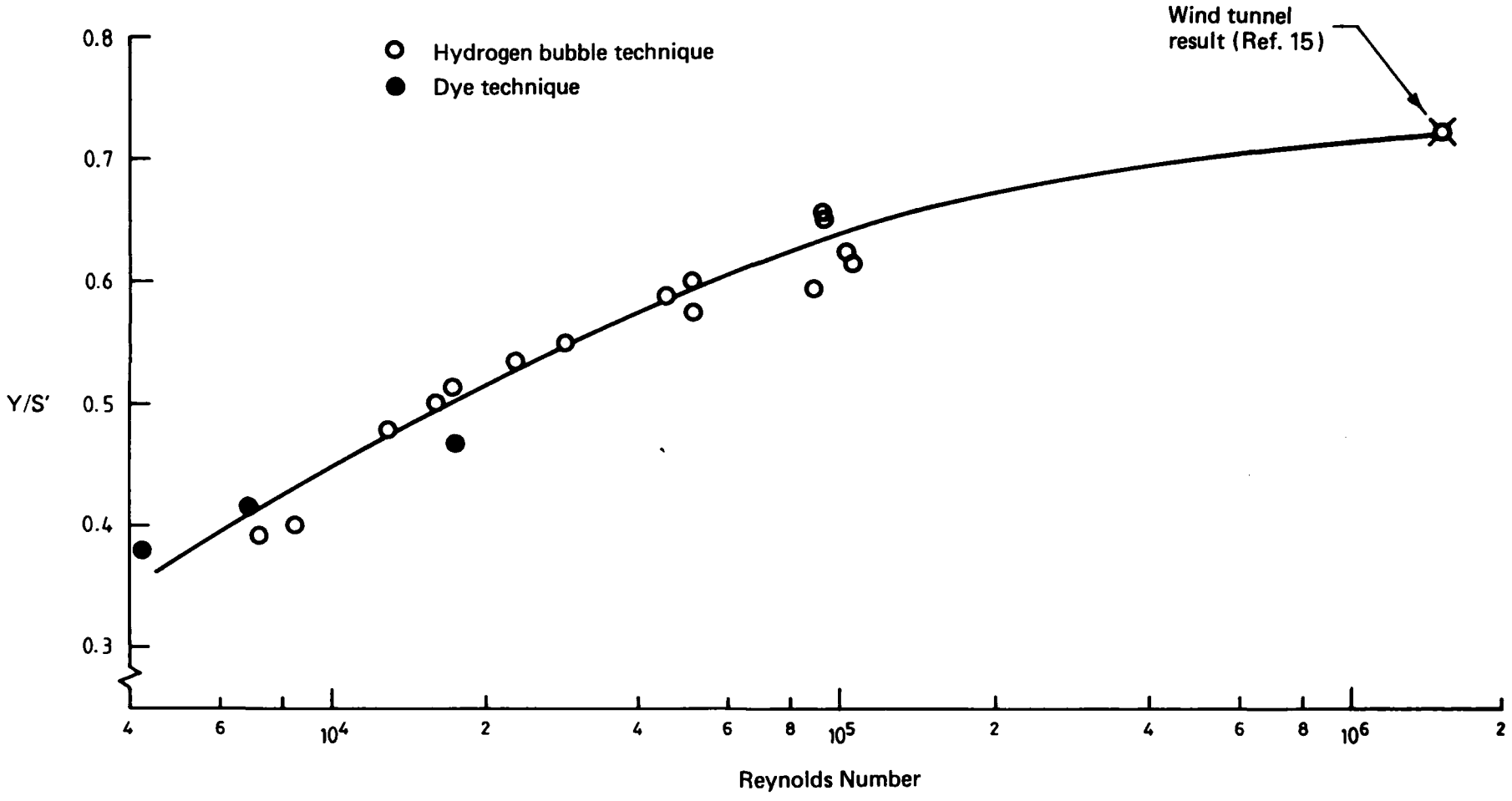

FIG. 25(a) EFFECT OF REYNOLDS NUMBER ON SPANWISE POSITION OF MERGED VORTEX. 80°/60° WING; $\alpha = 12°$; X/C = 1.0.

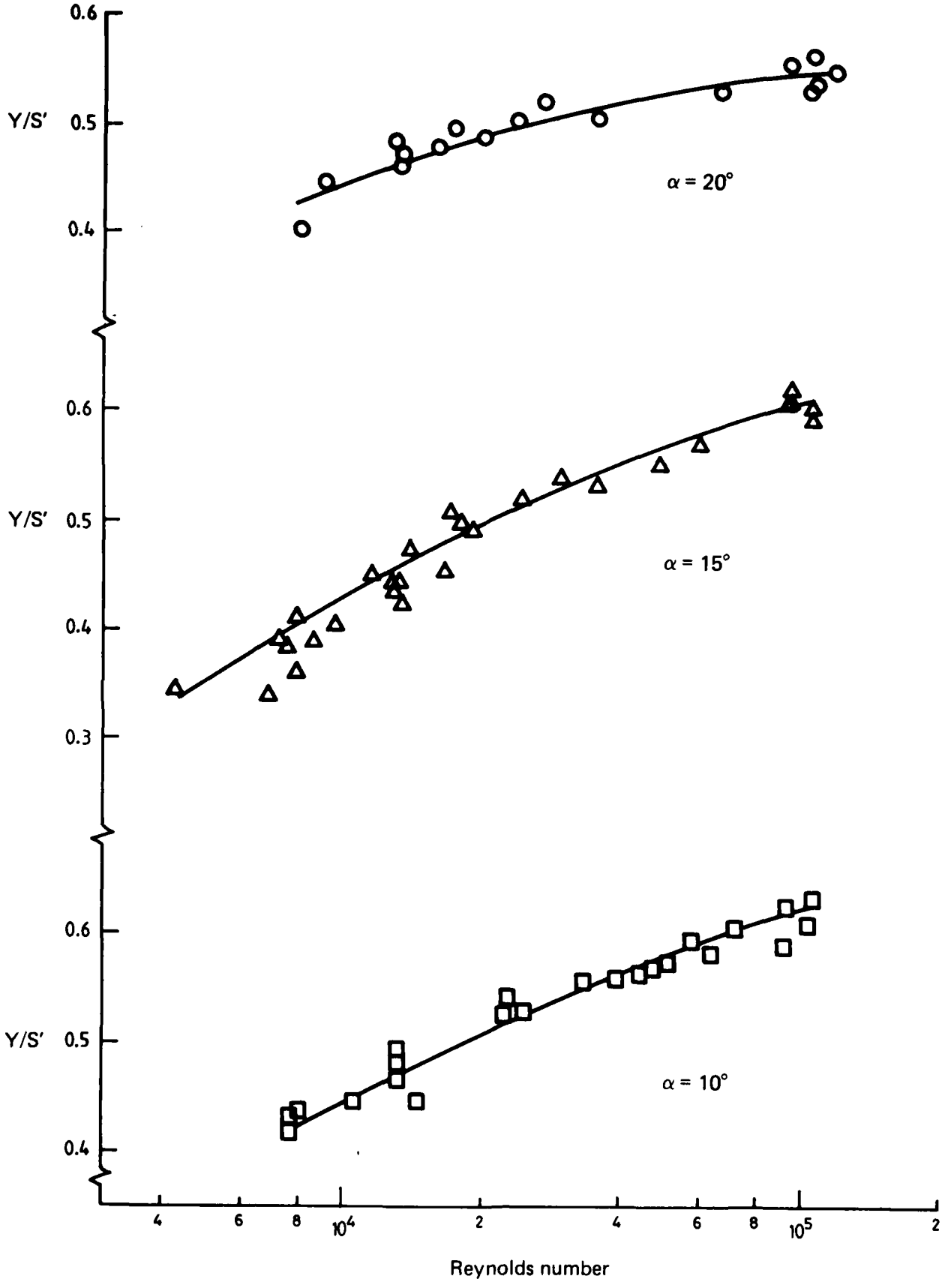

FIG. 25(b) EFFECT OF REYNOLDS NUMBER ON POSITION OF MERGED VORTEX. 80°/60° WING; X/C = 1.0.

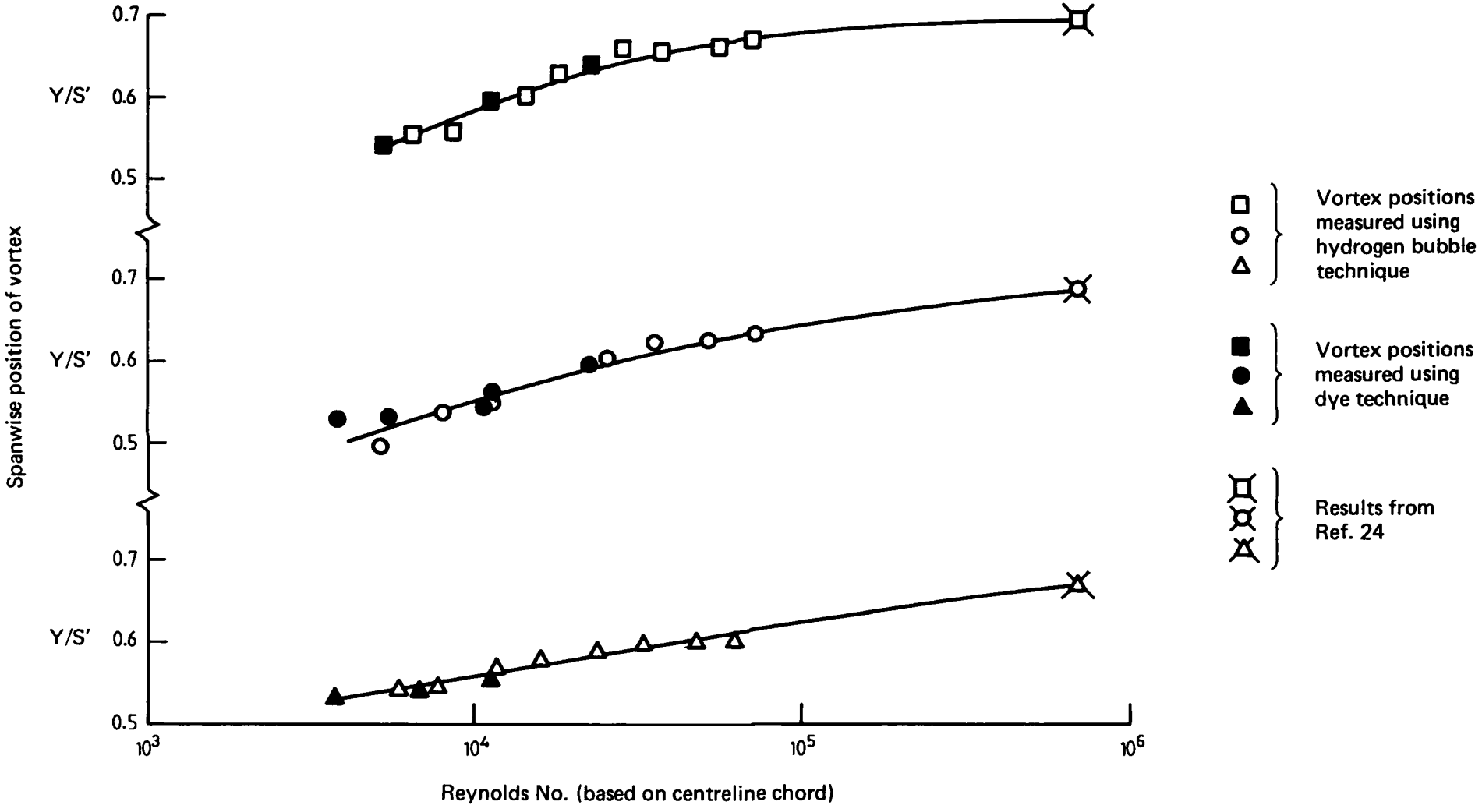

FIG. 26 EFFECT OF REYNOLDS NUMBER ON SPANWISE VORTEX POSITION. 70° DELTA WING. X/C = 0.9.

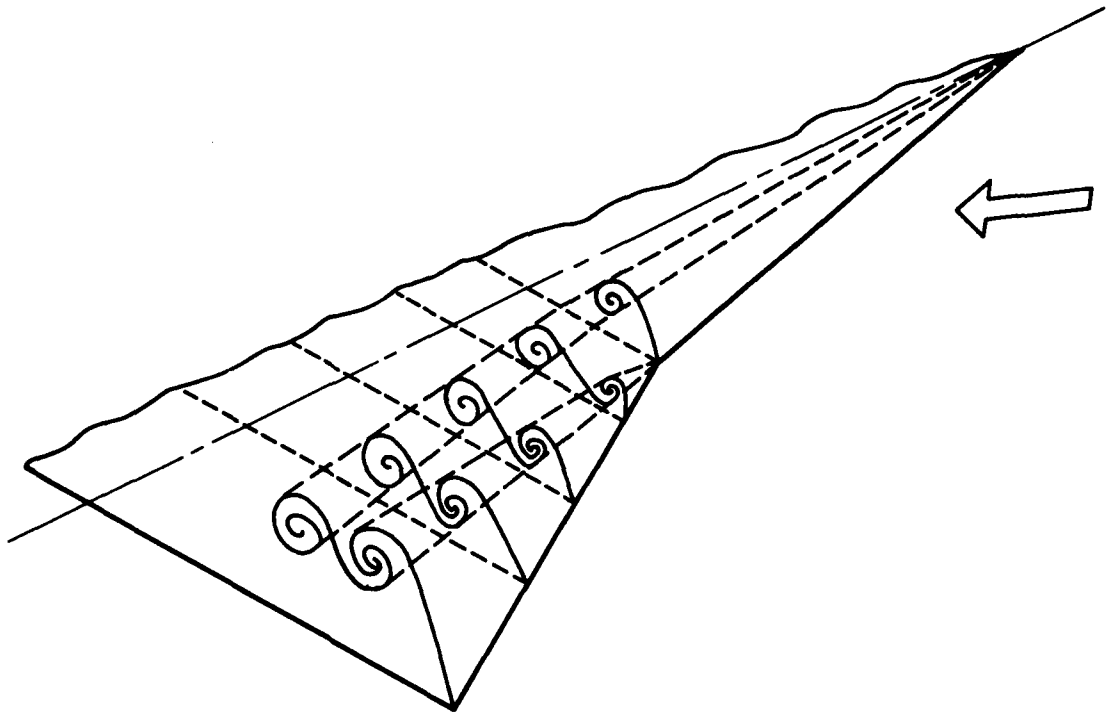

FIG. 27 DOUBLE BRANCHED VORTEX SYSTEM ON DOUBLE DELTA WING WITH SMALL LEADING EDGE KINK. (AFTER SMITH, REF. 2)

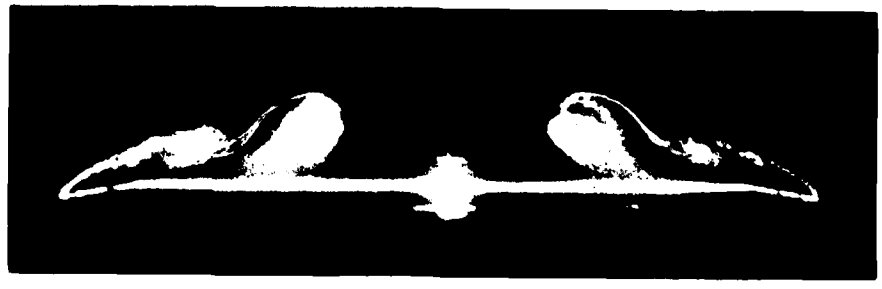

FIG. 28 DOUBLE BRANCHED VORTEX ABOVE 80°/40° WING. INCIDENCE = 15°; REYNOLDS NO. = 3.4×10^4; X/C = 0.6.

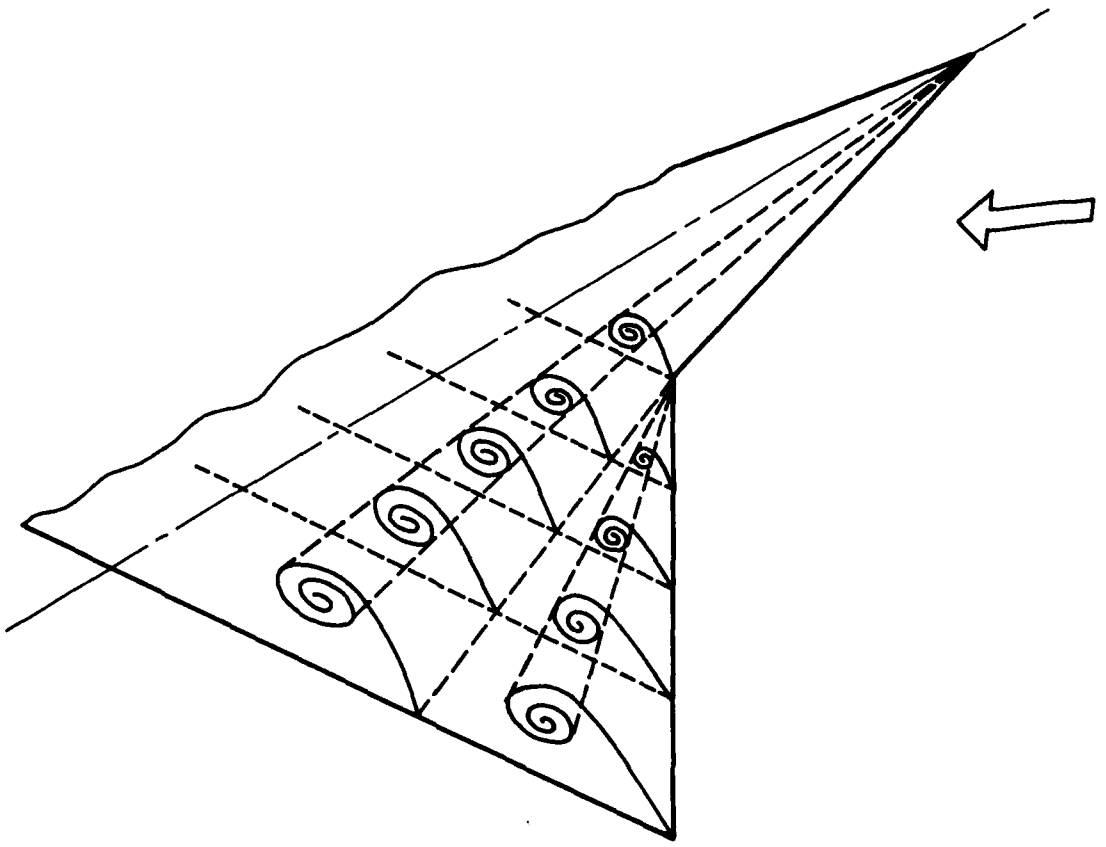

FIG. 29 POSSIBLE VORTEX SYSTEM ABOVE DOUBLE-DELTA WING WITH LARGE LEADING-EDGE KINK. (AFTER SMITH, REF. 2)

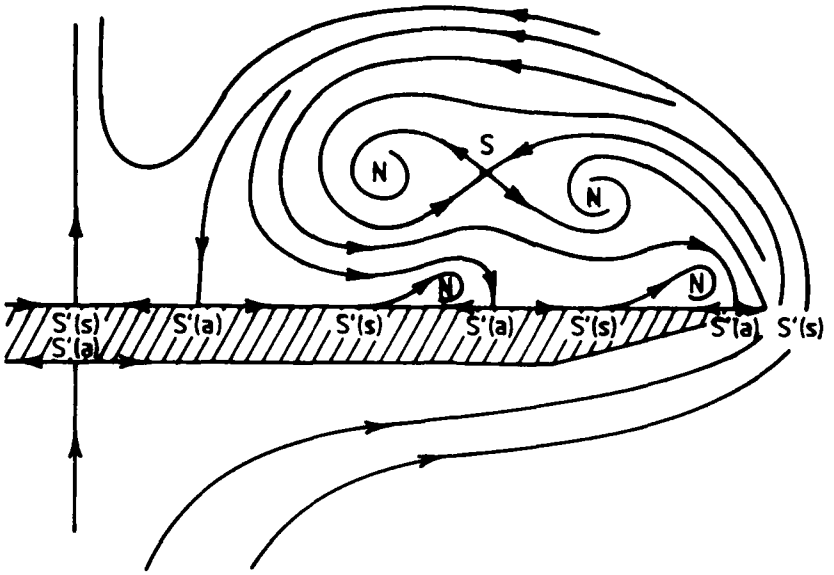

(a) Double branched vortex system (from Ref. 12)

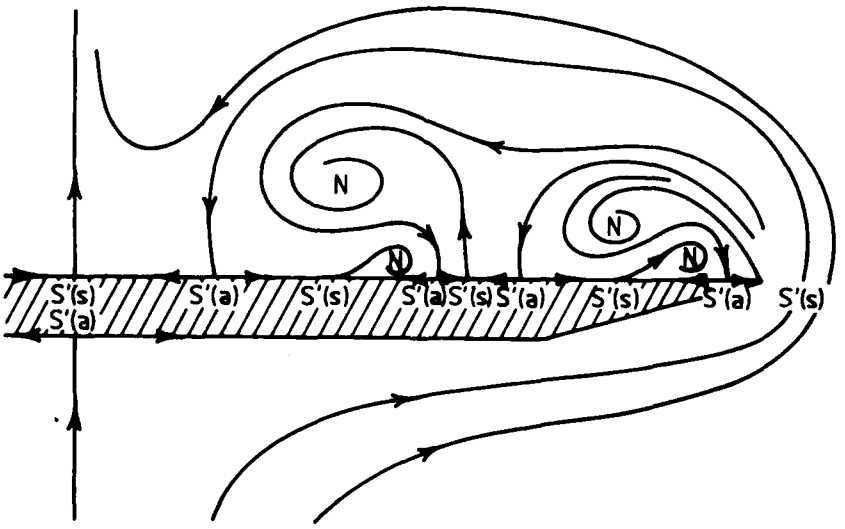

(b) Single branched vortex system

FIG. 30 CONJECTURED CROSS-FLOW STREAMLINES AROUND DOUBLE DELTA WINGS.

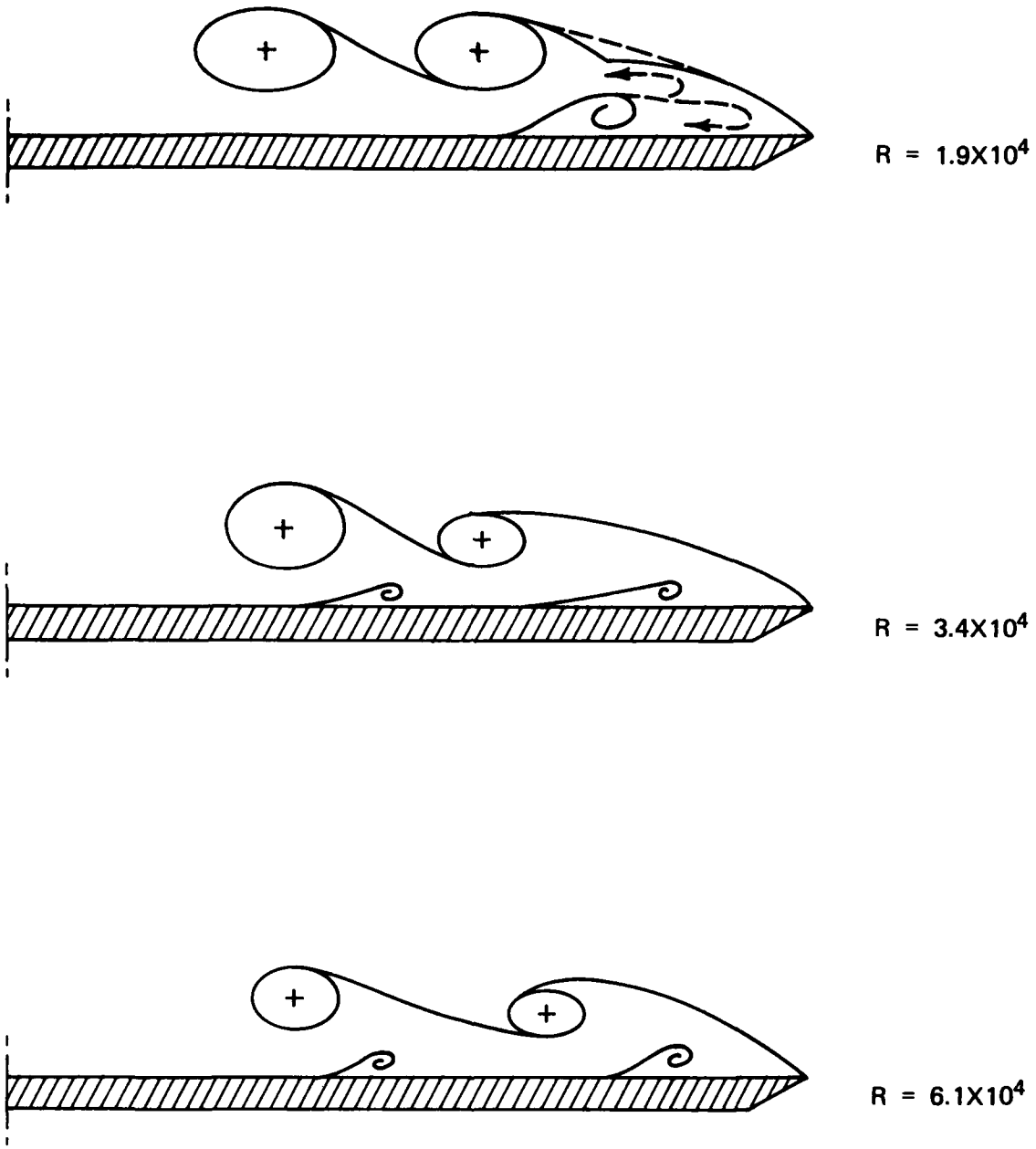

FIG. 31 EFFECT OF REYNOLDS NO. ON VORTEX SYSTEM CROSS-SECTIONS. 80°/40° WING; NEGATIVE CAMBER, INCIDENCE = 8°; X/C = 0.65.

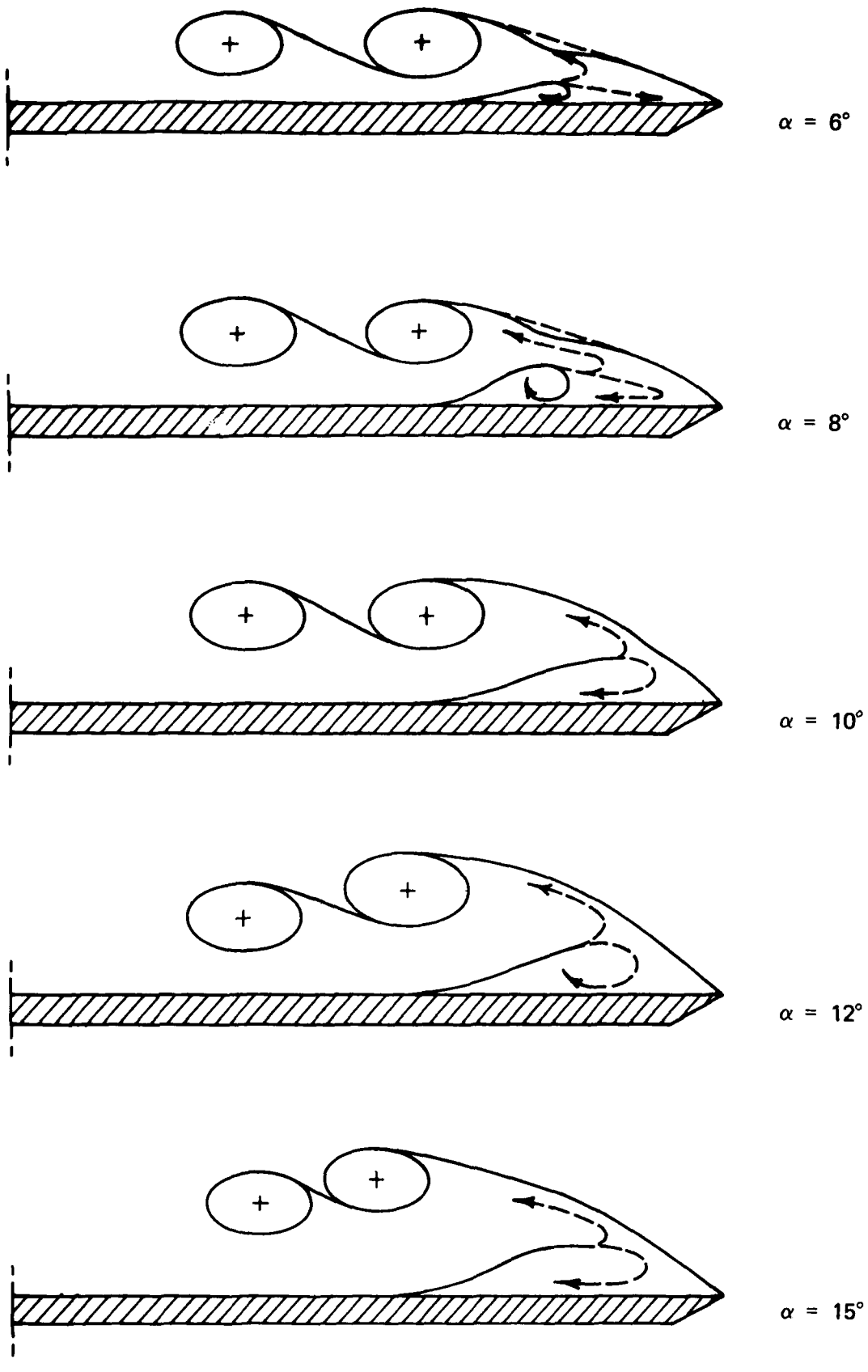

FIG. 32 VORTEX SYSTEM CROSS-SECTIONS. 80°/40° WING; NEGATIVE CAMBER, X/C = 0.65; REYNOLDS NO. = 1.9×10^4.

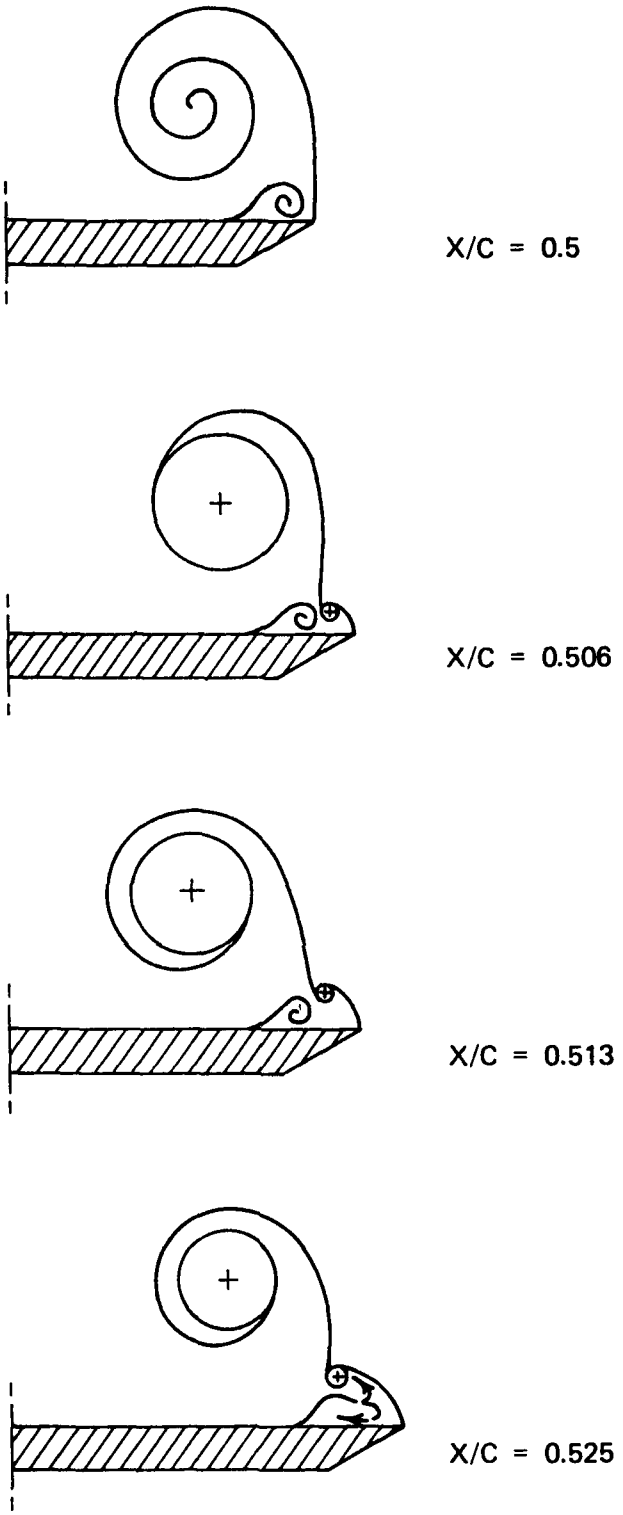

FIG. 33 VORTEX SYSTEM CROSS-SECTIONS. 80°/40° WING;
NEGATIVE CAMBER; INCIDENCE = 20°; REYNOLDS NO. = 1.9×10^4.

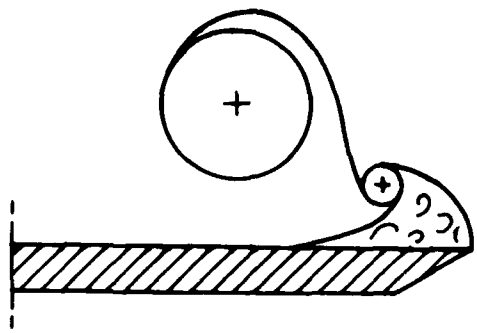

X/C = 0.538

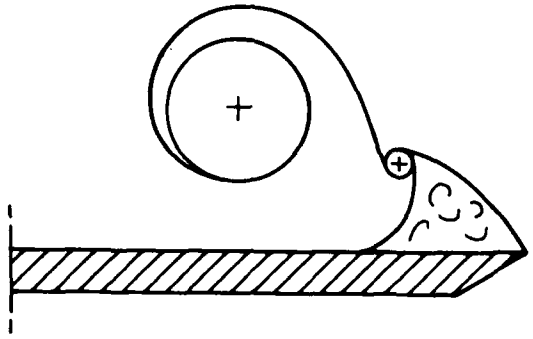

X/C = 0.55

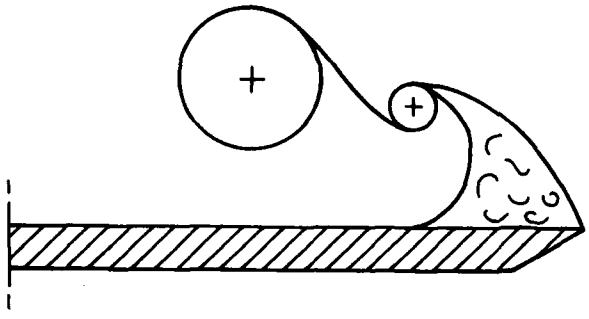

X/C = 0.575

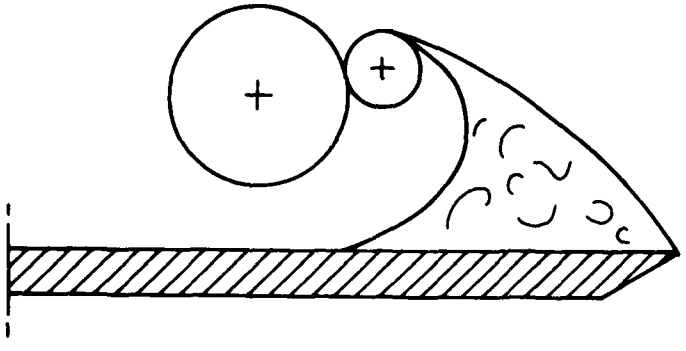

X/C = 0.60

FIG. 33 (contd) VORTEX SYSTEM CROSS-SECTIONS. 80°/40° WING; NEGATIVE CAMBER; INCIDENCE = 20°; REYNOLDS NO. = 1.9×10^4.

DISTRIBUTION

AUSTRALIA

DEPARTMENT OF DEFENCE

Defence Central
Chief Defence Scientist
Deputy Chief Defence Scientist
Superintendent, Science and Program Administration
Controller, External Relations, Projects and Analytical Studies
(1 copy)
Defence Science Adviser (UK) (Doc Data sheet only)
Counsellor, Defence Science (USA) (Doc Data sheet only)
Defence Science Representative (Bangkok)
Defence Central Library
Document Exchange Centre, DISB (18 copies)
Joint Intelligence Organisation
Librarian H Block, Victorian Barracks, Melbourne

Aeronautical Research Laboratories
Director
Library
Superintendent-Aerodynamics
Divisional File-Aerodynamics
N Pollock
Author: D H Thompson (4 copies)

Materials Research Centre
Director/Library

Defence Research Centre
Library

RAN Research Laboratory
Library

Navy Office
Navy Scientific Adviser

Army Office
Scientific Adviser-Army
Royal Military College Library

Air Force Office
Air Force Scientific Adviser
Aircraft Research and Development Unit
Scientific Flight Group
Library
RAAF Academy, Point Cook

Government Aircraft Factories
Library

DEPARTMENT OF AVIATION

Library

INDUSTRY

Commonwealth Aircraft Corporation, Library
Hawker de Havilland Aust. Pty. Ltd., Bankstown, Library

Universities and Colleges

Adelaide	Barr Smith Library
Melbourne	Engineering Library
Monash	Hargrave Library
Newcastle	Library
Sydney	Engineering Library
NSW	Physical Sciences Library
Queensland	Library
Tasmania	Engineering Library
Western Australia	Library
RMIT	Library

CANADA

NRC
Aeronautical & Mechanical Engineering Library

Universities and Colleges

Toronto	Institute for Aerospace Studies

CZECHOSLOVAKIA

Aeronautical Research and Test Institute (Prague), Head

FRANCE

ONERA, Library

INDIA

Defence Ministry, Aero Development Establishment, Library
Hindustan Aeronautics Ltd, Library
National Aeronautical Laboratory, Information Centre

JAPAN

National Aerospace Laboratory

NETHERLANDS

National Aerospace Laboratory (NLR)
Library
Dr. H. W. M. Hoeijmakers
Delft University of Technology
Mr. N. G. Verhaagen, Dept. of Aerospace Engineering

NEW ZEALAND

Defence Scientific Establishment, Library

Universities

Canterbury	Library

SWEDEN

Aeronautical Research Institute, Library

SWITZERLAND

F&W (Swiss Federal Aircraft Factory)

UNITED KINGDOM

Ministry of Defence, Research, Materials and Collaboration
CAARC, Secretary
Royal Aircraft Establishment
Bedford, Library
Farnborough
Library
Mr. J. H. B. Smith
National Physical Laboratory, Library
British Library, Lending Division
Aircraft Research Association
Library
Dr. A. J. Peace
Rolls-Royce Ltd., Aero Division Bristol, Library
British Aerospace
Kingston-upon-Thames, Library
Hatfield-Chester Division, Library
Short Brothers Ltd., Technical Library

Universities and Colleges

Bristol	Engineering Library
Cambridge	Library, Engineering Department
	Whittle Library
London	Professor G. J. Hancock, Aero Engineering
Manchester	Professor N. Johannesen, Fluid Mechanics
Nottingham	Science Library

Southampton	Library
Strathclyde	Library
Cranfield Inst. of Technology	Library
Imperial College	Aeronautics Library

UNITED STATES OF AMERICA

NASA Scientific and Technical Information Facility
Vigyan Research Associates, Dr. D. M. Rao
Boeing Company
Lockheed-Californian Company
Lockheed Georgia
McDonnell Aircraft Company, Library

Universities and Colleges

Florida	Aero Enginereing Department
	Professor D. C. Drucker
Princeton	Professor G. L. Mellor, Mechanics
Massachusetts Inst. of Tech.	MIT Libraries

SPARES (10 copies)

TOTAL (115 copies)

AD A 167004

Department of Defence

DOCUMENT CONTROL DATA

1. a. AR No.	1. b. Establishment No.	2. Document Date	3. Task No.
AR-004-047	ARL-AERO-R-165	AUGUST, 1985	DST85/027

4. Title	5. Security	6. No. Pages
A VISUALISATION STUDY OF THE VORTEX FLOW AROUND DOUBLE-DELTA WINGS	a. document: Unclassified b. title: U c. abstract: U	30 7. No. Refs: 30

8. Author(s)	9. Downgrading Instructions
D. H. THOMPSON	—

10. Corporate Author and Address	11. Authority (*as appropriate*)
Aeronautical Research Laboratories PO Box 4331, Melbourne, Vic., 3001	a. Sponsor b. Security: — c. Downgrading d. Approval

12. Secondary Distribution (*of this document*)

Approved for public release

Overseas enquirers outside stated limitations should be referred through ASDIS, Defence Information Services Branch, Department of Defence, Campbell Park, CANBERRA, ACT, 2601.

13. a. This document may be ANNOUNCED in catalogues and awareness services available to . . .

No limitations

13. b. Citation for other purposes (*i.e. casual announcement*) may be (*select*) unrestricted (*or*) as for 13 a.

14. Descriptors	15. COSATI Group
Flow visualization Vortices Delta wings Wings	01010 01030 20040

16. Abstract

A family of double-delta wings with leading-edge sweep combinations of 80/80, 80/70, 80/60, 80/50 and 80/40 deg. was tested in a small towing tank. The hydrogen bubble technique was used to visualise the vortex patterns above the wings over a range of Reynolds numbers (based on centreline chord) from 7,000 to 100,000. The effects of variations in incidence and leading-edge kink angle were examined. Reynolds number and leading-edge cross-section shape were found to have significant effects on the vortex structure. Attempts to visualise details of the upper surface secondary vortex flows met with only partial success.

This page is to be used to record information which is required by the Establishment for its own use but which will not be added to the DISTIS data base unless specifically requested.

16. Abstract (*Contd*)		
17. Imprint Aeronautical Research Laboratories, Melbourne.		
18. Document Series and Number Aerodynamics Report 165	19. Cost Code 547765	20. Type of Report and Period Covered ——
21. Computer Programs Used		
22. Establishment File Ref(s)		

END

DTIC

5-86